DIRECT GEOREFERENCING AND ORTHORECTIFICATION OF
AIRBORNE DIGITAL IMAGES

A THESIS SUBMITTED TO
THE GRADUATE SCHOOL OF NATURAL AND APPLIED SCIENCES
OF
MIDDLE EAST TECHNICAL UNIVERSITY

BY

ALİ COŞKUN KİRACI

IN PARTIAL FULFILLMENT OF THE REQUIREMENTS
FOR
THE DEGREE OF MASTER OF SCIENCE
IN
GEODETIC AND GEOGRAPHIC INFORMATION TECHNOLOGIES

SEPTEMBER 2008

Approval of the thesis:

DIRECT GEOREFERENCING AND ORTHORECTIFICATION OF AIRBORNE DIGITAL IMAGES

submitted by **ALİ COŞKUN KİRACI** in partial fulfillment of the requirements for the degree of Master Thesis in **Geodetic and Geographic Information Technologies Department, Middle East Technical University** by,

Prof. Dr. Canan Özgen   _____
Dean, Graduate School of **Natural and Applied Sciences**

Assoc.Prof. Dr. Şebnem Düzgün   _____
Head of Department, **Geodetic and Geographic Information Technologies**

Assoc. Prof. Dr. Mahmut Onur Karslıoğlu   _____
Supervisor, **Civil Engineering Dept., METU**

Examining Committee Members

Prof.Dr. Vedat Toprak   _____
Geological Engineering Dept., METU

Assoc.Prof.Dr. M. Onur Karslıoğlu   _____
Civil Engineering Dept., METU

Prof.Dr. Kerim Demirbaş   _____
Electrical and Electronics Engineering Dept., METU

Assoc.Prof.Dr. Sadık Bakır   _____
Civil Engineering Dept., METU

Erol Tunalı   _____
TÜBİTAK UZAY

                                                    Date: 01.09.2008

I hereby declare that all information in this document has been obtained and presented in accordance with academic rules and ethical conduct. I also declare that, as required by these rules and conduct, I have fully cited and referenced all material and results that are not original to this work.

Name, Last name: Ali Coşkun KİRACI

Signature   :

ABSTRACT

DIRECT GEOREFERENCING AND ORTHORECTIFICATION OF AIRBORNE DIGITAL IMAGES

Kiracı, Ali Coşkun

M. Sc., Department of Geodetic and Geographic Information Technologies

Supervisor   : Assoc.Prof. Mahmut Onur Karslıoğlu

September 2008, 131 pages

GPS/INS (Global Positioning System / Inertial Navigation System) brings possibility of relaxing the demand for aerial triangulation in stereo model construction and rectification. In this thesis a differential rectification algorithm is programmed with Matlab software for aerial frame camera images. This program is tested using exterior orientation parameters obtained by GPS/INS and images are ortho-rectified. Ground Control Points (GCP) are measured in the ortho-rectified images and compared with other rectification methods according to RMSE and mean error.

Besides, direct georeferencing accuracy is investigated by using GPS/INS data. Therefore, stereo models and ortho-images are constructed by using exterior orientation parameters obtained with both aerial triangulation and GPS/INS integration. GCPs are measured in both stereo models and ortho-images, compared with respect to their RMSE and mean error. In order to determine Digital Elevation Model (DEM) effect in ortho-rectification, different DEM data are used and the results are compared.

Keywords: Direct georeferencing, GPS/INS, orthoimages, orthorectification, rectification.

ÖZ

HAVADAN ALINAN DİJİTAL GÖRÜNTÜLERİN DOĞRUDAN YÖNELTİLMESİ VE ORTOREKTİFİKASYONU

Kiracı, Ali Coşkun

Yüksek Lisans, Jeodezi ve Coğrafi Bilgi Teknolojileri Bölümü

Tez Yöneticisi: Doç. Dr. Mahmut Onur Karslıoğlu

Eylül 2008, 131 sayfa

GPS/INS, stereo model oluşturulmasında ve rektifikasyonda havai nirengi gereksinimi için esneklik getirmektedir. Bu tezde Matlab yazılımı ile havadan alınan çerçeve kamera görüntüleri için bir diferensiyel rektifikasyon algoritması programlandı. Bu program, GPS/INS entegrasyonu ile elde edilen dış yöneltme parametreleri kullanılarak orto-görüntüler oluşturuldu ve test edildi. Orto-görüntüler üzerinde Yer Kontrol Noktaları ölçüldü ve diğer rektifikasyon yöntemleri ile karesel ortalama hataları (KOH) ve ortalama hatalarına göre karşılaştırıldı.

Bunun yanında, GPS/INS verileri kullanılarak doğrudan yöneltmenin doğruluğu araştırıldı. Bunun için, hem havai nirengi hem de GPS/INS entegrasyonu ile edilen dış yöneltme parametreleri kullanılarak stereo modeller ve ortogörüntüler oluşturuldu. Stereo modeller ve orto-görüntüler üzerinde YKN. ları ölçüldü, KOH ve ortalama hatalarına göre karşılaştırıldı. Sayısal Yükseklik Modeli (SYM) nin orto-rektifikasyondaki etkisini belirlemek için farklı SYM verileri kullanıldı ve sonuçlar karşılaştırıldı.

Anahtar Kelimeler: Doğrudan yöneltme, GPS/INS, orto-görüntü, ortorektifikasyon, rektifikasyon.

To My Wife

ACKNOWLEDGEMENTS

TABLE OF CONTENTS

LIST OF TABLES

TABLES

LIST OF FIGURES

FIGURES

LIST OF ABBREVIATIONS

ABGPS : Airborne GPS

AINS   : Aided INS

CIM   : Image Coordinate

CP   : Photo Coordinate

CC   : Camera Coordinate

CCD   : Charge Coupled Device

CB   : Body Coordinate

CE   : Earth Fixed Coordinate

CL   : Local Coordinate

CG   : Geodetic Coordinate

CM   : Map Coordinate

CPDP   : Carrier Phase Differential Positioning

C/A   : Coarse Acquisition

DEM   : Digital Elevation Model

DG   : Direct Georeferencing

DGPS   : Differential Global Positioning System

DRM   : Differential Rectification Method

ECEF   : Earth Centered Earth Fixed

GCP   : Ground Control Point

GPS   : Global Positioning System

INS   : Inertial Navigation System

IMU   : Inertial Measurement Unit

NED   : North East Down

NP   : Navigation Processor

PPP   : Precise Point Positioning

RMSE   : Root Mean Square Error

SRTM   : Shuttle Radar Topography Mission

UTM   : Universal Transverse Mercator

CHAPTER 1

INTRODUCTION

GPS/INS systems are rapidly emerging as a main component of airborne mapping and remote sensing systems. In recent years, GPS/INS has been a great of interest for direct georeferencing. In order to determine camera perspective center position, GPS application has already become a common process in airborne applications. Aerial triangulation is performed to determine the unknown exterior parameters $(X_0, Y_0, Z_0, \omega, \varphi, \kappa)$ generally with the use of four full control points and pass points homogenously scattered on the overlap area among the images. Then bundle block adjustment is performed to estimate exterior orientation parameters. To decrease the use of ground control points (GCP) has always been focus of the photogrammetric studies. Theoretically there is no need for GCP with the use of GPS/INS. Integrated GPS/INS provides exterior orientation parameters directly. According to the accuracy requirement and the aim of the study it is possible not to use or decrease the number of GCP is possible.

Aerial photos and satellite images do not show features in their correct locations due to displacements caused by the tilt of the sensor and terrain relief. Orthorectification transforms the central projection of the photograph into an orthogonal view of the ground, thereby removing the distorting effects of tilt and terrain relief. Orthorectification is the process of transforming raw imagery to an accurate orthogonal projection, as against the perspective projection of the raw image. The product of orthorectification process is orthoimage or orthophotos. Without orthorectification, scale is not constant in the image and accurate measurements of distance and direction cannot be made. In order to orthorectify imagery, a transformation model is required which takes into account the various

sources of image distortion generated at the time of image acquisition. These include sensor orientation, relief displacement, earth shape and rotation, orbit and attitude variations, systematic error associated with the sensor. [14]

Various studies were performed about direct georeferencing and orthorectification and their accuracy assessments. One of the study conducted by Jacobsen (2000), combined bundle block adjustment and direct sensor orientation results were compared and boresight misalignment was determined. They found the results in mean square errors of the horizontal coordinate component in the range of +/- 0.43 m. and 0.78 m for vertical component for 1:3500 photo scale.

Cramer, Stallmann and Haala (2000) performed direct georeferencing using GPS/INS tests and compared the results with combined aerial triangulation. The root mean squares of object coordinates as east, north and vertical component were 4.5 cm, 6.3 cm, 12.1 cm for aerial triangulation and 8.8 cm, 11.9 cm, 17.8 cm for direct georeferencing.

Another study conducted by Wegmann (2003) was image orientation by combined aerial triangulation (AT) with GPS/IMU. Boresight misalignment was determined and combined (AT) results were assessed. The test resulted in 5 cm in horizontal and 10 cm in vertical coordinate component for 1/5000 photo scale.

Skaloud and Lichti (2006) studied on a rigorous approach to boresight self calibration in airborne laser scanning. The results for their approach showed that RMS residuals 3 cm in height, 2 arc seconds in angles and 1 cm in laser range with 200 m flying height.

Heipke et al. (1992) studied in SPOT Imagery for point determination, DEM generation and orthorectification by the automatic photogrammetric processing. For the DEM generated, an empirical height accuracy of better than 10 m. was achieved with small base-to-height ratios of 0.4 and 0.6.

Pala and Pons (1995) tested the incorporation of relief in polynomial-based geometric correction of SPOT and Landsat TM imagery. It is investigated that sub-pixel accuracy can be reached with this method.

El-Manadili and Novak (1996) studied in Direct Linear Transformation (DLT) for the geometric modeling of SPOT imagery. The approach does not need the interior and ephemeris information. The solution is based on only ground control points. When sensor model and ephemeris information are not available this is advantageous for processing of the new high resolution satellite images. Corrections for other systematic errors are considered through the adjustment.

Accuracy of the rectification methods was compared and applicability of them was assessed by Ok in his MS thesis (2005). The thesis examines rectification models including affine transformation to rigorous analytical rectification.

Erdoğan has studied on methods and inputs of orthorectification process and effects of them over this process are described in his M.S. thesis (2000). In particular, SPOT satellite system and stereoscopic aspects of this system are studied in detail. Measurements and accuracy results of photogrammetric process, DEMs and orthoimages are presented.

A new differential rectification algorithm for monoscopic images taken by CCD frame cameras was proposed by Karslıoğlu and Friedrich (2005). The method directly assigns the geodetic coordinates of the images so it avoids earth curvature corrections. This method was performed in this thesis for digital aerial frame camera and the results were examined.

Bettemir has studied on sensitivity analysis of differential rectification method proposed by Karslıoğlu and Friedrich for CCD frame cameras and pushbroom scanners (2006). Sensitivity and error analysis of a differential rectification method were performed by using digital images taken by a frame camera onboard BILSAT and pushbroom scanner on ASTER. The effectiveness and accuracy of

3

the differential rectification method was compared with other rectification methods and results were compared.

In this thesis a differential rectification algorithm proposed by Karslıoğlu and Friedrich is applied to UltracamX Vexcel digital aerial frame camera images. For this, an operational software was developed, implemented and tested to generate orthorectified image on the basis of this algorithm in Matlab environment which is explained step by step in Chapter 3. The test of the software is accomplished by using exterior orientation parameters delivered by GPS/INS integrated system on board the airplane. GCPs of which the coordinates are determined by adjustment of GPS observations are measured in ortho-rectified images obtained with the software and rectified images with polynomial method (2nd and 3rd degree), RMSE (Root Mean Square Error) and mean error is computed using the adjusted and measured coordinates of GCPs.

Besides, combined aerial triangulation and direct georeferencing are performed using exterior orientation parameters obtained by GPS/INS integration. Stereo models and ortho-images are constructed with each method and RMSE and mean error are computed for GCPs measured in stereo models and ortho-images. The results are compared and assessed with respect to their accuracies. Various GCP combinations are used for combined aerial triangulation to see the effect of decreasing number of GCP. Additionally various DEM (Digital Elevation Model) data are used to determine the effect of DEM in orthorectification.

This thesis is divided into seven parts. In the following chapter (Chapter 2), aerial triangulation methods, Global Positioning System and Inertial Navigation System are presented. Development of the aerial triangulation and the effect of decreasing GCP numbers are studied. Georeferencing algorithm and boresight calibration are presented which were used in this thesis.

In Chapter 3, common rectification methods are introduced and colinearity equations as a basis of differential rectification method are described for aerial

frame camera. DRM algorithm procedure which is programmed in this thesis is explained step by step.

In Chapter 4, 5 and 6, test area, data and the methodology used in the study are presented. Data inputs and processes are defined and implementation of the algorithm is completed.

In chapter 7, an overall discussion of the thesis study is made. Analysis results are commented briefly and some recommendations were suggested for future studies related with direct goereferencing and orthorectification applications.

CHAPTER 2

AERIAL TRIANGULATION AND DIRECT GEOREFERENCING

2.1   AERIAL TRIANGULATION

Aerial triangulation is an important procedure in photogrammetric workflow. It provides the exterior orientation parameters of all images and ground coordinates of all pass points within a photogrammetric block, based on photogrammetric measurements and a few control points. And normally aerial triangulation is a very hard and time-consuming procedure.

Traditionally, aerial triangulation begins with preparing and annotating photographs, whereby a suitable number of well distributed points are carefully selected such that they appear on as many photographs as possible. Once preparation is completed, the points must be transferred to all photographs. This latter phase is quite crucial; particularly the transform of strip tie points. In fact, the success of an aerial triangulation project depends largely on the quality of the point transfer. Only after points are transferred or clearly identified can the measuring process begin [30].

Here automatic triangulation improvements play an important role. The point transfer can be combined with simultaneous measurement of conjugate points on all images involved. Basically, aerial triangulation is suitable for automation. While preparation, block points can be automatically selected at proper locations. An important advantage is the possibility to determine conjugate points that appear on more than two photographs by a multiple image matching procedure simultaneously. In traditional aerial triangulation, an operator can only view two images at the same time.

In modern photogrammetry, the relative orientation is not implemented as a separate stand-alone process, but it is part of a broader point measurement and triangulation module. However, it provides the theoretical and practical basis of automated point measurement during aero-triangulation. Aero-triangulation is often characterized as one of the more complex procedures in terms of user knowledge of the underlying principles of a photogrammetric block adjustment. Its objective is to relate multiple images to each in order to: [30, p 957]

-determine the orientation parameters of each image in the block, namely the (Xo,Yo,Zo) coordinates the exposure station and omega, phi, kappa, rotations and to

-determine the ground coordinates (X, Y, Z) of points observed in them.

This is performed by the measurement of photo coordinates of the ground control points and the measurement of conjugate points in the overlapping areas of the block imagery (tie, and pass points).

Virtually all vendors provide triangulation algorithms that are based on rigorous physical sensor models and the well established principle of least squares bundle adjustment in which all parameters are fully weight constrained [30, p 957].

2.2   AERIAL TRIANGULATION METHODS

Aerial triangulation can be defined as the determination of point coordinates (X, Y, Z) by means of photogrammetric devices. From the aspects of photogrammetric applications, it is the determination of control points to perform absolute orientation in order to evaluate a single or a pair of photograph(s) (stereo compilation) (Photogrammetry Lecture Notes, 2002)

Densification of the control points (3rd and 4th degree points based on 1st and 2nd degree triangulation network) for the production of 1:25.000 scaled topographic maps has been completed in Turkey. However this does not satisfy the enough point density necessary to produce maps having scales larger than 1:25.000 (e.g

1:5000, 1:2000, and 1:1000). Most of this kind of points lost or destroy in the course of time. Aerial triangulation is the most useful way of constructing the required number of control points in map production processes.

Point densifications by means of photogrammetric method can be arranged by their historical developments namely pool method, serial method, aerial triangulation method, and aerial triangulation with kinematic GPS support respectively.

2.2.1 Pool Method

Independent of the flight direction at least 3 control points must exist in a stereo model, comprised of adjacent two photographs, to perform the absolute orientation.

A circle called as pool circle that encircles an equilateral triangle and whose diameter can be measured is used to provide the required number of triangulation points. Pool circle is drawn on a transparent base such as tracing paper, astrolon etc. in a scale of triangulation canavas. 3 points must be in the circle or at least on the circle wherever the pool circle is placed on a triangulation and flight planning sheets (Figure 2.1)
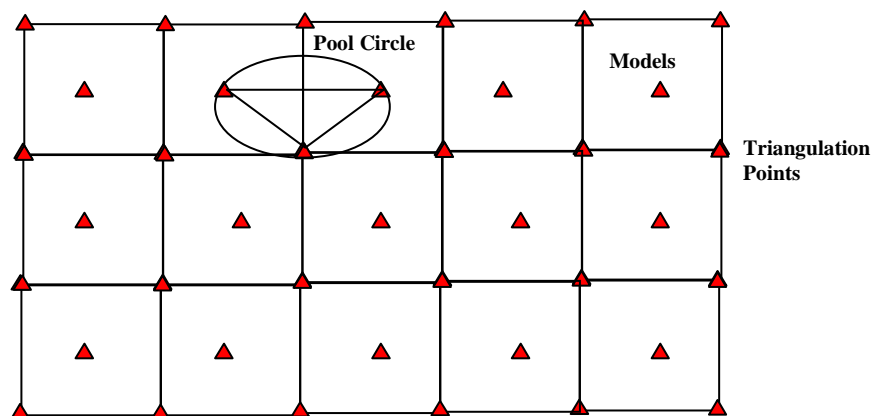
Figure 2.1 Triangulation and flight planning by means of pool method

2.2.2 Serial Method

Triangulation and flight planning by means of serial method is made by placing one point at nearly the corners of model which therefore provides absolute orientation in a restricted way. To achieve this, firstly the flight direction, photo scale, and the along track overlapping ratio is considered to determine the optimal or optimum model area. After then how many points at which spacing along the X and Y direction is determined. Considering the length of model along the X direction is equal to base of model, base length (B) is adopted to for the triangulation point spacing. Until 1960 pool method and after that time serial method had been used in Turkey. Because the pool method necessitates establishing lots of points and the flights can not be covered along the colon in serial method, most of the studies performed by GCM have to be redone. Therefore the expected accuracy and economy from pool and serial method has not been provided (Figure 2.2) (Photogrammetry Lecture Notes, 2002).
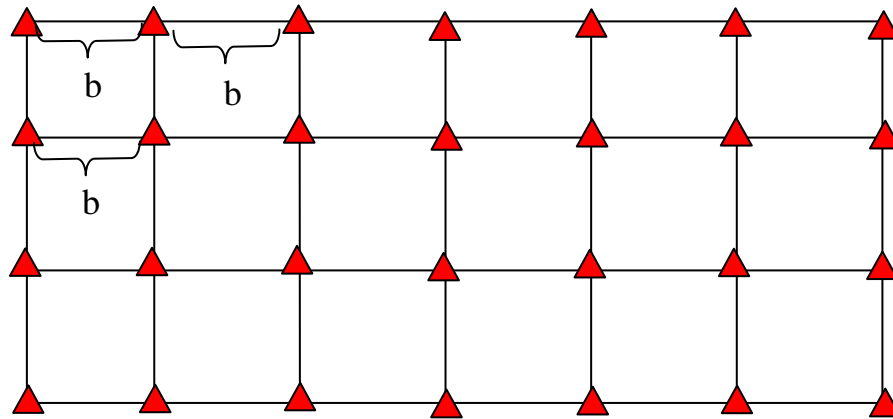
Figure 2.2 Triangulation and flight planning by means of serial method.

2.2.3 Aerial Triangulation Method

It is a triangulation method developed during 1970s which eliminates the drawbacks occurred in pool and serial method and provides establishing fewer points in the field. The basic purpose of the method is to establish minimum number of ground control points and determine the sufficient number of control points present in stereo models by means of photogrammetric techniques to perform absolute orientation to evaluate the models. In this method there must be a triangulation point at the beginning and the end of the strips.

Practically a flight plan containing map sheets to be evaluated, flight directions and available triangulation points is prepared. Within this plan a selection for the triangulation points lie on photograph area and spacing 2B between each other is done at the outer frame of working area. At least 2 points are selected at the beginning and the end of every strip, above and beneath of strip line. These points should fall in the same model. Full control (X, Y, Z) spacing nearly 4B or only a height control point (Z) selections is done above and beneath every strip if they are in the block (Figure 2.3).

In aerial triangulation method natural or artificial points are marked and measured as strip and model tie points and then their 3-D coordinates as well as the 12 exterior orientation parameters for each model (X_o, Y_o, Z_o, $К$, φ, ω) are calculated after an adjustment process by the help of point densification by means of photogrammetric method with a few ground control points established in the field.
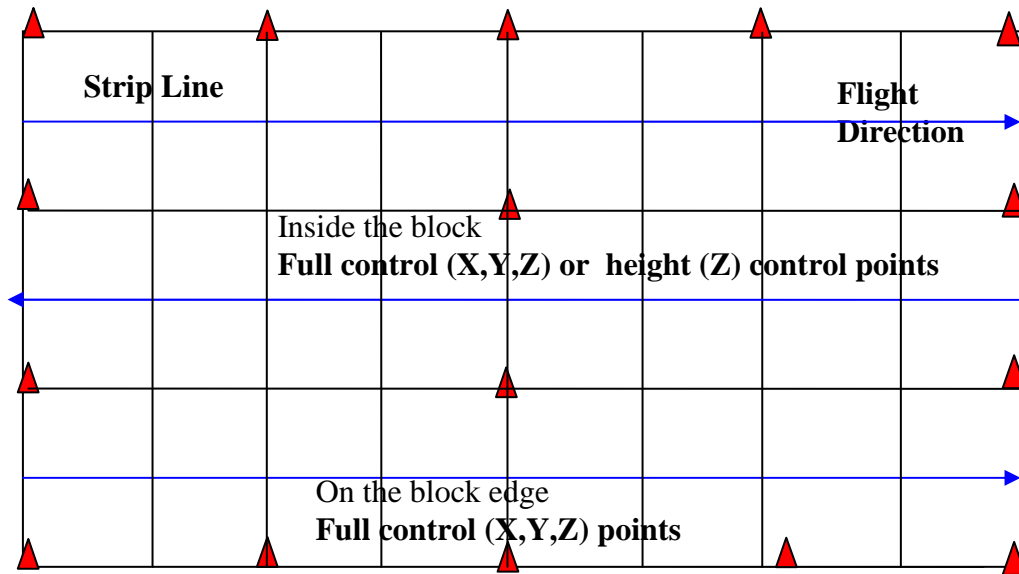
Figure 2.3 Triangulation and flight planning by means of aerial triangulation

2.2.4 Aerial Triangulation Method with Kinematic GPS Support

Aerial triangulation controlled by kinematic GPS observation in the aircraft has been established as a precise method of photogrammetric point determination with a few control points marked on the ground. New developments of kinematic GPS processing yield accurate exposure locations (X_o, Y_o, Z_o) instantaneously. Thus, it leads to reduce 90-95% field survey and production cost and can meet the specification of topographic mapping at small or medium scale (Photogrammetry Lecture Notes, 2002).

Practically depending on the flight plan at least 4 but ideally 8 points around the corners of block area are marked and measured. These points are positioned by geodetic techniques (Figure 2.4) (Photogrammetry Lecture Notes, 2002).
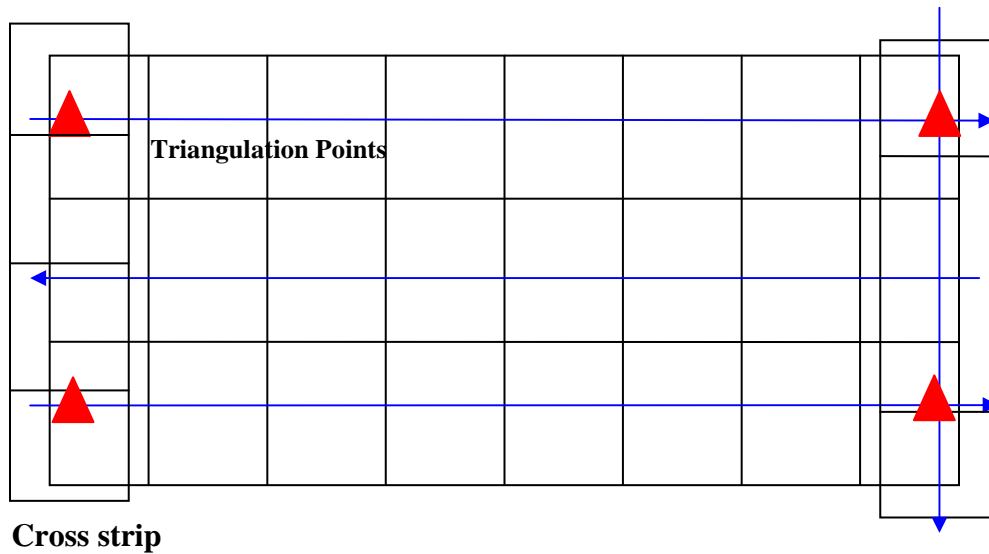
Figure 2.4 Triangulation and flight planning by means of aerial triangulation with kinematic GPS support

2.2.5 GPS/IMU Supported Aerial Triangulation Adjustment

An inertial navigation system is a navigation aid that uses a computer and motion sensors to continuously track the position, orientation, and velocity (direction and speed of movement) of a vehicle without the need for external references. INS includes at least a computer and a platform or module containing accelerometers, gyroscopes, or other motion-sensing devices. The INS is initially provided with its position and velocity from another source (a human operator, a GPS satellite receiver, etc.), and thereafter computes its own updated position and velocity by integrating information received from the motion sensors. An INS can detect a change in its geographic position (a move east or north, for example), a change in its velocity (speed and direction of movement), and a change in its orientation (rotation about an axis). It does this by measuring the linear and angular accelerations applied to the system. [41].

Inertial Measurement Unit (IMU) is the most important component of INS and consists of a gyroscope and an accelerometer. Gyroscopes measure the angular

velocity of the system in the inertial reference frame. By using the original orientation of the system in the inertial reference frame as the initial condition and integrating the angular velocity, the system's current orientation is known at all times. Accelerometers measure the linear acceleration of the system in the inertial reference frame, but in directions that can only be measured relative to the moving system (since the accelerometers are fixed to the system and rotate with the system, but are not aware of their own orientation). However, by tracking both the current angular velocity of the system and the current linear acceleration of the system measured relative to the moving system, it is possible to determine the linear acceleration of the system in the inertial reference frame. Performing integration on the inertial accelerations (using the original velocity as the initial conditions) using the correct kinematic equations yields the inertial velocities of the system, and integration again (using the original position as the initial condition) yields the inertial position.

GPS and INS are used in collaboration to take the advantages of both (Figure 2.5). GPS/INS refers to the use of GPS satellite signals to correct or calibrate a solution from an INS. INS usually can only provide an accurate solution for a short period of time. The INS accelerometers will produce an unknown bias signal that appears as a genuine specific force. This is integrated to produce an error in position. Additionally, the INS software must use an estimate of the angular position of the accelerometers when conducting this integration. Typically, the angular position is tracked through an integration of the angular rate from the gyro sensors. These also produce unknown biases that affect the integration to get the position of the unit. The GPS gives an absolute drift-free position value that can be used to reset the INS solution or may be blended with it by use of a mathematical algorithm such as a Kalman Filter. The angular orientation of the unit may be inferred from the series of position updates from the GPS. The change in the error in position relative to the GPS may be used to estimate the unknown angle error. The benefits of using GPS with an INS are that the INS may be calibrated by the GPS signals and that the INS can provide position and angle updates between the 1 second

GPS updates. Additionally, GPS may lose its signal and the INS can continue to compute the position and angle during the period of lost GPS signal. The two systems are complementary and are often employed together [41].
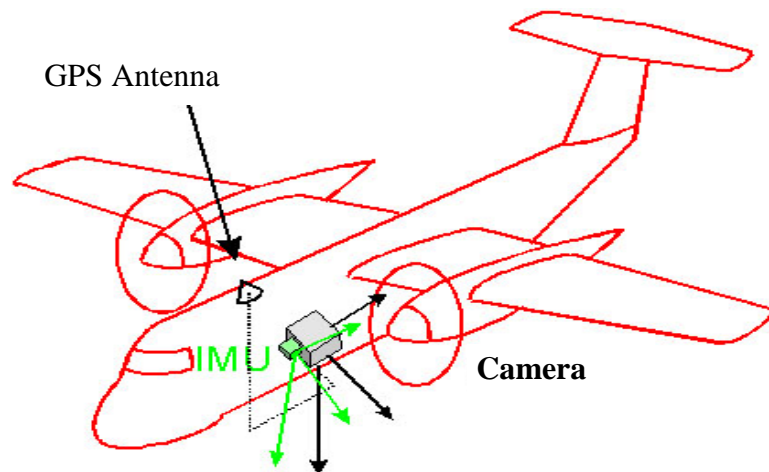
Figure 2.5 GPS/INS system.

In summary, the advent and commercial availability of high-quality integrated GPS/INS and GPS/IMU systems allows for direct georeferencing without use of any ground control data in remote sensing and photogrammetric mapping applications at least theoretically.

2.3   GLOBAL POSITIONING SYSTEM (GPS)

The global positioning system is a satellite-based navigation system consisting of a network of 24 Medium Earth Orbit satellites (32 by March 2008) that are eleven thousand nautical miles in space and in six different orbital paths. The satellites precise microwave signals that enable GPS receivers to determine their location, speed, direction, and time.

A GPS receiver calculates its position by carefully timing the signals sent by the constellation of GPS satellites high above the Earth. Each satellite continually transmits messages containing the time the message was sent, a precise orbit for the satellite sending the message (the ephemeris), and the general system health and rough orbits of all GPS satellites (the almanac). These signals travel at the speed of light through outer space, and slightly slower through the atmosphere. The receiver uses the arrival time of each message to measure the distance to each satellite, from which it determines the position of the receiver using geometry and trigonometry. The resulting coordinates are converted to more user-friendly forms such as latitude and longitude, or location on a map, and then displayed to the user.

It might seem that three satellites would be enough to solve for a position, since space has three dimensions. However, a three satellite solution requires the time be known to a nanosecond or so, far better than any non-laboratory clock can provide. Using four or more satellites allows the receiver to solve for time as well as geographical position, eliminating the need for a super accurate clock. In other words, the receiver uses four measurements to solve for four variables: x, y, z, and t.

While many GPS applications have no particular use for the computed time, it is used in some GPS applications such as time transfer.

Although four satellites are required for normal operation, fewer may be needed in some special cases. If one variable is already known (for example, a sea-going ship knows its altitude is 0), a receiver can determine its position using only three satellites. Also, in practice, receivers use additional clues (doppler shift of satellite signals, last known position, dead reckoning, inertial navigation, and so on) to give degraded answers when fewer than four satellites are visible.

2.3.1   Types of Positioning

GPS can be used for either point positioning or relative (differential) positioning. A simple mathematical resection computation is used to determine a point's position. GPS receivers use other constants (Keplerian elements) broadcast by the satellite in its ephemeris to compute X, Y, Z coordinates of each satellite for each instant (epoch) observations are made. When the distances to four or more satellites are measured, the X, Y, Z, coordinates of the point occupied can be computed by resection formulas. Four instead of three satellites are needed due to the fact that the true range or distance to each satellite is not measured by GPS. The distance measured is called a pseudo or quasi-range because it consists of true range plus or minus a constant bias error due to the clock error of the receiver. If the receiver were connected to an atomic clock that was set to the proper GPS time, the true range to each satellite could be measured. Thus in point positioning four equations (distances to satellites) in four unknowns (X, Y, Z and clock error) exists and therefore provides a unique solution. When more than four satellites are observed an over-determined solution can be handled, using a least squares solution which also provides estimates of the position. Relative positioning requires two or more GPS receivers and is commonly used in aerial photography to navigate and position the aircraft more precisely. By using at least two receivers it is aimed to eliminate orbital and clock errors [30].

2.3.2 Positioning Errors

There are a number of electronic system errors that can occur using GPS; however, most of the equipment sold today has resolved these system errors so that they can be considered negligible. Three major sources of errors, orbital, ionospheric and multipath can be mitigated using both software and hardware techniques.

2.3.2.1 Orbital Errors

The broadcast ephemeris is normally accurate to one part per million (1 ppm) or about 20 m and is often accurate 1 meter. A 20-meter orbital can result in a 10 cm error in position for a 100 km line when relative positioning techniques are used. The precise ephemeris is accurate within 5 to 20 cm depending upon when it has been computed, so the errors introduced by the precise ephemeris are negligible for most surveys [30].

2.3.2.2 Atmospheric Errors

Another source of inaccuracy is the reduced speed of propagation in the troposphere and ionosphere. While radio signals travel with the velocity of light in the outer space, their propagation in the ionosphere and troposphere is slower.

In the ionosphere in a height of 80 – 400 km a large number of electrons and positive charged ions are formed by the ionizing force of the sun. The electrons and ions are concentrated in four conductive layers in the ionosphere These layers refract the electromagnetic waves from the satellites, resulting in an elongated runtime of the signals. These errors are mostly corrected by the receiver by calculations [27].

2.3.2.3 Multipath Errors

The multipath effect is caused by reflection of satellite signals (radio waves) on objects. It was the same effect that caused ghost images on television when antennae on the roof were still more common instead of todays satellite dishes.

For GPS signals this effect mainly appears in the neighbourhood of large buildings or other elevations. The reflected signal takes more time to reach the receiver than the direct signal. The resulting error typically lies in the range of a few meters [27].

2.3.3 Airborne GPS (AGPS) Control

Airborne GPS is a method, which drastically reduces the number of ground control points necessary on larger projects. When performing airborne GPS projects, a geodetic quality GPS system is installed in the airplane. The GPS receiver records an event marker from the camera, logging the precise time of each exposure station or photo center. This time record is then correlated to the location of GPS ground stations (at known, surveyed locations), which were recording during the flight. It has been completed several Airborne GPS projects where minimal ground control is supplemented by precisely locating the camera's projection center in three dimensions.

Today many ABGPS project is able to collect the GPS data (L1/ L2 code and carries phase) every second. For the best accuracy, data should be collected more frequently. The photo-center positions are determined by interpolating between the adjacent GPS determined positions. At low altitudes the aircraft may not be suitably stable and one second position samples may introduce unacceptable errors. The need for one-half second data can be checked by flying a mission using the one-half second data to compute photo-positions, and then thinning the data to one second and re-computing the photo-centers. A comparison of the two sets of positions will show whether the more frequent data are needed [30].

2.3.4 Base Stations

The optimum location for an ABGPS base station is in a grassy area at an airport near the center of the project area. The grass will not reflect the satellite signal as much as paved areas and thus reduce the possibility of multipath errors. Furthermore, airports are excellent sites since there are few obstructions to block the satellites signals. Additionally, the aircraft, GPS receiver will be able to quickly initialize (fix integer ambiguities) in a few minutes when the base station is located close to the aircraft. A base station can usually be left unattended at an airport, saving the cost of an operator [30].

2.3.5 Processing GPS Data

2.3.5.1 Point Positioning

Point positioning is normally performed in the GPS receiver in near real-time. Point position errors include the ephemeris error, ionosphere error, pseudo-range error, and any multipath errors that may be present. Some post-processing software recomputes the point positions using the precise ephemeris. These positions should be considerably more accurate than the ones computed using the broadcast ephemeris; however, they still are not as accurate as relative point positions [30].

2.3.5.2 Differential Code Phase positioning

Differential Global Positioning System (DGPS) is an enhancement to Global Positioning System that uses a network of fixed, ground-based reference stations to broadcast the difference between the positions indicated by the satellite systems and the known fixed positions. These stations broadcast the difference between the measured satellite pseudoranges and actual (internally computed) pseudoranges, and receiver stations may correct their pseudoranges by the same amount. When a positioning service is used, corrections received from a communications satellite or ground radio station are applied to the measured (code-phase) pseudo ranges to obtain satellite ranges from which many of the systematic errors have been eliminated. These more accurate pseudo ranges are then used in a classical resection computation to compute coordinates of the point [30].

2.3.5.3 Carrier Phase Differential Positioning (CPDP)

Most ABGPS uses the L1 (19cm), L2 (24 cm), and L1-L2 (86 cm) carrier phase data to compute the base vector length between a base station and a rover receiver. Since the coordinates of the base station are known (or can be accurately determined) the vector between the base and rover permits the computation of the

19

accurate coordinates of the rover. In the case of photo-control operations the rover may remain stationary for several minutes (static survey), while the rover is constantly moving in the case of ABGPS [30].

The vector computation using carrier phase is much the same as the differential pseudo-range computation. In pseudo range computation, the distances between the GPS receivers and the satellites are unambiguously (if not precisely) known. The vector between the GPS stations results from the projection of the eight (or more) pseudo-ranges measured at the one known and one unknown point. The pseudo-range measurement error varies form 0.5 to 3 meters depending upon the receiver used.

The carrier phase observation also measures the range to the satellite; however this range is ambiguous since it consists of an unknown integer number of 19 cm cycles plus a precisely known (measured) fractional cycle. In other words, the carrier phase satellite range would be determined to millimeter accuracy if the integer number of whole cycles were known. GPS processing software, in effect, determines this number integer cycles so that the satellite range data (actually difference in range) is determined to millimeter accuracy.

This determination of the precise difference in satellite ranges is performed in a multi step computation [30]:

1. The (unambiguous) pseudo-ranges are differed to provide a preliminary solution of the vector to meter accuracy.

2. The L1 and L2 carrier phases are linearly combined to produce an 86 cm wide-lane phase. These wide-lane observables are double differenced (between sites and again between one satellite and the remaining satellites) for each epoch. Since the relative position of the unknown point has been determined to meter accuracy in step one, a search cube is set upcentered on the preliminary position to search for the correct ambiguity (difference in range integers). For example, if data from five satellites are observed, four integer ambiguities are formed (since one satellite

is reference). The various sets of ambiguities are then statistically tested to arrive at the set of integer ambiguities which give the correct vector. This computation yields the answer correct to a centimeter.

3. When the wide-lane ambiguity has been determined, the L1 ambiguity can be quickly determined and the final answer computed to a few millimeter accuracy. For long lines with noisy data it may be impossible to determine the integer ambiguities so that only a float solution can be computed.

4. As described above, the double differences are formed by subtracting the L1 carrier phases between sites (rover, base) and between the highest satellite and the remaining satellites to form both the integer ambiguities and the normal four unknowns (difference latitude, longitude, height and clock error). This yields seven unknowns for four satellites. Since four knowns are observed every epoch, it would be theoretically possible to solve the vector in two epochs; however the set of equations is ill conditioned and a solution is not possible with so little data. When a sufficient data set has been observed (usually 15 to 20 minutes for an L1 receiver), a three integer ambiguities as real numbers (e.g, ambiguity 1234 would be served as 1234.0876) so that all seven unknowns are solved for. If there is a sufficient amount of data, the float ambiguities are very close to integers and the numbers can be rounded off to produce the correct answers. These estimated (rounded off) ambiguities are used to complete the computation.

5. The final solution is computed by treating the estimated ambiguities computed in the float solutions as known and solving the set of equations for the normal four unknowns. The set of equations is then re-solved, increasing or decreasing each ambiguity by one cycle in turn. Each time the computation is made, the standard error of the solution is determined. The correct set of ambiguities is the set that has the smallest standard error, and the solution is considered correct when the ratio of the standard error of the best solution to that of the next best solution is two to three times. In this case the solution of the vector is said to be a fixed solution and the vector determined to centimeter accuracy [30].

2.4   INERTIAL NAVIGATION SYSTEMS

An inertial Navigation System (INS) has two main components. The first is the inertial measurement unit (IMU), which comprises three accelerometers, three gyros and electronics to provide digitally encoded samples of the accelerometer and gyro data on a serial interface. The accelerometers are arranged as an orthogonal triad and measure the specific force vector that is the vector sum of the local gravity vector and the acceleration vector experienced by the IMU [30]. The gyros are also arranged into an orthogonal triad that measures the angular rate vector. The angular rate vector is the sum of the Earth rotation vector plus the angular rate vector experienced by the IMU with respect to the earth.

The second component is the navigation processor (NP). It solves Newton's equations of motion of the IMU on the rotating Earth based on the measured accelerations and angular rates. In order to do so, the NP must establish the local North, East and Down directions of the navigation coordinate frame (Figure 2.6) using a procedure called alignment. Determining the down direction is called leveling, and is based on the assumption that the local gravity vector is the vertical reference. Once leveling is completed, the horizontal axes of the navigation frame define a plane that is tangent to the local geoidal surface, and hence is said to be locally level. Aligning a locally level navigation frame to the true North direction is called heading alignment. A mechanism called gyro compassing uses the horizontal component of the Earth angular rate vector as heading reference. A stationary or otherwise non-accelerating INS uses the Earth rate vector measured by the gyros to gyrocompass its navigation frame to true North. A typical aircraft INS must undergo a stationary alignment lasting 10 to 30 minutes to accurately align its navigation frame. Thereafter it navigates free-inertially, which implies that it computes its navigation solution using only the acceleration and angular rate data from the IMU without any subsequent corrections to its alignment or position solution [30].
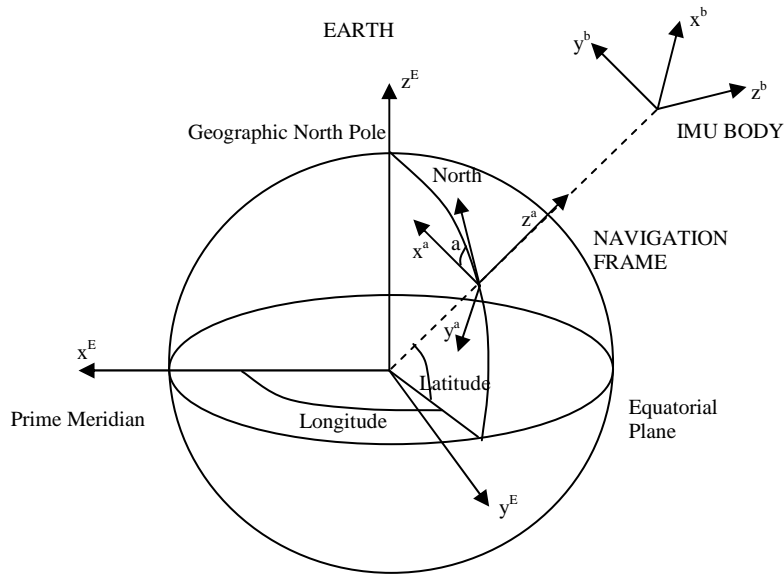
Figure 2.6   Frames of references used in inertial navigation [30, p.705].

2.4.1   GPS-Aided Inertial Navigation System

An aided INS (AINS) (Figure 2.7) combines the components of an INS with navigation-aiding sensors for the purpose of regulating the INS errors to those of the aiding sensors during vehicle navigation. The typical AINS uses Kalman Filter to estimate the errors in the inertial navigation solution and the inertial sensor errors. The Kalman filter uses measurements of the current inertial navigation solution differenced with aiding sensor navigation data to observe and estimate the INS errors. This is possible only when the aiding sensor error characteristics are different from the INS errors. A GPS position solution contains errors that can be characterized as noisy and statistically bounded within an error ellipse of fixed volume. By contrast, the INS position errors are characterized as smooth but unbounded. These error characteristics are complementary, and hence amenable to Kalman filter error estimation. The Kalman filter processes measurements that are the differences of the inertial navigator and GPS positions, and thus comprises the noisy but bounded GPS position errors plus the growing INS position error. The Kalman filter contains a model for these errors, and thereby is able to suppress the

23

GPS short-term errors and estimate the INS errors. The accuracy of the INS error estimates depends on the magnitude of the GPS position error. When the GPS solution is a kinematic ambiguity resolution solution, a better estimate error is obtained with decimeter accuracy than an uncorrected CA solution.

The AINS uses the Kalman filter's estimated inertial navigation errors to correct the position, velocity and attitude computations in the inertial navigation algorithm. This error correction closes the loop around the INS and thereby regulates the INS errors to be consistent with the aiding sensor errors. In a GPS-AINS, it regulates the INS position and velocity errors to be consistent with smoothed GPS position and velocity errors. It furthermore regulates the INS attitude errors and thereby continuously improves the INS alignment. Thus a GPS-AINS is able to align from a cold initialization while the vehicle is moving. This is called a mobile alignment, or in the case of an airborne AINS, an air start [30].

2.5   Direct Georeferencing

Direct Georeferencing (DG) is the direct determination of the position and orientation parameters of a sensor. It is an enabling technology for quantitive data acquisition and mapping applications where precise orientation and the position of the sensor are required [30]. A direct georeferencing system provides the position and orientation of the sensor required to register the acquired data in geographic coordinates. In photogrammetry, direct georeferencing is used to produce measurements of the exterior orientation parameters for each photograph without the use of ground control points or aerial triangulation.

If the IMU attitude vector $[\omega \; \varphi \; \kappa]^t$ and the GPS antenna position vector $[X \; Y \; Z]^t$ are measured with sufficient accuracy for the application at hand, there is no need to perform triangulation on the block of images involved. This can result significant savings in time and money. The boresight angles $[\omega_B \; \varphi_B \; \kappa_B]^t$ and antenna offsets $[\Delta X \; \Delta Y \; \Delta Z]^t$ still have to be accurately known and correctly

applied to the attitude and antenna vectors. The rotation angles also have to be properly exploited.

The attitude and position data are sometimes available with the boresight and offset corrections are applied, making the implementation of this method straightforward. In this method, the corrections for drift and shift for both IMU attitude angles and GPS position are assumed to be zero ($[\Delta\omega_0 \ \Delta\varphi_0 \ \Delta\kappa_0]^t$, $[\Delta\omega_1 \ \Delta\varphi_1 \ \Delta\kappa_1]^t$, $[\Delta X_0 \ \Delta_0 Y_0 \ \Delta Z_0]^t$, $[\Delta X_1 \ \Delta Y_1 \ \Delta Z_1]^t$) making the time variable irrelevant [30].

2.5.1 Coordinate Frame Definitions

Geographic coordinate frame (g): This frame is local level frame tangent to the reference ellipsoid. Its X-axis points North, Y-axis East, Z-axis Down, it is also called as NED frame.

IMU body coordinate frame (b): IMU sensor axes are the axes of this orthogonal frame. The orientation of this frame is fixed with respect to the camera body frame (c). The DG system provides the roll, pitch and heading (φ,ω,κ) of the body frame (b) with respect to the local Geographic or NED frame (g) [30].

Camera body coordinate frame (c): This frame is a right handed orthogonal coordinate frame. Its origin is the perspective center of the camera lens, direction of flight is X-axis, Y-axis pointing to the right of the camera, and Z-axis down. The IMU body frame is misaligned with boresight angles with respect to this frame.

Mapping coordinate frame (m): This is any local coordinate mapping frame, such as the UTM.

Image coordinate frame (i): It is fixed to the image and orthogonal right handed coordinate frame. Its origin is at the perspective center of the camera lens, direction of the flight is X-axis, Y-axis pointing toward the left of the image, and Z-axis up.

Pixel coordinate frame (p): This frame is defined by the rows and columns of pixels that make up the image, either from a scanned photograph or CCD.

Earth frame (ECEF): The Earth frame is fixed to the reference ellipsoid and is also referred to as Earth Centered Earth Fixed (ECEF). Its origin is at the center of the ellipsoid, with its X-axis pointing through the intersection of the equator and the Greenwich meridian, its Y-axis toward the equator and the +90 deg meridian, and Z-axis through the geographic North Pole [30].
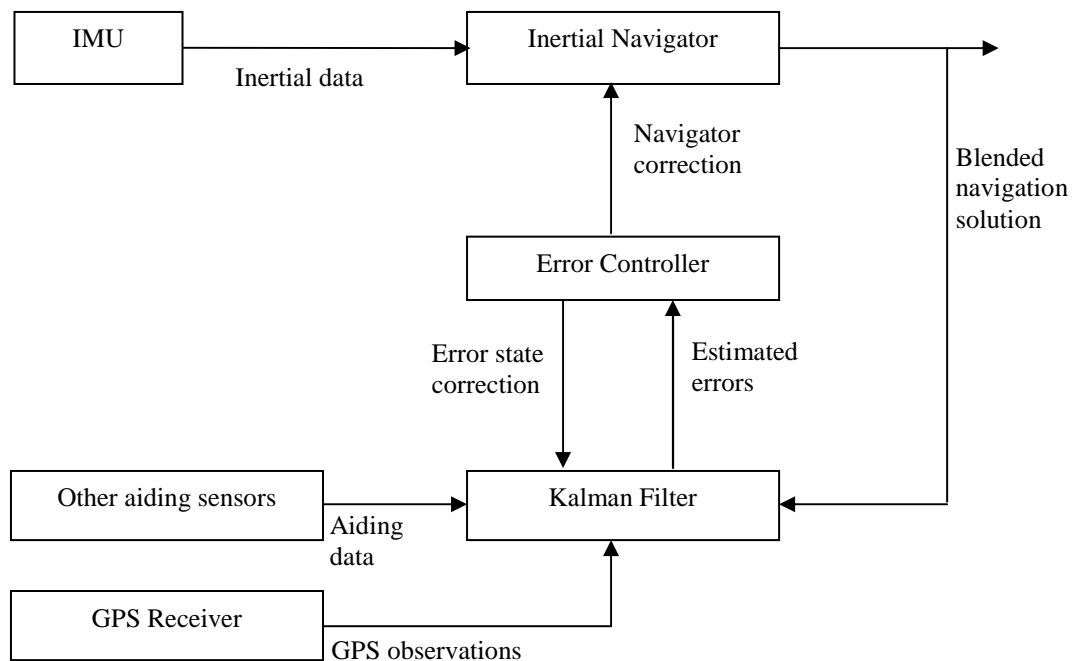
Figure 2.7 GPS aided INS architecture [30, p.711]

2.5.2   Mapping with Direct Georeferencing

2.5.2.1 Computation of 2 dimensional image vector

The first step is to compute the vector from the principle point (PP) to the point g (R_{PP-g}), corrected for the radial distortion of the lens.

Figure 2.8 shows the two dimensional image vector from the principal point (PP) to the point g measured in the image coordinate frame. Its origin is at the center of the image (O). The vector is computed as follows:

$$(\vec{R}_{PP\text{-}g}) = \begin{bmatrix} x_g - x_{PP} - dx_r \\ \\ y_g - y_{PP} - dy_r \end{bmatrix} \tag{2.1}$$

where:

x_g, y_g coordinates of point g in the image frame,

x_{PP}, y_{PP} coordinates of the principal point in the image frame,

dx_r, dx_r radial distortions correction terms.

2.5.2.2 Compute 3D image vector in IMU body frame.

In order to perform this step first three dimensional image vector to point g is constructed, using the two dimensional image vector and the focal length of the camera, and resolve it in the IMU body frame (b). Once the vector is resolved in the IMU body frame, the vector is transformed to the local NED frame (g) using roll, pitch and heading from the GPS/INS.

As shown in Figure 2.9, the three dimensional image vector $\vec{R}^i_{E\text{-}g}$ is from the camera perspective center E to point g. It is computed from the two dimensional image vector, $\vec{R}^p_{PP\text{-}g}$ resolved in the pixel frame, and the focal length f as follows:

$$\vec{R}^i_{E\text{-}g} = \begin{bmatrix} 0 & -1 & 0 \\ -1 & 0 & 0 \\ 0 & 0 & 1 \end{bmatrix} \begin{pmatrix} \vec{R}^p_{PP\text{-}g} \end{pmatrix} = \begin{bmatrix} -(y_g - y_{PP} - dy_r) \\ -(x_g - x_{PP} - dx_r) \\ -f \end{bmatrix} \tag{2.2}$$
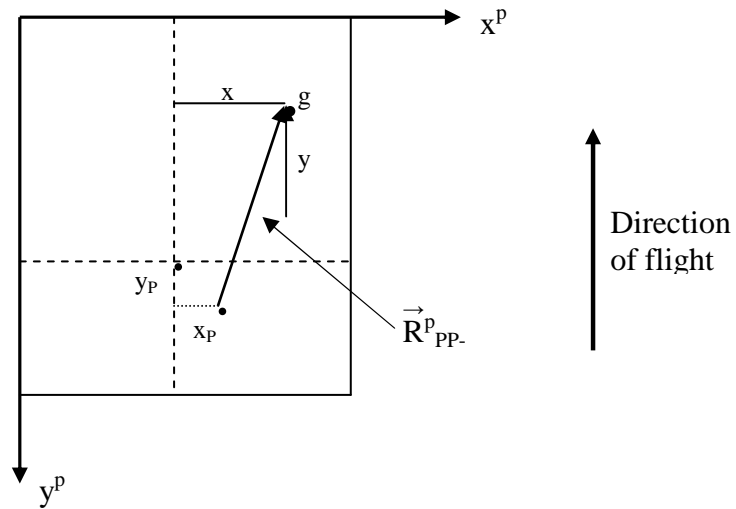
Figure 2.8: Two dimensional image vector [3, p.712].

The IMU body frame (b) is defined as x forward, y right, z down. It is misaligned from the image frame (i) by the so called boresight angles, which are physical mounting angles between the IMU and camera. The boresight angles are determined via a calibration flight, with traditional photogrammetric techniques used to work backwards to solve for the boresight angles [30].
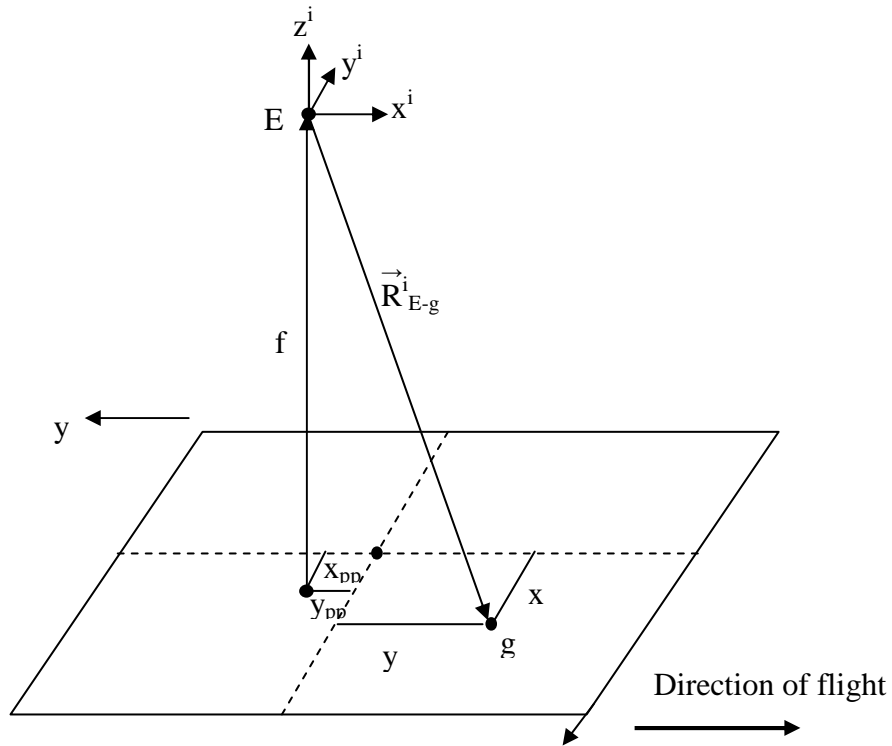
Figure 2.9 Three dimensional image vector [30, p.712].

The simplest way of relating the boresight angles to the image frame is to first define an arbitrary camera frame (c) that is collinear with the image frame (i), but has x forward, y right, and z down. The boresight angles are then computed as the angular offsets of the IMU body frame (b) with respect to this frame. The relationship among the three frames is given in figure 2.10.
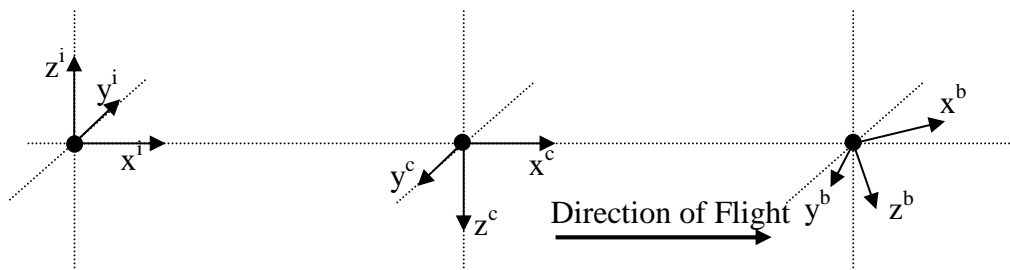
Figure 2.10 Relationship among different frames in space [30, p.713].

29

The image vector from the camera perspective center E to point g resolved in the IMU body frame (b) is described as follows:

where:

$$\vec{R}^b_{E\text{-}g} = C^b_c \, C^c_i \, \vec{R}^i_{E\text{-}g} \tag{2.3}$$

$$C^c_i = \begin{pmatrix} 1 & 0 & 0 \\ 0 & -1 & 0 \\ 0 & 0 & -1 \end{pmatrix} \tag{2.4}$$

and

$$C^b_c = \begin{pmatrix} 1 & 0 & 0 \\ 0 & \cos\theta_x & \sin\theta_x \\ 0 & -\sin\theta_x & \cos\theta_x \end{pmatrix} \begin{pmatrix} \cos\theta_y & 0 & -\sin\theta_y \\ 0 & 1 & 0 \\ \sin\theta_y & 0 & \cos\theta_y \end{pmatrix} \begin{pmatrix} \cos\theta_z & \sin\theta_z & 0 \\ -\sin\theta_z & \cos\theta_z & 0 \\ 0 & 0 & 1 \end{pmatrix} \tag{2.5}$$

The boresight angles are constant as long as IMU remains rigidly mounted to the camera. These are determined once for a given installation by performing a calibration flight over known ground control. The boresight angles are defined as to bring the camera frame into alignment with the body frame. The sequence of rotations is described as follows [30].

    a. Clockwise rotation about the camera frame Z axis by the angle θ_z.

    b. Clockwise rotation about the once rotated Y axis by the angle θ_y.

    c. Clockwise rotation about the twice rotated X axis by the angle θ_x.

2.5.2.3 Resolve Image Vector in Local NED Geographic Frame

The next step is to transform image vector which is in the IMU body frame into the local NED Geographic frame (g) using the roll, pitch and heading at the time of exposure measured by the GPS/INS:

$$\vec{R}^g_{E\text{-}g} = \begin{pmatrix} x^g_{E\text{-}g} \\ y^g_{E\text{-}g} \\ z^g_{E\text{-}g} \end{pmatrix} = C^g_b \, \vec{R}^b_{E\text{-}g} \tag{2.6}$$

Where:

Φ, θ, Ψ are the roll pitch and heading (yaw) angles,

The roll, pitch and heading angles are defined by the sequence of rotations that bring the NED Geographic frame into alignment with the IMU body frame, and are described as follows [3]:

    a. Clockwise rotation about the down axis by the heading Ψ

    b. Clockwise rotation about the once rotated East axis by the pitch angle θ

    c. Clockwise rotation about the twice rotated North axis by the roll angle Φ

This can be expressed as the following rotation matrix:

$$C^b_g = \begin{pmatrix} 1 & 0 & 0 \\ 0 & \cos\Phi & \sin\Phi \\ 0 & -\sin\Phi & \cos\Phi \end{pmatrix} \begin{pmatrix} \cos\theta_y & 0 & -\sin\theta_y \\ 0 & 1 & 0 \\ \sin\theta_y & 0 & \cos\theta_y \end{pmatrix} \begin{pmatrix} \cos\Psi & \sin\Psi & 0 \\ -\sin\Psi & \cos\Psi & 0 \\ 0 & 0 & 1 \end{pmatrix} \tag{2.7}$$

from which:

$$C_b^g = C_g^{bT} = \begin{pmatrix} \cos\Psi & -\sin\Psi & 0 \\ \sin\Psi & \cos\Psi & 0 \\ 0 & 0 & 1 \end{pmatrix} \begin{pmatrix} \cos\theta & 0 & \sin\theta \\ 0 & 1 & 0 \\ -\sin\theta & 0 & \cos\theta \end{pmatrix} \begin{pmatrix} 1 & 0 & 0 \\ 0 & \cos\Phi & -\sin\Phi \\ 0 & \sin\Phi & \cos\Phi \end{pmatrix} \quad (2.8)$$

GPS/INS provides the roll, pitch and heading angles are directly available from the at the camera exposure times directly.

2.5.2.4 Project the Image Vector to the Ground

If the Image vector is in the local NED Geographic frame, it can than be projected to the ground. The vector $\vec{R}^g_{E\text{-}G}$ from the camera perspective center **E** to the point **G** on the ground (Figure 2.11), is computed from the image vector $\vec{R}^g_{E\text{-}g}$ as follows:

$$\vec{R}^g_{E\text{-}G} = \begin{pmatrix} X^g_{E\text{-}G} \\ Y^g_{E\text{-}G} \\ Z^g_{E\text{-}G} \end{pmatrix} = \vec{R}^g_{E\text{-}g} \; \frac{H}{z^g_{E\text{-}g}} \quad (2.9)$$

Where:

$$H = H^e - h_s - h_d \quad (2.10)$$

H^e height above ellipsoid from GPS/INS

h_s geoidal seperation

h_d orthometric height from DEM

$z^g_{E\text{-}g}$ vertical component of image vector in the NED geographic frame
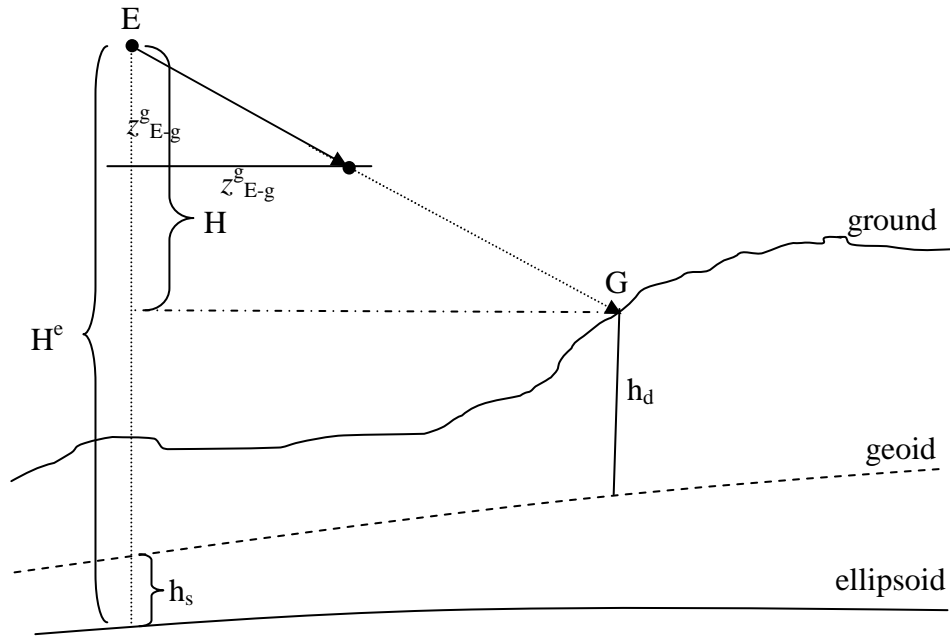
Figure 2.11: NED goegraphic frame to ground [30, p.715].

with this vector ground coordinates for point G can be computed.

2.5.2.5 Computation of ECEF Coordinates

Using equations 2.1 through 2.10, compute:

$$\vec{R}^i_{E\text{-}g} = \begin{bmatrix} -(y_g - y_{PP} - dy_r) \\ -(x_g - x_{PP} - dx_r) \\ -f \end{bmatrix}^i \tag{2.11}$$

$$\vec{R}^g_{E\text{-}g} = \begin{bmatrix} x^g_{E\text{-}g} \\ y^g_{E\text{-}g} \\ z^g_{E\text{-}g} \end{bmatrix} = C^g_b C^b_c C^c_i \; \vec{R}^b_{E\text{-}g} \tag{2.12}$$

$$\vec{R}^g_{E\text{-}G} = \begin{bmatrix} X^g_{E\text{-}G} \\ Y^g_{E\text{-}G} \\ Z^g_{E\text{-}G} \end{bmatrix} = \vec{R}^g_{E\text{-}g} \; \frac{H}{z^g_{E\text{-}g}} \tag{2.13}$$

Then resolve vector $\vec{R}^g_{E\text{-}g}$ in the earth frame (ECEF) and add to the coordinates of the perspective center **E** computed by the GPS/INS [30]:

$$\begin{bmatrix} X_G \\ Y_G \\ Z_G \end{bmatrix} = \begin{bmatrix} X_E \\ Y_E \\ Z_E \end{bmatrix} + C^{ECEF}_g \begin{bmatrix} X_{E\text{-}G} \\ Y_{E\text{-}G} \\ Z_{E\text{-}G} \end{bmatrix} \tag{2.14}$$

$$C^{ECEF}_g = \begin{bmatrix} -\sin\lambda\cos l & -\sin l & -\cos\lambda\cos l \\ \sin\lambda\sin l & \cos l & -\cos\lambda\sin l \\ \cos\lambda & 0 & -\sin\lambda \end{bmatrix} \tag{2.15}$$

λ latitude of camera perspective center E computed by the DG system,

l longitude of camera perspective center E computed by the DG system,

Once the ground coordinates are computed in the ECEF frame they can be transformed into any mapping projection, datum or Local Rectangular (LSR) frame [30].

The local mapping frame projection (m) can be computed by generating the position of the camera perspective center in the mapping frame, and the rotations of the Image frame (i) with respect to the local mapping frame (φ, ω, κ):

$$\vec{R}^i_{E\text{-}g} = \begin{bmatrix} -(y_g - y_{PP} - dy_r) \\ -(x_g - x_{PP} - dx_r) \\ -f \end{bmatrix}^i \tag{2.16}$$

34

Then resolve the image vector into the local mapping frame (m) via:

$$\vec{R}^g_{E\text{-}g} = \begin{pmatrix} x^g_{E\text{-}g} \\ y^g_{E\text{-}g} \\ z^g_{E\text{-}g} \end{pmatrix} = C^m_i \ \vec{R}^b_{E\text{-}g} \ + \ \begin{pmatrix} x^m_0 \\ y^m_0 \\ z^m_0 \end{pmatrix} \tag{2.17}$$

Where:

$$C^m_i = C^m_E \ C^E_g(\lambda, l) C^g_b(\Phi, \theta, \Psi) C^b_c(\theta_x, \theta_y, \theta_z) C^c_i \tag{2.18}$$

$$C^g_b = \begin{pmatrix} \cos\kappa & -\sin\kappa & 0 \\ \sin\kappa & \cos\kappa & 0 \\ 0 & 0 & 1 \end{pmatrix} \begin{pmatrix} \cos\omega & 0 & \sin\omega \\ 0 & 1 & 0 \\ -\sin\omega & 0 & \cos\omega \end{pmatrix} \begin{pmatrix} 1 & 0 & 0 \\ 0 & \cos\varphi & -\sin\varphi \\ 0 & \sin\varphi & \cos\varphi \end{pmatrix} \tag{2.19}$$

$$= \begin{pmatrix} \cos\omega\cos\kappa & \sin\varphi\sin\omega\cos\kappa\text{-}\cos\varphi\sin\kappa\text{-}\cos\varphi\sin\omega\cos\kappa & \sin\varphi\sin\kappa \\ \cos\omega\sin\kappa & \sin\varphi\sin\omega\sin\kappa\text{+}\cos\varphi\cos\kappa & \cos\varphi\sin\omega\sin\kappa\text{-}\sin\varphi\cos\kappa \\ -\sin\omega & \sin\varphi\cos\omega & \cos\varphi\cos\omega \end{pmatrix}$$

Equation 2.18 can be used to solve directly for the traditional exterior angles ω, φ, κ which can then be input directly to orient a photogrammetric plotter or to use in an aerial triangulation package. The transformation matrices C^E_g, C^b_c, C^c_i, C^g_b are directly available from the GPS/INS data, whereas the transformation C^m_E matrix is dependent upon local mapping frame [30].

If DEM is available, it not necessary to set up a stereo pair. Using equation 2.13 the image vector is directly projected down to the mapping frame using:

35

$$\vec{R}^m_{\text{E-G}} = \begin{pmatrix} X_{\text{E-G}} \\ Y_{\text{E-G}} \\ Z_{\text{E-G}} \end{pmatrix}^m = \vec{R}^g_{\text{E-g}} \; \frac{Z^m_{\text{E}} - h_d}{z^g_{\text{E-g}}} \tag{2.20}$$

From which the mapping frame coordinates of point **G** are computed as:

$$\begin{pmatrix} X_{\text{G}} \\ Y_{\text{G}} \\ Z_{\text{G}} \end{pmatrix}^m = \begin{pmatrix} X_{\text{E}} \\ Y_{\text{E}} \\ Z_{\text{E}} \end{pmatrix}^m + \begin{pmatrix} X_{\text{E-G}} \\ Y_{\text{E-G}} \\ Z_{\text{E-G}} \end{pmatrix}^m \tag{2.21}$$

2.6   Boresight Calibration

The distance between camera and IMU is measured physically when IMU mounted. It is hoped that the axes of IMU would be parallel with respect to the camera but this is not possible and cannot be measured. Hence the angles between camera and IMU have to be computed.

The boresight angles between the IMU and camera image plane are computed in an aerial triangulation of a block flown are a well-controlled test field. A minimum of four opposing strips is usually flown, with 60 percent overlap and 20 percent sidelap (Figure 2.12). Photo scale is typically between 1:5000 and 1:8000. Even number strips are used, each with at least five to eight photographs. Ground control points are signalized and distributed around the perimeter of the test field [30].

The block is then triangulated in a least squares bundle adjustment using the ground control and the GPS derived photo centers. The boresight angles are computed by constructing the mean differences of the orientation angles from the bundle adjustment with the angles from DG system, or are solved for directly in the bundle adjustment.
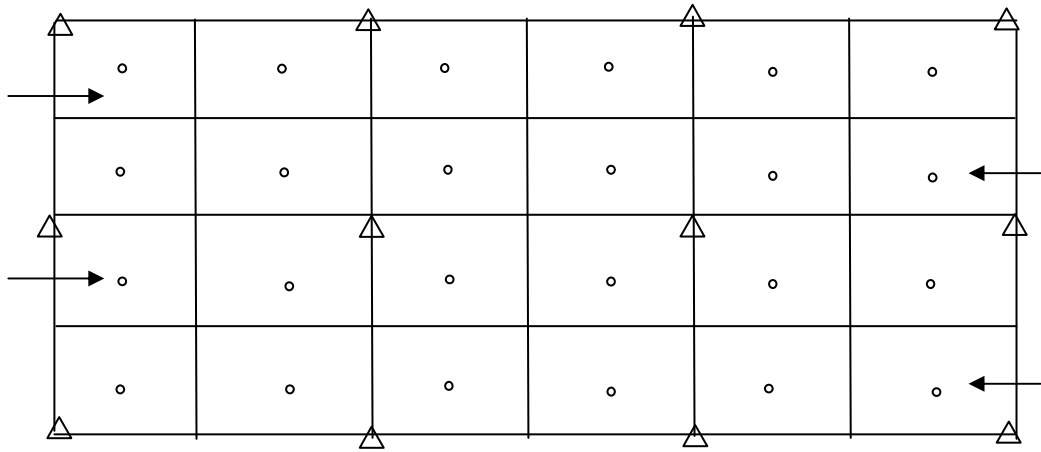
Figure 2.12 Boresight calibration flight design [30, p 720].

CHAPTER 3

ORTHORECTIFICATION

3.1 Common Rectification Methods

In this subchapter some of the widespread rectification methods will be presented.

3.1.1 Helmert Transformation

There are four parameters in 2-D Helmert transformation; the scale, shift and rotation. The rotation is orthogonal beacuse two axes are rotated by same amount so the rotation is orthogonal [3].The formula of Helmert transformation can be given as;

$$\begin{aligned} x &= au + bv + c \\ y &= -bu + av + d \end{aligned} \tag{3.1}$$

where a and b are the rotation parameters, c and d are translation parameters, u and v are the image coordinates. Scale is the norm of a and b. At least two GCPs are needed to solve the parameters. The effect of tilt and curvature of the earth can not be eliminated successfully by Helmert transformation [3].

3.1.2 Affine Transformation

An affine transformation is any transformation that preserves collinearity (i.e., all points lying on a line initially still lie on a line after transformation) and ratios of distances (e.g., the midpoint of a line segment remains the midpoint after transformation). In Affine Transformation rotation is not orthogonal but parallel lines remains parallel after the rotation [3]. The mathematical formula of the transformation can be written as;

$$X = au + bv + c$$
$$Y = du + ev + f \tag{3.2}$$

In Equation 3.2 a and b are the both rotation and scaling, c is the translation parameters of the x axis, similarly d and e are the rotation and scaling parameters and f is the translation parameter for the y axis. X and Y are the ground coordinates of the corresponding pixel with respect to a certain datum and finally u and v are image coordinates. Totally there are 6 parameters to be solved, so at least 3 GCPs are required in order to determine the transformation parameters [3].

3.1.3 Pseudo Affine Transformation

Pseudo Affine is an eight parameter transformation used for the rectification of satellite images. In order to solve eight parameters at least four GCPs are required. This method has three rotation parameters and one translation parameter for each axis [3]. The mathematical formula of the Pseudo Affine Transform is given as;

$$x = a_1 uv + a_2 u + a_3 v + a_4$$
$$y = a_5 uv + a_6 u + a_7 v + a_8 \tag{3.3}$$

Pseudo Affine Transformation is neither an orthogonal transformation nor parallel lines stay parallel. Because of a_1 and a_5 terms rotation and scaling will not be the same for every pixel in the raw image.

3.1.4 Projective Transformation

To perform a projective rectification, a geometric transformation between the image plane and the projective plane is necessary. For the calculation of the eight unknown coefficients of the projective transformation, at least four control points in the object plane are required. Projective transformation is applicable to rectifying aerial photographs of flat terrain or images of facades of buildings, since it does not correct for relief displacement [3]. The equations for projective rectification are given as follows:

$$X = \frac{a_1 x + b_1 y + c_1}{a_3 x + b_3 y + 1} , \quad Y = \frac{a_2 x + b_2 y + c_2}{a_3 x + b_3 y + 1} \qquad (3.4)$$

In Equation 3.4 X and Y are the rectified coordinates expressed in terms of x and y, which are tilted photo coordinates. a_1, b_1, c_1, a_2, b_2, c_2, a_3 and b_3 are the transformation parameters to be solved.

3.1.5   Second Order Conformal Transform

As its name implies, this method rotates the image axes with same angle but the amount of rotation is not the same at every location of the image. In other words rotation amount may not be the same for different pixel locations but the both axis will be rotated by the same amount. There are four parameters for rotation of the two axes and one parameter for the translation of each axis. In order to determine all parameters, at least three GCPs are required [3]. The mathematical formula of the method can be written as;

$$x = a_1 u + a_2 v + a_3\left(u^2 - v^2\right) + 2a_4 uv + a_5$$
$$y = -a_2 u + a_1 v + 2a_3 uv - a_4\left(u^2 - v^2\right) + a_6 \qquad (3.5)$$

When second order conformal transformation is applied, parallel lines may not remain parallel after the transformation.

3.1.6   Polynomial Transformation

For the rectification of satellite images, Polynomial transformations are generally used. The order of polynomial can be taken as two or three. Higher order polynomials increase the parameter number considerably which results an increase in demand for GCPs. Furthermore higher order terms may be correlated with each other and cause rank deficiency in the coefficient matrix leading to inaccurate solution [3]. The general formula for the polynomial transform can be written as;

$$x = \sum_i \sum_j a_{ij} u^{i-1} v^{j-1}$$
$$y = \sum_i \sum_j b_{ij} u^{i-1} v^{j-1}$$

(3.6)

In Equation 3.6 a and b are coefficients to be determined for rectification, *u* and *v* are raw image coordinates of the ground point and x and y are the assigned ground point for the corresponding image point [3].

3.2 Orthorectification

Existing imagery may be resampled to produce a new image that conforms to specific geometric properties, such as the production of a vertical view from oblique imagery. This may be a one to one process, where a single source image is modified into another resampled one, as is commonly the case when producing an orthophoto, Resampling can be defined typically as two step process comprising:

- the establishment of a geometric correspondence between the coordinate systems of the source image s(x, y) and the resampled image r(x', y') and

- the establishment of a function to express the radiometric relationship between two images.

Orthorectification is a special case of image resampling whereby the effects of the image perspective and relief displacement are removed so that the resulting orthoimage has uniformly scaled pixels, resembling a planimetric map. There are two basic approaches to orthoimage generation: forward and backward (direct or indirect) projection. In forward projection, pixels from the image are projected onto DEM to ascertain their object space coordinates, which are subsequently projected into the orthoimage. In backward projection, the object space coordinates are projected into the source image to derive the radiometric information for the corresponding orthoimage pixel. In either case, image resampling is required to account for terrain variation and perspective effects. Orthophoto generation typically proceeds following a differential rectification,

using the collinearity equations to describe the above mentioned geometric relationships between two coordinate systems [30].

The method illustrated in the Figure 3.1 is the process commonly referred to as differential rectification. In figure, point P is imaged at location P` on the mapping plane due to relief displacement. An orthogonal projection is achieved by placing a rectification plane at the average terrain height of the terrain falling within the bounds of the rectification segment containing point P [13].
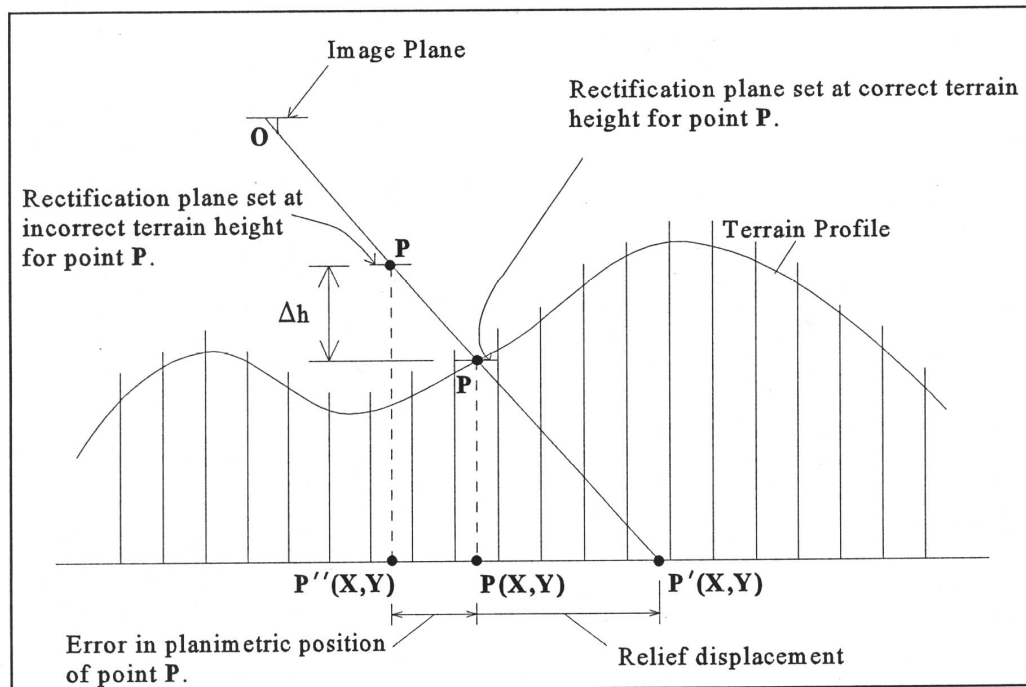
Figure 3.1 An illustration of the concept of differential rectification.

In a digital context such as in softcopy photogrammetry, digital images are used in the process and are differentially transformed to a rectification plane on a pixel-by-pixel basis and digitally projected to a mapping plane thereby eliminating tilt and relief displacements. The terrain profile shown in Figure 3.1 can be considered to be a scan line in the digital image. If one-to-one correspondence

between the orthophoto and the footprint of the raw image pixels is established, then one can imagine a rectification plane introduced into each image pixel. The true orthographic positions of image points are determined by placing a rectification plane along a terrain profile at regular intervals called rectification segments. The rectification plane is placed at the average elevation of the terrain for each segment and the image data contained within the segment is rectified to this plane. Figure 3.1 illustrates this concept.

The image pixels are projected to the mapping plane, or equivalently the orthophoto matrix, through the assignment of a gray scale value to each grid element of a regular gridded DEM. This ensures that both the elevation and photographic density of ground surface elements are stored at the same planimetric location. If the gridded pattern of the DEM does not correspond to the pixel pattern of the raw image, then the elevations corresponding to each image pixel must be interpolated.

The geometric accuracy of orthophotos mainly depends on the quality of the underlying surface description. The definition of the surface can be made mainly with two data sources: (a) ground control or exterior orientation parameters, (b) digital elevation model, which are the main inputs for the orthorectification process. Therefore, a user of orthophoto data should be aware of the effects inherent to orthophotos such as misplacement of objects that are not modelled by the DEM. Furthermore, the terms accuracy and pixel size should be strictly separated which are generally confused by the users. Metadata about the orthophoto including information about the input data directly connected to the orthophoto would be helpful in order to avoid the use of orthophotos for applications where the accuracy of orthophoto data is not sufficient. Orthophotos may be computed with a quite small pixel size for the sake of interpretation, but their positional accuracy may be less (Weidner, 1999).

Orthoimages are the end product of orthorectification. Once created, these digital images can be merged with other data sources and mosaiced with adjacent

orthoimages. The resulting digital file makes an ideal image backdrop for many applications, including feature collection, visualization, and input into GIS/Remote Sensing systems [13].

3.2.1 Orthorectification Methods

The process of orthorectification differentially transforms, on a pixel-by-pixel basis, a space imagery into an orthogonal projection. The correspondence between an image pixel and its corresponding ground element can be established in one of the two ways:

(i) Direct orthorectification model: source image (l,p) $\rightarrow$ geocoded image (i,j)

(ii) Inverse orthorectification model: geocoded image (i,j) $\rightarrow$ source image (l,p)

In the direct method of orthorectification, the image coordinates of the center of the input pixel in the original digital image are used to calculate the output space coordinates of the corresponding ground element to which the image pixel gray value is transferred. This direct projection of each image pixel onto a mapping plane is accomplished using the reprojection case of collinearity equation. Although this direct method results in an output pixel for each input pixel, it creates a problem in that the elevation data required in the process must be stored in a rectangular matrix that is based on the digital image coordinates. This can be difficult to accomplish when a DEM has been collected from a source other than the image being orthorectified because the geographic extents of the image and the DEM may not correspond exactly and geocoding the image to the DEM can be problematic, as it must be performed in an off-line process. For these reasons, the indirect approach is the preferred method of orthorectification.

The indirect or inverse model is the most convenient. It consists in computing, for each rectified pixel, the radiometric value according to the corresponding pixels of the raw image. Actually, to limit computing time without noticeable errors, a regular grid can be used instead of applying the model for every image pixel. The

44

grid is called Geometric Interpolation Grid (GIG). In that process, the grid-cell corner coordinates (I,J) are known. One pixel of the rectified image (i,j) is selected. Using the inverse model, the location of the each corner of the grid-cell is calculated (L,P) in the raw image. The location of the concerned pixel is calculated using a resampling method between the grid cell corners. The radiometric value of the rectified pixel is calculated using the adjoining pixels of the corresponding pixel in the raw image, by a resampling method [13].

3.2.2 The Role of Exterior Orientation Parameters

GCPs are used to calculate the position and orientation (i.e. roll, tilt, and yaw) of the imaging system at the moment of image taken. This calculation is accomplished using standard photogrammetric algorithms, such as a space resection or bundle adjustment. Orientation parameters can be obtained directly with the use of GPS/INS so there is no need for GCPs to compute them if the accuracy requirement is provided. The position and orientation of the imaging system are expressed as six values: x, y, z, roll, pitch, and yaw (or alternatively, x, y, z, omega, phi, and kappa), which collectively define the exterior orientation of the imaging system for each image [13]. They are needed in order to map each pixel of the digital image to its precise location on the ground. These processes can change according to the characteristics of the imaging system.

When GPS/INS is not used orthoimage generation uses the method of space resection to determine the relation between the object space and image space. Thus, the accuracy of the ground control so directly or indirectly exterior orientation parameters used in the process effects the accuracy of the digital orthophoto. The absolute accuracy of an orthoimage depends also upon the quality of the ground control information or orientation parameters.

Any errors in the exterior orientation parameters or ground control information will be propagated into the pixel positions through the digital rectification process. It is therefore important to control this error source.

3.2.3 The Role of DEM

A digital elevation model (DEM) is a digital representation of a portion of the Earth terrain over a two dimensional surface. The role of DEM in orthorectification process is that it eliminates terrain-induced displacements so as to transform an imagery into an orthogonal projection. The role of DEM is illustrated in Figure 3.2 where it can be seen that the DEM matrix, where individual elements have an elevation associated with them, can be made to correspond to a selected orthophoto matrix. Any ground sample distance (GSD) can be chosen for a given orthophoto. The GSD is then used to create an empty orthophoto matrix by basically dividing the specified study area into a regular gridded pattern. The digital imagery is orthorectified through the assignment of a gray-level value to each element in the DEM matrix. In fact, this is the essence of digital orthorectification whereby the pixels are projected to the specified orthophoto matrix through the assignment of a gray-level value to each grid element of the DEM. Thus, the role of DEM is twofold: (i) it sets the height of the elemental rectification planes (defined by the DEM grid interval) by storing the ground elevation corresponding to each plane and, (ii) it serves as the storage array for the gray-level values of each element.

DEM accuracy plays an important role in digital orthorectification process as it affects the accuracy of planimetry in the orthophoto. The accuracy of DEMs depends on a number of factors including source data scale, resolution and quality, DEM gridding interval and processing algorithms.
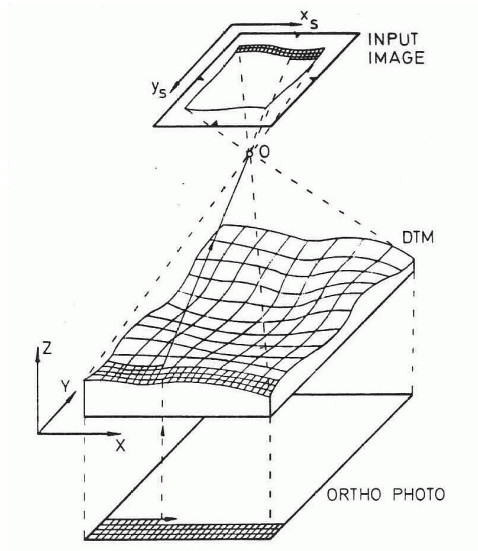
Figure 3.2 Principle of orthophoto generation (Wiesel, 1984).

3.3   DRM Algorithm for Aerial Frame Cameras

DRM is based on colinearity equations to provide a relationship between pixel positions and corresponding positions on ground. The procedure of differential rectification is applied in combination with the forward projection (direct) method of orthoimage reprojection. This is based on the collinearity principle, which states that the projection center of a central perspective image, an object point, and its photographic image lie upon a straight line. (Figure 3.3).
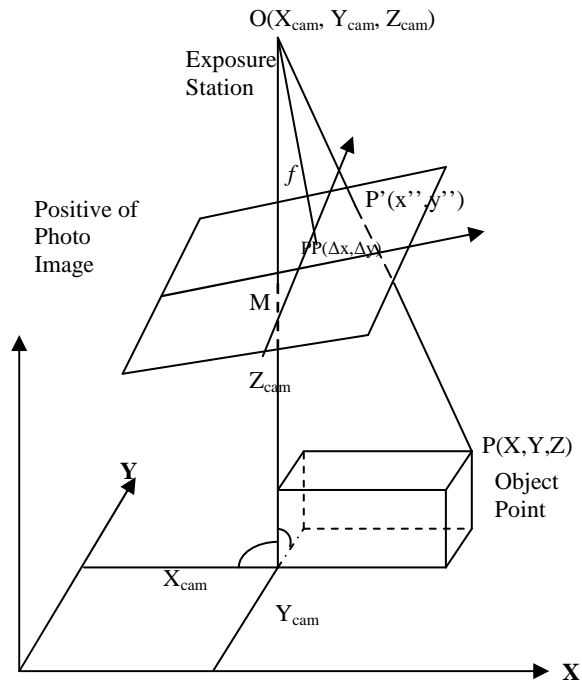
Figure 3.3 Illustration of Colinearity Conditions [3].

M is the photographic nadir point,

PP is the principal point,

P' is the image position of the object point P and x", y" are the image coordinates of point P.

Colinearity equations are written by interior and exterior camera parameters.

Interior orientation parameters of the camera are as below;

- f focal length (mm)

- $\Delta x, \Delta y$ principal point coordinates (mm)

- k_1, k_2 radial lens distortion   ($1/mm^2$ and $1/mm^4$ respectively)

48

- p_1, p_2 asymmetric radial lens distortion   (1/mm)

Exterior orientation parameters of the camera are as below;

- X_{cam}, Y_{cam}, Z_{cam} Camera coordinates at exposure time with respect to a given datum (meter)

- ω, φ, κ Attitude angles of the S_B with respect to S_L at exposure time

3.3.1 Transformation from C_{IM} to C_P

Algorithm of DRM for aerial digital frame cameras consists of 6 stages and the data needed for each step are shown in Figure 3.4. Pixel coordinates of image are computed in C_{IM} to begin the rectification procedure.

The first step of the algorithm is transformation of image coordinates from C_{IM} to C_C. Image coordinates are converted to C_P by using Equation 3.7. In this transformation, origin of coordinate system is translated from left corner to the middle of the CCD array by moving half of the size of the CCD array by applying the correction of the misalignment of the principal point to the CCD center by an amount of Δx and Δy. Furthermore, direction of y axis is reversed and coordinate system is shifted from Left Hand system to Right Hand system. Additionally, unit of this coordinate system is converted from pixel to mm by using parameter 'c' the size of the sensing element in CCD array [3]. Transformation from C_{IM} to C_P can be formulated as in Equation 3.7.

49
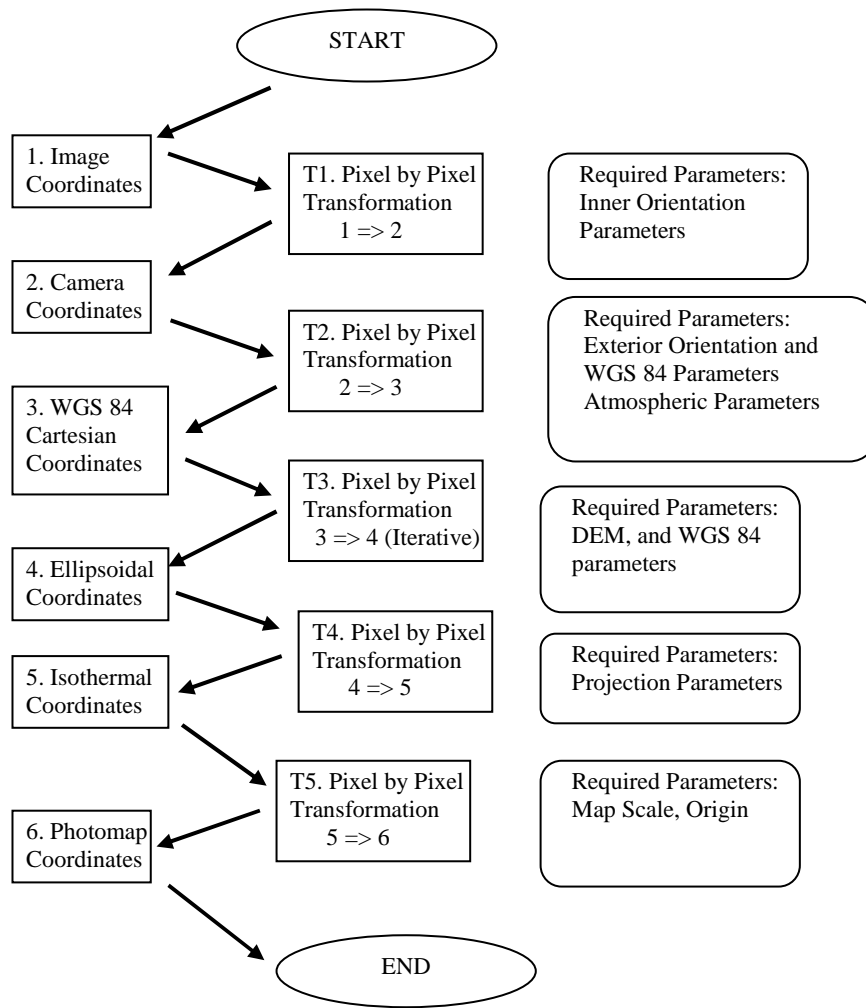
Figure 3.4 Illustration of the algorithm of DRM [26].

$$x' = \left(x'' - \frac{width}{2} \right) * c - \Delta x \qquad (3.7)$$

$$y' = \left(-y'' + \frac{heigth}{2} \right) * c - \Delta y$$

where;

x'' and y'' are cartesian pixel coordinates in the digital image (pixel)

width and *height* are the image width and image height (pixel)

Δx, Δy are the x and y coordinates of the principal point (mm)

c is the image scale (mm/pixel)

x' and y' are the coordinates in C_C (mm)

Obtained photo coordinates are not at right positions. There are small displacements in their ideal positions because of the lens distorsion effects. These displacements have to be corrected by using mathematical models [3].

3.3.2 Lens Distortion Corrections

Lens distortions are corrected by a polynomial model. The radial distortion value is the radial displacement from the ideal location to the actual image of the collimator cross, with positive values indicating outward displacements. Radial and asymmetric lens distortions are corrected by the following formulae [3];

$$x = x' * (1 - k_1 * r^2 - k * r^4 - 2 * p_1 * x' - 2 * p_2 * y' - \frac{p_1 * r^2}{x'})$$

$$y = y' * (1 - k_1 * r^2 - k_2 * r^4 - 2 * p_2 * y - 2 * p_1 * x' - \frac{p_2 * r^2}{y'}) \qquad (3.8)$$

$$z = -f$$

$$r = \sqrt{x'^2 + y'^2} \qquad (3.9)$$

where;

r is the distance of the corresponding pixel from the principal point on the CCD array (mm)

x' is the x coordinate of the image point in C_P,

y' is the y coordinate of the image point in C_P,

x, y and z values are the for lens distortion free image coordinates in C_C,

k1 and k2 are radial lens distortion parameters,

p1 and p2 are decentering lens distortion parameters,

f is the focal length of the camera.

3.3.3 Transformation from C$_P$ to C$_C$

Transformation to C$_C$ can be performed with the use of focal length of the camera and pixel positions in S$_P$. The origin of coordinate system is moved from principal point to focus, for this reason all image points' z coordinates are –f (Equation 3.10).

Direction vector of each pixel is calculated with respect to the camera coordinate system, by;

$$\overset{C}{D} = [x, y, z]' / \sqrt{x^2 + y^2 + z^2} \tag{3.10}$$

where;

x and y are the corrected pixel coordinates in C$_P$ and z is the negative value of focal length

$\overset{C}{D}$ is the direction vector with respect to C$_C$.

3.3.4 Transformation from C$_C$ to C$_B$

Transformation from C$_C$ to C$_B$ is applied by 180° rotation respect to X axis and -90° rotation with respect to Z axis. Two coordinate systems are shown in Figure 3.5a and 3.5b.

$$\overset{B}{D} = R_3(-90^o)R_1(180^o)\overset{C}{D} \tag{3.11}$$

where;

$\overset{B}{D}$ is the direction vector of the corresponding image point with respect to C$_B$

$$R_1(180^o) = \begin{bmatrix} 1 & 0 & 0 \\ 0 & -1 & 0 \\ 0 & 0 & -1 \end{bmatrix} \qquad R_3(-90^o) = \begin{bmatrix} 0 & -1 & 0 \\ 1 & 0 & 0 \\ 0 & 0 & 1 \end{bmatrix} \tag{3.12}$$
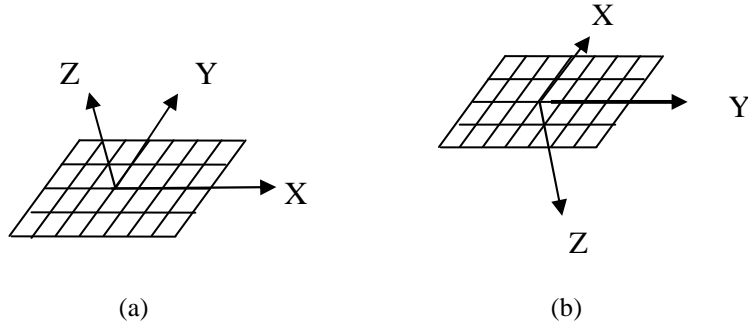
Figure 3.5 (a) Orientation of C_C (b) Orientation of C_B [2, p38]

3.3.5 Transformation from C_B to C_L

Roll, pitch and yaw angles derived from INS are the angles with respect to Geodetic Local Frame (NED). Once the direction vector is resolved in the body frame, it is then resolved into the local NED Geographic frame (C_L) using the roll, pitch and heading at the time of exposure measured by the GPS/INS:

$$\overset{L}{D} = \overset{L}{R_B} \overset{B}{D} \tag{3.13}$$

$$R_B^L = \begin{pmatrix} 1 & 0 & 0 \\ 0 & \cos\Phi & \sin\Phi \\ 0 & -\sin\Phi & \cos\Phi \end{pmatrix} \begin{pmatrix} \cos\theta_y & 0 & -\sin\theta_y \\ 0 & 1 & 0 \\ \sin\theta_y & 0 & \cos\theta_y \end{pmatrix} \begin{pmatrix} \cos\Psi & \sin\Psi & 0 \\ -\sin\Psi & \cos\Psi & 0 \\ 0 & 0 & 1 \end{pmatrix} \tag{3.14}$$

Where:

Φ, θ, Ψ are the roll pitch and heading angles,

The roll, pitch and heading angles are defined by the sequence of rotations that bring the NED Geographic frame into alignment with the IMU body frame, and are described as follows [30]:

53

a. clockwise rotation about the down axis by the heading Ψ

b. clockwise rotation about the once rotated East axis by the pitch angle θ

c. clockwise rotation about the twice rotated North axis by the roll angle Φ

3.3.6 Computation of Intersection Point

Applying Equation 3.13 completes the first step of the rectification algorithm. Second step of the algorithm involves the computation of cartesian coordinates of intersection point with the direction vector computed in step 1 with the WGS84 ellipsoid. In order to compute the cartesian coordinates of the intersection point, the direction vector with respect to C_L should be transformed to C_E and the intersection equation involving the direction vector in C_E and camera position should be generated [3].

3.3.6.1 Transformation from C_L to C_E

To proceed the next step transformation of direction vector from Geographic Local Frame (NED) to Earth Fixed Refence Frame (ECEF) is needed.

Equation of the rotation from C_L to C_E can be written as;

$$\overset{E}{D} = \overset{E}{R}_L \overset{L}{D} \tag{3.15}$$

Both are rectangular coordinate frames and geometrical relationship between two system can be established by two consecutive rotations given as

$$R_L = \mathbf{R}_3(-\lambda_A)\mathbf{R}_2(\varphi_A - 90)\mathbf{R}_3(-90) \tag{3.16}$$

where φ_A and λ_A are latitude and longitude of origin of LGF; and $\mathbf{R}3$ and $\mathbf{R}2$ are counterclockwise rotations (positive when viewed toward origin) around Z and Y axes.

$$R_L = \begin{bmatrix} -\sin\lambda_A & -\sin\varphi_A\cos\lambda_A & \cos\varphi_A\cos\lambda_A \\ \cos\lambda_A & -\sin\varphi_A\sin\lambda_A & \cos\varphi_A\sin\lambda_A \\ 0 & \cos\varphi_A & \sin\varphi_A \end{bmatrix} \tag{3.17}$$

$\overset{E}{D}$ is the direction vector of the corresponding image point with respect to C_E.

Direction vector of corresponding image point with respect to C_E is obtained. The direction vector goes through from aerial camera focus and passes the corresponding sensing element of the CCD array and intersects the WGS84 ellipsoid. The intersection point of direction vector with the WGS84 ellipsoid surface should be computed to complete step 2. Aerial camera's position is known with respect to C_E at the instant of the image acquisiton, if the intersection point on the reference ellipsoid is assumed as P_0 with the coordinates [X_0, Y_0, Z_0] then the following equation can be written [26];

$$\begin{bmatrix} X_0 \\ Y_0 \\ Z_0 \end{bmatrix} = \begin{bmatrix} X_{cam} \\ Y_{cam} \\ Z_{cam} \end{bmatrix} + s * \begin{bmatrix} \overset{E_X}{D} \\ \overset{E_Y}{D} \\ \overset{E_Z}{D} \end{bmatrix} \tag{3.18}$$

where;

X_0, Y_0, Z_0 are the coordinates of the intersection point with respect to C_E,

X_{cam}, Y_{cam}, Z_{cam} are the coordinates of the satellite camera with respect to C_E,

s is the distance between satellite's camera focus and the intersection point on the reference ellipsoid,

$\overset{E_X}{D}$, $\overset{E_Y}{D}$, $\overset{E_Z}{D}$ are the components of direction vector from camera focus to image plane with respect to C_E.

In Equation 3.18 there are 4 unknowns to be solved which are X_0, Y_0, Z_0 and s. However, Equation 3.18 contains only 3 equations which is inadequate for solving the equation set. One more equation is required for the solution for the intersection point. Since P_0 is on the reference ellipsoid's surface, ellipsoidal surface equation can be written for this point [3],

$$\frac{X_0 + Y_0}{a^2} + \frac{Z_0}{b^2} = 1 \qquad (3.19)$$

where;

a is the semimajor axis

b is the semiminor axis of the WGS84 reference ellipsoid.

This leads to a system of four equations and four unknowns

If Equation 3.18 is substituted into Equation 3.19 the following intersection equation will be obtained,

$$\left[\frac{\overset{E}{D_x^2} + \overset{E}{D_y^2}}{a^2} + \frac{\overset{E}{D_z^2}}{b^2} \right] * s^2 + 2 * \left[\frac{\overset{E}{D_x} * X_{cam} + \overset{E}{D_y} * Y_{cam}}{a^2} + \frac{\overset{E}{D_z} * Z_{cam}}{b^2} \right] * s \\ + \frac{X_{cam}^{\;2} + Y_{cam}^{\;2}}{a^2} + \frac{Z_{cam}^{\;2}}{b^2} - 1 = 0 \qquad (3.20)$$

Solving Equation 3.20 for s will lead to two solutions for s, which are

$$s_{1,2} = \frac{-\beta \pm \sqrt{\beta^2 - 4\alpha\gamma}}{2\alpha} \qquad (3.21)$$

where;

$$\alpha = \frac{\overset{E}{D_x^2} + \overset{E}{D_y^2}}{a^2} + \frac{\overset{E}{D_z^2}}{b^2} \qquad (3.22)$$

$$\beta = 2 * \left(\frac{\overset{E}{D_x} * X_{cam} + \overset{E}{D_y} * Y_{cam}}{a^2} + \frac{\overset{E}{D_z} * Z_{cam}}{b^2} \right) \qquad (3.23)$$

$$\gamma = \frac{X_{cam}^{\;2} + Y_{cam}^{\;2}}{a^2} + \frac{Z_{cam}^{\;2}}{b^2} - 1 \qquad (3.24)$$

Among the two s values the shorter one is the proper solution because the bigger distance gives the other side of the ellipsoidal surface [26]. The smaller root is

used in the intersection equation and intersection point's coordinates (X_0, Y_0, Z_0) are computed [3]. Solution for the smaller root is as following

$$s = \frac{-\beta - \sqrt{\beta^2 - 4\alpha\gamma}}{2\alpha}$$

(3.25)

If s is substituted into Equation 3.18 Cartesian coordinates of the intersection point can be computed. This may be thought as the end of Step 2 but this is not the case. Since the light ray passes through the atmosphere which is a dispersive medium, it is refracted and its path is not a straight line anymore. For this reason, computed cartesian coordinates of the ground point should be corrected. The correction is performed by the zenith angle of the direction vector. In order to compute zenith angle the direction vector should be transformed from C_E to C_L. The rotation matrix of this transformation is computed by means of the geodetic coordinates of the corresponding ground point. For this reason, cartesian coordinates should be transformed into geodetic coordinates. Cartesian coordinates are converted to ellipsoidal coordinates by an iterative method [3].

$$\phi_i = \tan^{-1}\left(\frac{Z}{\sqrt{X^2 + Y^2}}\left(1 - e^2 \frac{N_i}{N_i + h_i}\right)^{-1}\right)$$

(3.26)

$$\lambda = \tan^{-1}\left(\frac{Y}{X}\right)$$

(3.27)

$$h_i = \frac{\sqrt{X^2 + Y^2}}{\cos\phi_i} - N_i$$

(3.28)

The algorithm shown in Equation 3.26 is an iterative method, in order to start iteration, it is a good approximation to take initial value of h as 0 and compute ϕ and correct the h. This iteration continues until the difference in h is less than a predefined threshold value [3].

3.3.6.2 Atmospheric Refraction Correction

According to the Snell's law light rays are bended while traveling through a medium of changing refraction index. Besides the refractivity of the medium, change in direction is proportional to the entrance angle also [3, p43]. The relation between the entrance and exit angles to the boundary is given as;

$$n_1 \sin\theta_1 = n_2 \sin\theta_2 \qquad (3.29)$$

where;

n_1 is the refractivity index of the first medium

n_2 is the refractivity of the second medium

θ_1 is the entrance angle of the light ray to the boundary

θ_2 is the exit angle of the light from the boundary

Entrance angle of the light ray will be equal to its zenith angle.

$$N = (n-1)10^6 \qquad (3.30)$$

[3, p.43] where

N is the refractivity and computed for visible light by the formula [3, p.43]

$$\frac{\partial N}{\partial h} = -78\frac{p}{T^2}\left(0.034 + \frac{\partial T}{\partial h}\right) - \frac{11}{T}\frac{\partial e}{\partial h} \qquad (3.31)$$

where;

h is the elevation with respect to mean sea level

p is atmospheric pressure in hPa

T is the temperature of the atmosphere in Kelvin

e is humidity measured as the water vapor pressure in hPa

Parameters in the Equation 3.31 are not constant and they should be computed for each atmosphere layer. In order to compute the refractivity, the atmosphere is

divided into layer of 1 km thickness. Within each layer refractivity is considered as constant [3, p. 43].

Atmosphere pressure, p is computed from the barometric formula [3].

$$p = p_0 e^{\frac{-Mgh}{RT}} \tag{3.32}$$

where;

h is the height in meter

P_0 is pressure at ground level in hPa

M is the mass of 1 mole of air 0.029 kg mol^{-1}

R is the gas constant (8.314 J K^{-1} mol^{-1})

g_0 is the acceleration due to gravity (9.81 m s^{-2})

By taking the initial values for temperature as 300 Kelvin, atmospheric pressure as 1023 hPa and water vapor pressure as 16 hPa the following values are obtained for the atmospheric conditions for the first 8 km.

3.3.6.3 Transformation from C_E to C_L

To perform atmospheric corrections, zenith angle of the direction vector should be computed. To compute zenith and azimuth angles, direction vector in C_E should be transformed to C_L [3].

In order to transform from S_E to S_L first from the third axis (Z-axis) the frame is rotated by λ degrees and from the second axis (Y-axis) the frame is rotated by 90 – φ degrees. To convert the local system to left hand system the first axis is multiplied by -1. The total rotation is

$$\mathbf{R}_E^L = \mathbf{Q}_1 \mathbf{R}_2(90 - \varphi)\mathbf{R}_3(\lambda) \tag{3.33}$$

59

where;

ϕ is the latitude of the point on the ground,

λ is the longitude of the point on the ground,

If the matrix multiplications represented in Equation 3.33 are performed, the following matrix will be obtained,

$$\mathbf{R}_E^L = \begin{bmatrix} -\sin\phi\cos\lambda & -\sin\phi\sin\lambda & \cos\phi \\ -\sin\lambda & \cos\lambda & 0 \\ \cos\phi\cos\lambda & \cos\phi\sin\lambda & \sin\phi \end{bmatrix} \tag{3.34}$$

In this matrix $sin(90 - \varphi)$ is substituted by $cos(\varphi)$ and $cos(90 - \varphi)$ is substituted by $sin(\varphi)$.

$$D^L = \mathbf{R}_E^L \, D^E \tag{3.35}$$

This can be written in matrix form as;

$$\begin{bmatrix} D_x^L \\ D_y^L \\ D_z^L \end{bmatrix} = \begin{bmatrix} -\sin\phi\cos\lambda & -\sin\phi\sin\lambda & \cos\phi \\ -\sin\lambda & \cos\lambda & 0 \\ \cos\phi\cos\lambda & \cos\phi\sin\lambda & \sin\phi \end{bmatrix} \begin{bmatrix} D_x^E \\ D_y^E \\ D_z^E \end{bmatrix} \tag{3.36}$$

By using the direction vector with respect to C_L, azimuth and zenith angles of the direction line can be computed by the following formulae:

$$\alpha = \tan^{-1}\left(\frac{D_y^L}{D_x^L}\right) \tag{3.37}$$

$$z = \tan^{-1}\left(\frac{\sqrt{D_x^{L\,2} + D_y^{L\,2}}}{D_z^L}\right) \tag{3.38}$$

where;

α is the azimuth angle,

z is the zenith angle.

3.3.7 Relief Displacement Correction

The intersection point of the direction vector with the WGS84 ellipsoid is exactly on the reference ellipsoid, in other words its ellipsoidal height is zero which is usually not the real case. Height differences of the objects with respect to datum cause relief displacements which alter the place of the objects in the image. In order to eliminate relief displacements, exact elevation of ground objects should be known. While studying with mono images to eliminate relief displacements a DEM is required. First at the position of intersection, elevation of that point is read from DEM and a correction for relief displacement for the geodetic position is done on reference ellipsoid, then height value of the corrected position is read from DEM and another correction is performed considering the elevation differences between two successive height values obtained from DEM. The iterative procedure continues until the elevation difference between two successive elevation values reduces to a predetermined threshold value [26].

The iteration algorithm is shown in Figure 3.4. The intersection point of direction vector with WGS84 ellipsoid is shown as P_0 in the figure. From its geodetic coordinates an elevation value is obtained from DEM. By using azimuth & zenith angles and ellipsoidal parameters geodetic coordinates of the intersection point is corrected [26]. The correction formulae are shown in Equation 3.30. After the first iteration the present point is called P_1 which has different geodetic coordinates from the previous points, this will cause a different ellipsoidal normal as shown in the Figure 3.6. The direction vector is again transformed from C_E to C_L in order to compute the correct zenith and azimuth angles, after correcting the zenith and azimuth a new height value obtained from DEM, h_1, and geodetic coordinates are corrected if the difference between two height values, $|h_1 - h_0|$, is greater than the pre-defined threshold value, ϵ. Magnitude of the correction is computed by the

61

elevation differences obtained at current and previous iteration steps. This is the modification for the DRM which was using only the previous elevation data. Iteration procedure continues until the difference between two successive height values are below the threshold value [3].

Figure 3.6 Illustration of relief displacement correction algorithm [26].

The procedure can be formulated as;

$$\Delta h_n = h_n(\lambda_{n-1}, \phi_{n-1}) - h_{n-1}(\lambda_{n-1}, \phi_{n-1})$$ (3.39)

$$d_n = \Delta h_n \tan(z)$$ (3.40)

$$\lambda_n = \lambda_{n-1} + d_n \sin(\alpha) * \left(\frac{V}{c}\right)_{n-1} \left(\frac{1}{\cos(\phi_{n-1})}\right)$$ (3.41)

$$\phi_n = \phi_{n-1} + d_n \cos(\alpha_{n-1}) * \left(\frac{V^3}{c}\right)_{n-1} \quad (3.42)$$

where;

$$c = \frac{a^2}{b}, \qquad V_n = \sqrt{1 - \frac{a^2 - b^2}{b^2} \cos^2(\phi_0)_n} \quad (3.43)$$

The threshold value to be satisfied is $|\Delta h_n| < \varepsilon$, finally

$$\lambda_a = \lambda_n, \qquad \phi_a = \phi_n, \qquad h_a = h_n.$$

$$(3.44)$$

After n iterations final position of the point becomes λ_n, ϕ_n and h_n.

Geodetic coordinates of the intersection points and the corrected points are not expected to be exactly on the DEM grids. For this reason, elevation of the point can not be obtained directly. Interpolation is required to predict the elevation of the point. Because of this four nearest grid point's elevation are obtained from DEM and a linear interpolation is applied if P_i is not exactly on the DEM grids [3].

3.3.8 Transformation from C_G to C_M

After computing the geodetic coordinates for each pixel position, the geodetic coordinates are converted to Universal Transverse Mercator (UTM) coordinates. Conversion of coordinates between the geodetic system of latitude and longitude and the UTM map projection involves complex mathematics. A UTM zone has a number of defining constants in addition to the required standard ellipsoid parameters [3].

These defining constants are;

k_0 is scale factor along the central meridian,

ϕ_0 is latitude of the grid origin,

λ_0 is longitude of the grid origin,

E$_0$ is false easting,

N$_0$ is false northing.

The longitude of the grid origin λ_0 is conventionally referred to as the longitude of the central meridian.

UTM conversion equations involve series expansion which is truncated to a limited number of terms. For this reason, the accuracy of the transformation is limited not only to the number of significant figures in the computations; but also the truncation of the series. When the following formulae are used, the accuracy should be satisfactory as long as the points are limited to the defined region of the particular UTM zone.

A key parameter involved in UTM conversions is the meridional distance M from the equator to a specific latitude ϕ. Calculation of M can be performed by a truncated series expansion which is given in the following equation [3].

$$M = a\left[\left(1 - \frac{e^2}{4} - \frac{3e^4}{64} - \frac{5e^6}{256}\right)\phi - \left(\frac{3e^2}{8} + \frac{3e^4}{32} + \frac{45e^6}{1024}\right)\sin(2\phi) + \left(\frac{15e^4}{256} + \frac{45e^6}{1024}\right)\sin(4\phi) \\ - \frac{35e^6}{3072}\sin(6\phi) \right] \quad (3.45)$$

where;

M is the meridian distance from the equator to a specific latitude φ,

a is the semimajor axis,

e is the eccentricity,

ϕ is the latitude.

The value of latitude ϕ in the first term must be in radian. This equation is accurate to 1 mm in any latitude.

A forward procedure that can convert latitude ϕ and longitude λ of a point to X and Y Transverse Mercator coordinates begins by computing the following preliminary quantities T, C, A [3].

$$T = \tan^2 \phi \qquad (3.46)$$

$$C = e'^2 \cos^2 \phi \qquad (3.47)$$

$$A = (\lambda - \lambda_0)\cos\phi \qquad (3.48)$$

where;

λ and λ_0 are in radians,

e' is second eccentricity,

λ_0 is the longitude of the grid origin (central meridian).

The following equations complete the forward conversion to X and Y.

$$X = k_0 N\left[A + (1 - T + C)\frac{A^3}{6} + (5 - 18T + T^2 + 72C - 58e'^2)\frac{A^5}{120}\right] + E_0 \qquad (3.49)$$

$$Y = k_0 \left\{ \begin{array}{l} M - M_0 + \\ N\tan\phi\left[\frac{A^2}{2} + (5 - T + 9C + 4C^2)\frac{A^4}{24} \\ + (61 - 58T + T^2 + 600C - 330e'^2)\frac{A^6}{720}\right] \end{array} \right\} + N_0 \qquad (3.50)$$

where;

k_0 is a scale factor at central meridian.

e' is the second eccentricity.

E_0, N_0 are false easting and false northing respectively.

M is the meridianal distance at latitude ϕ.

M_0 is the meridianal distance at latitude ϕ_0.

N is the length of ellipsoid normal at latitude ϕ.

3.3.9 Resampling

After geodetic coordinates of the ground point transformed to UTM coordinates, next step is resampling to produce the image map. The computed UTM coordinates will not be regularly spaced and placed. So, the position of the pixels in the image will be different. To obtain a regular shaped and spaced UTM grids, a mapping algorithm should be defined that maps Brightness Values of the image with irregular UTM grids to image with regular UTM grids.

When a digital image is acquired, no attempt is made to have the pixels line up with any particular map projection coordinates. It is therefore necessary to perform resampling to obtain a digital sample at an intermediate row, column location. Resampling involves interpolation between existing pixels' brightness value (BV) to synthesize pixels that correspond to fractional locations. Interpolation works by using known data to estimate values at unknown points.Determination of the appropriate fractional locations is often the result of a coordinate transformation [3].

There are various techniques for resampling digital images. The most widely used which are nearest-neighborhood interpolation, bilinear interpolation and bicubic convolution [3]. In this thesis bilinear interpolation is used for resampling procedure because of its smoothness. Bilinear interpolation considers the closest 2x2 neighborhood of known pixel values surrounding the unknown pixel. It then takes a weighted average of these 4 pixels to arrive at its final interpolated value. This results in much smoother looking images than nearest neighbor. After performing the resampling all requirements of the algorithm illustrated in Figure 3.4 will be accomplished.

CHAPTER 4

TEST AREA, DATA SETS AND SOFTWARE

In this chapter test area and data sets used in the implementation are explained. After describing the study area, the image data properties, flight plan and GCPs are given. Besides software used in aero-triangulation, direct georeferencing and rectification of images are described.

4.1 The Study Area

The study area (Figure 4.1) is located in Ankara. It covers an area of approximately 3600 km^2 and encloses the city of Ankara.

4.2 Flight Plan and GCPs

Flight is planned over the test area with 15 flight column and includes 571 images (Figure 4.1). Image scale is 1:60.000 with 6 km height above the average terrain height and ground sample distance (GSD) is 43 cm.

Totally 24 GCPs (Figure 4.2) are constructed homogeneously and 4 of them are on the corner of the test block. 3 hours GPS observation was done for each GCP and adjusted with least square adjustment method. GCPs adjusted coordinates are given in Appendix-A.
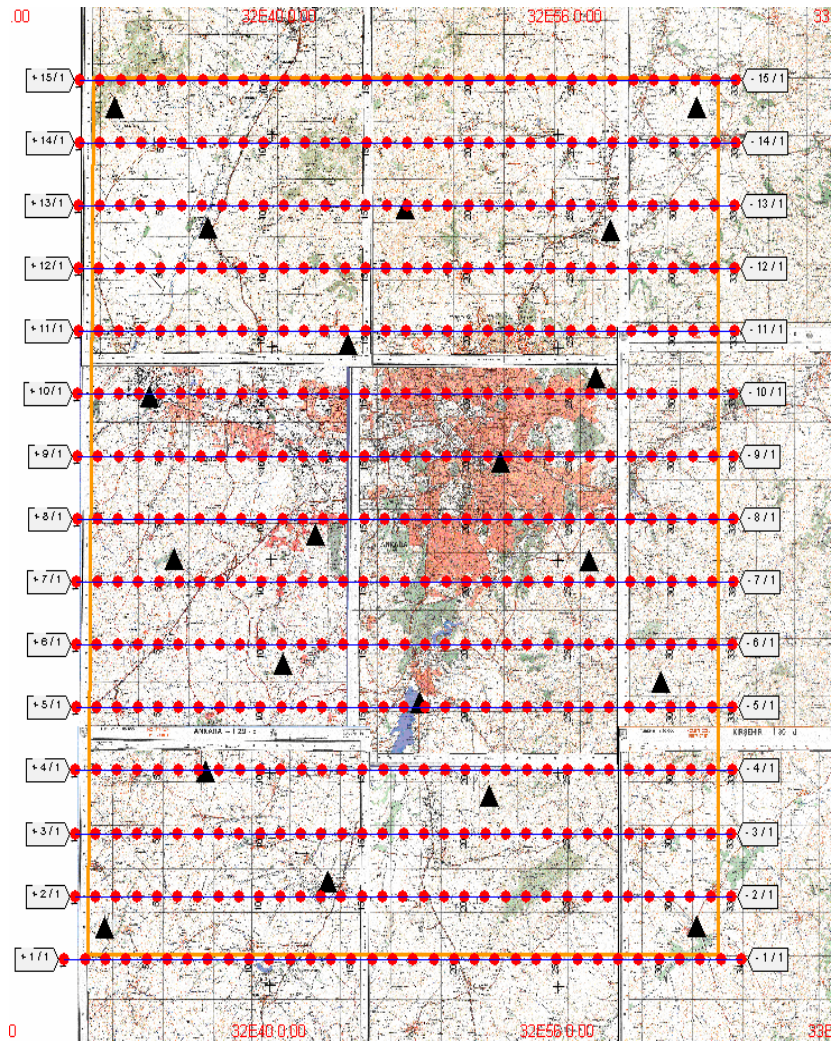
Figure 4.1 The Study Area.
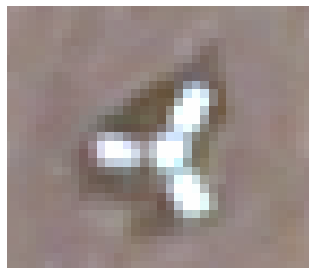
Figure 4.2 GCP example.

4.3 Digital Camera and Image Data

UltramcamX Vexcel digital camera (Figure 4.3) is used and tested in this thesis. It has 13 CCDs arrays (9 pan, 4 color). Camera properties are shown in Table 4.1.

Table 4.1 UltracamX Vexcel Technical Properties [44].

Panchromatic image size	14,430 * 9,420 pixels
Panchromatic physical pixel size	7.2 μm
Input data quantity per image	435 Mega Bytes
Physical format of the focal plane	104 mm * 68.4 mm
Panchromatic lens focal distance	100 mm
Lens aperture	f= 1/5.6
Angle-of-view from vertical, cross track (along track)	55° (37°)
Color (multi-spectral capability) 4 channels	RGB & NIR
Color image size	4810 * 3140 pixels
Color physical pixel size	7.2 μm
Color lens system focal distance	33 mm
Color lens aperture	f = 1/4.0
Color field of view from vertical, cross track (along track)	55° (37°)
Shutter speed options	1/500 to 1/32
Forward-motion compensation (FMC)	TDI controlled
Maximum FMC-capability	50 pixels
Pixel size on the ground (GSD) at flying height of 500 m (at 300m)	3.6 cm (2.2 cm)
Frame rate per second (minimum inter-image interval)	1 frame per 1.35 seconds
Analog-to-digital conversion at 14 bits Radiometric resolution in each color channel	14 bits

Figure 4.3 UltracamX Vexcel.

4.4 Software

Kinematic GPS data are post-processed with IGI GraffNav 8.1 and integrated with INS data with AeroOffice v5.1c software. Aero-triangulation is implemented with Inpho Match-AT 5.0, orthorectification and rectification of images is done with Erdas Imagine 9.1 and Inpho OrthoMaster 5.2 and the differential rectification algorithm explained in chapter 5 is programmed with Matlab 7.1. Stereo models are constructed by Datem Summit Evolution 4.1

4.5 DEM Data

YUKPAF is elevation data derived from 1:25.000 scaled topographic maps with 10 m interval. SRTM (Shuttle Radar Topography Mission) DEM is 30 m interval data (Level 2).

CHAPTER 5

IMPLEMENTATION OF AERO-TRIANGULATION AND DIRECT GEOREFERENCING

In this chapter aero-triangulation, direct georeferencing and boresight calibration implementation process are explained.

5.1 Direct Georeferencing

Aero-triangulation provides exterior orientation parameters with bundle block adjustment. In order to determine the parameters, sufficient amount of GCPs are needed. Perspective center coordinates (X_0, Y_0, Z_0) and rotation angles (ω, φ, κ) of each image in the block are solved by using GCP coordinates with space resection. With the use of the GPS/INS, it is possible to determine exterior orientation parameters by GPS/INS integration. Theoretically there is no need to GCP but the geometric accuracy of GPS/INS has to be determined.

Air GPS data and ground (base) GPS data are post-processed with GraffNav 8.1 and using Carrier Phase Differential Positioning method. GPS post-processing parameters are shown in Figure 5.1-5.4. Besides GPS trajectory and estimated position accuracy is shown in Figure 5.5 and Figure 5.6.
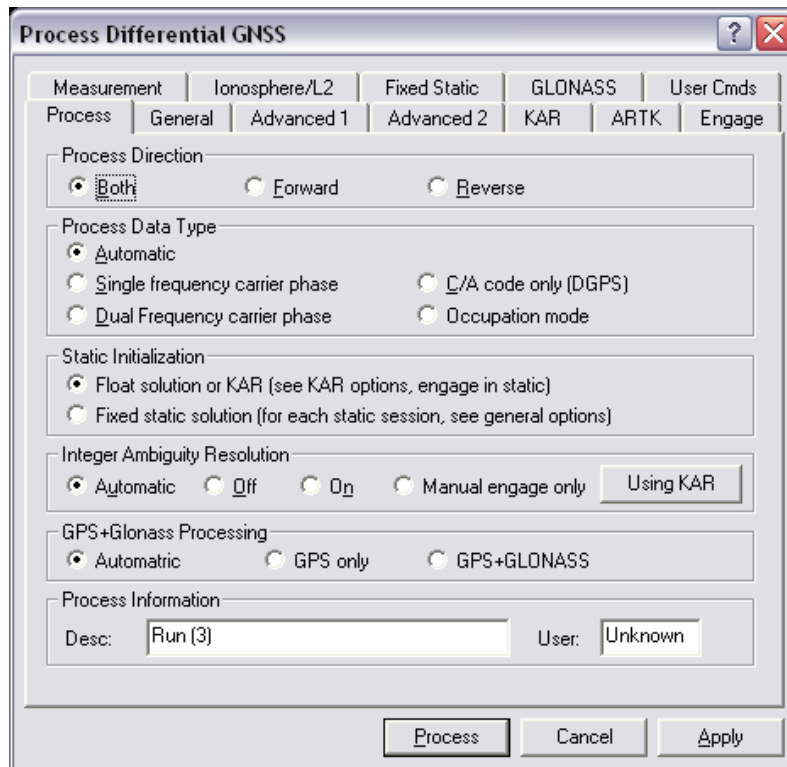
Figure 5.1 Process parameters.
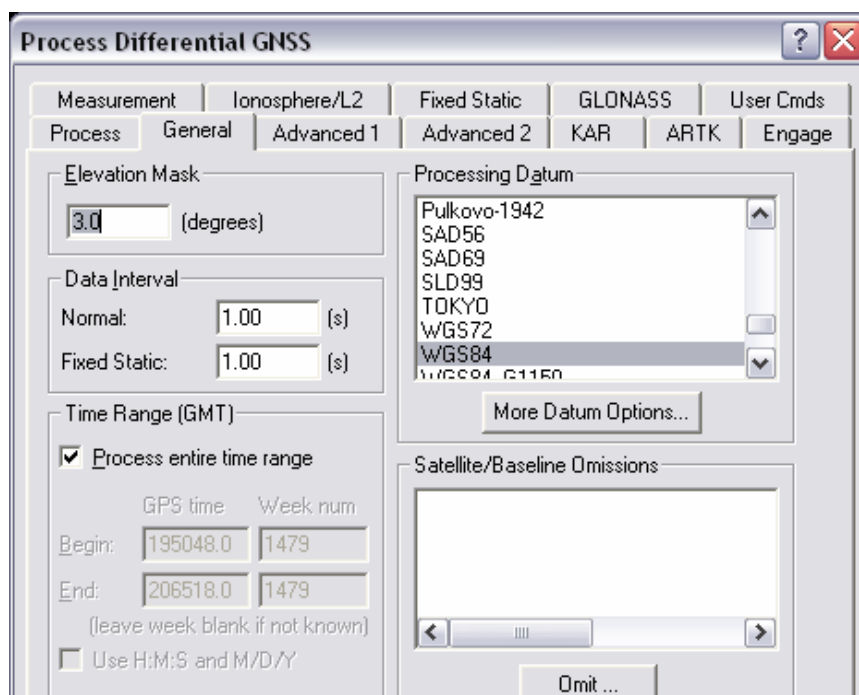
Figure 5.2 Elevation mask and processing datum.
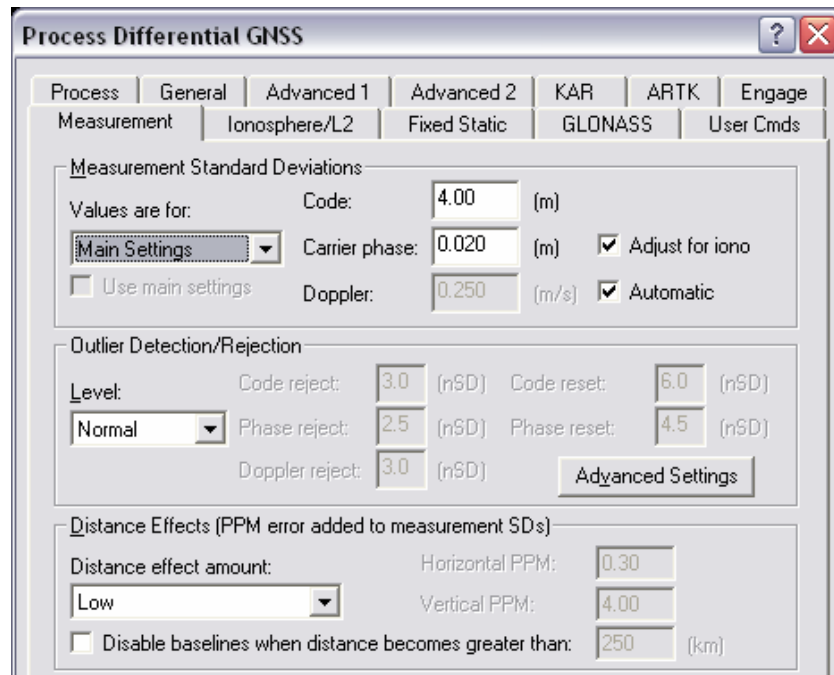
Figure 5.3. Measurement parameters.
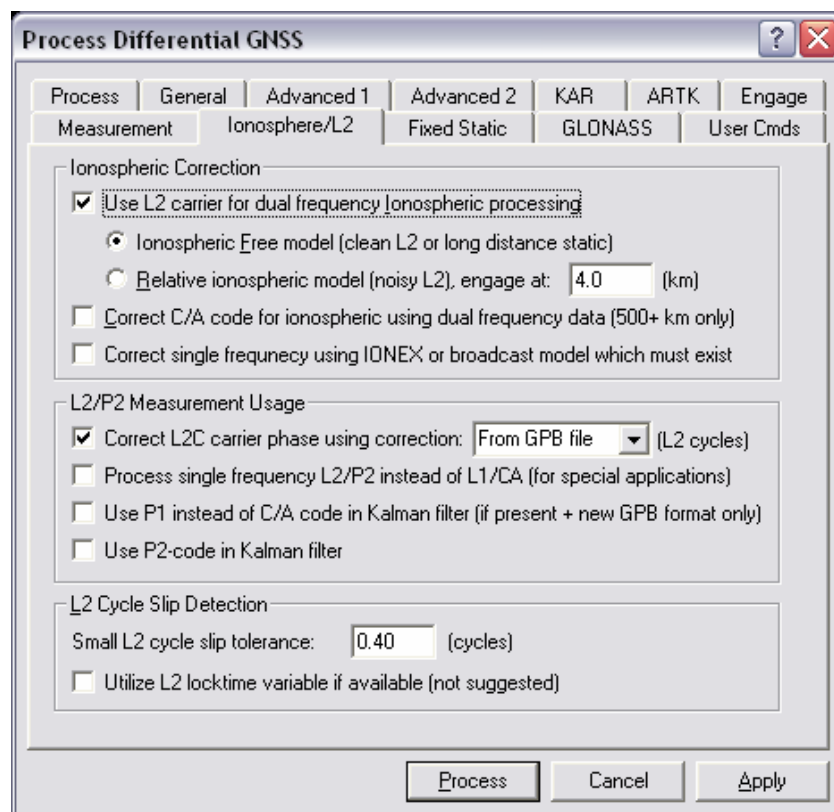
Figure 5.4 Ionospheric correction parameters.
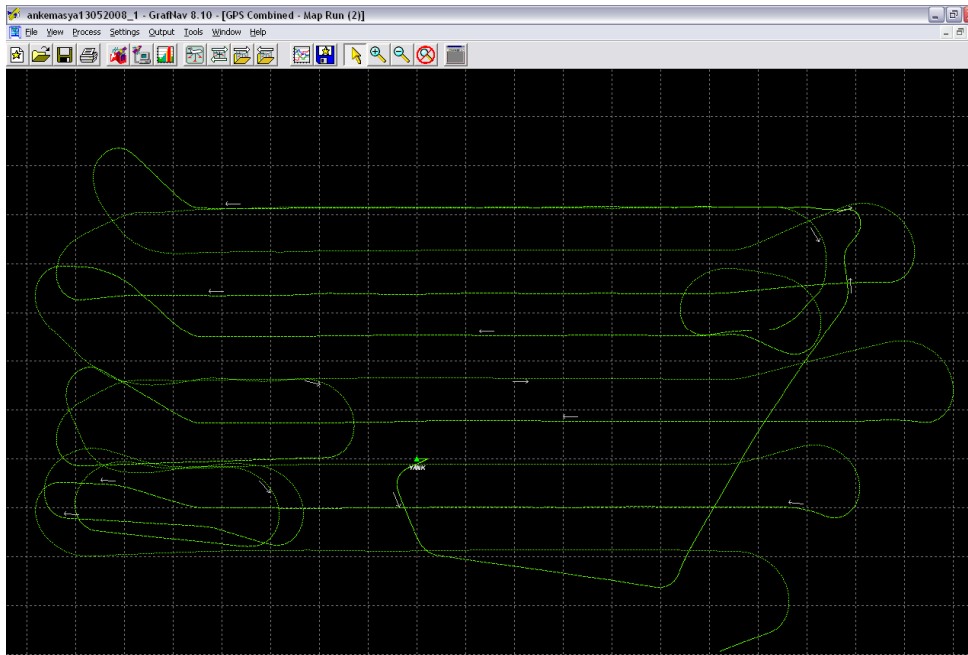
Figure 5.5 GPS trajectory.
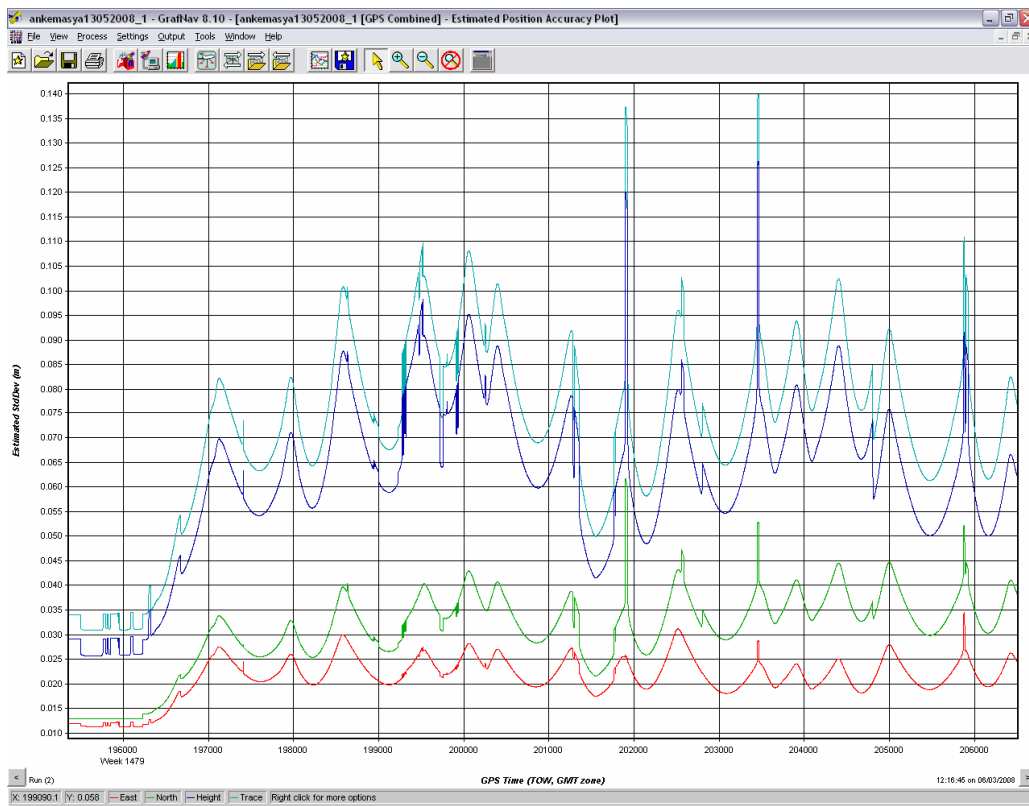
Figure 5.6 Estimated position accuracy.

GPS data and INS data are integrated with AeroOffice using Kalman Filtering Method as explained in Chapter 3. GPS/INS position differences are shown in Figure 5.7. Exterior orientation parameters obtained from integration are used for stereo model construction. Stereo models are constructed in Datem Summit Evolution software and GCPs of which the coordinates are determined by adjustment of GPS observations are measured in the models. Horizontal and vertical coordinate differences between the adjusted and measured coordinates are determined, mean error and root mean square error (RMSE) (Table 5.1) are computed. Detailed results are shown in Appendix-B.
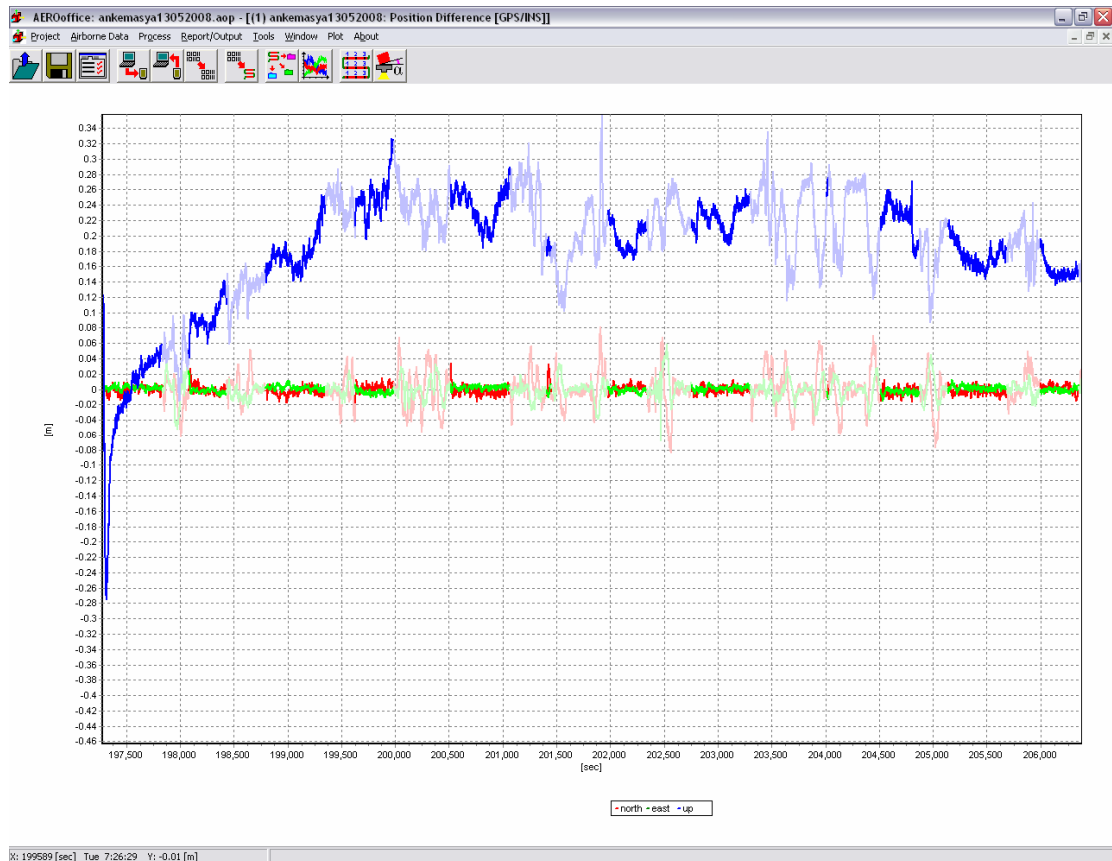
Figure 5.7 GPS/INS Position differences.

Table 5.1 RMSE and mean error of DG.

ROOT MEAN SQUARE ERROR (RMSE)			MEAN ERROR		
X (m)	Y (m)	Z (m)	X (m)	Y (m)	Z (m)
0,835	0,603	0,550	0,699	0,426	0,412

5.2 Aero-triangulation

Integrated GPS/INS data are corrected using boresight calibration results and used as initial parameters in aero-triangulation process. Corrected GPS/INS data and 4 GCPs at the corner of the test block are used and full automatic aero-triangulation is implemented to determine the tie points (Figure 5.8). Then bundle block adjustment is applied (Figure 5.9-5.13) with Inpho Match-AT using 4 GCPs, 2 GCPs, 1 GCP and no GCP in order to determine the effect of the GCP amount in the adjustment. GCPs are used as check points and computed in bundle block adjustment. Horizontal and vertical coordinate differences between the adjusted measured and adjusted GCP coordinates are determined, mean error and root mean square error (RMSE) are computed (Figure 5.14). Detailed results are shown in Appendix-C.
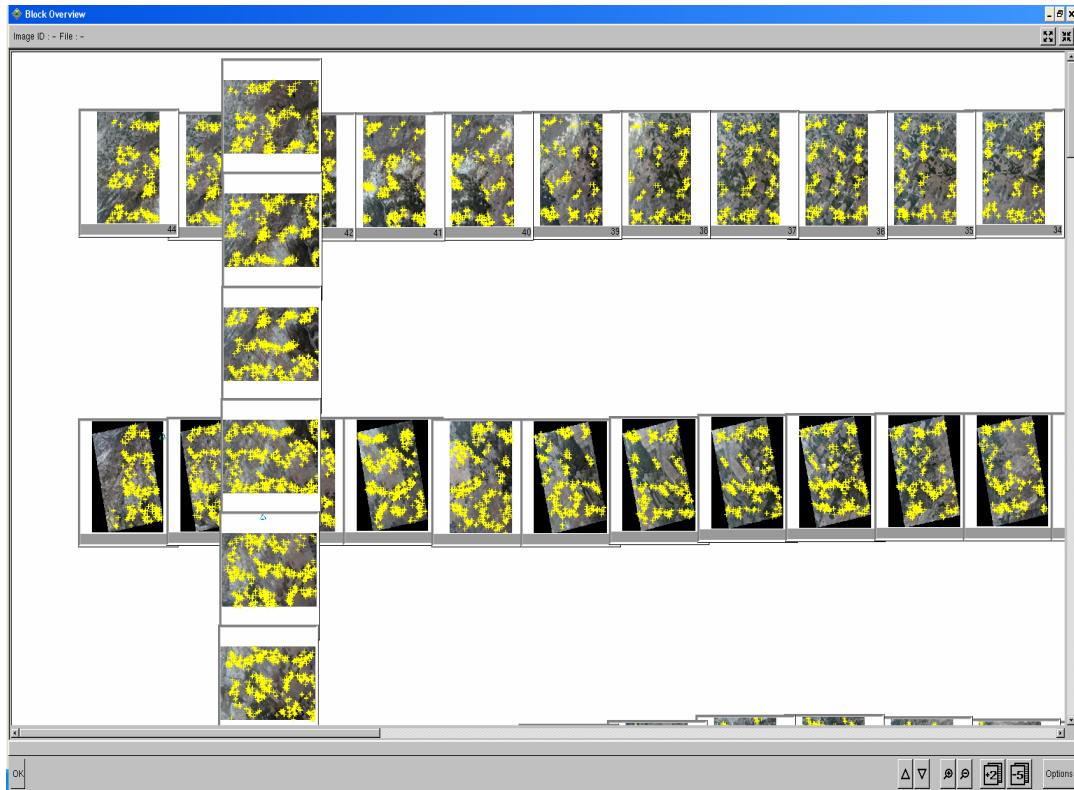
Figure 5.8 Automatic aero-triangulation example.
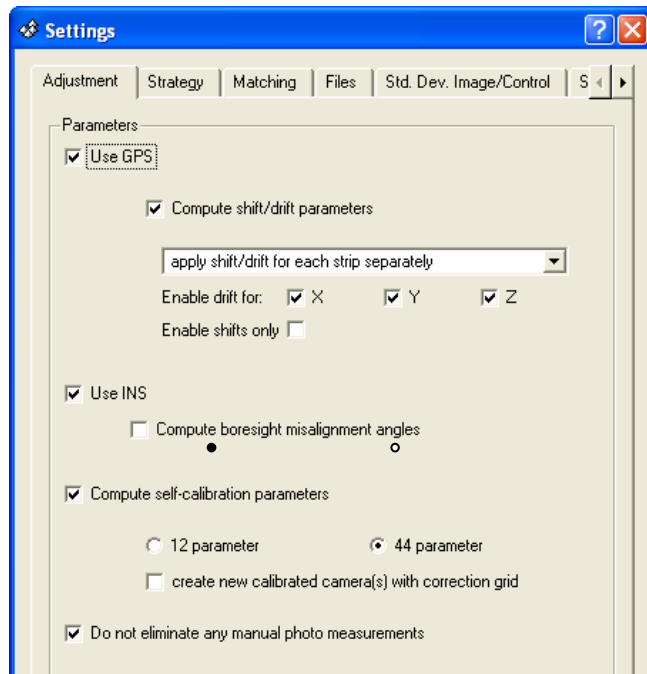
Figure 5.9 Adjustment settings.
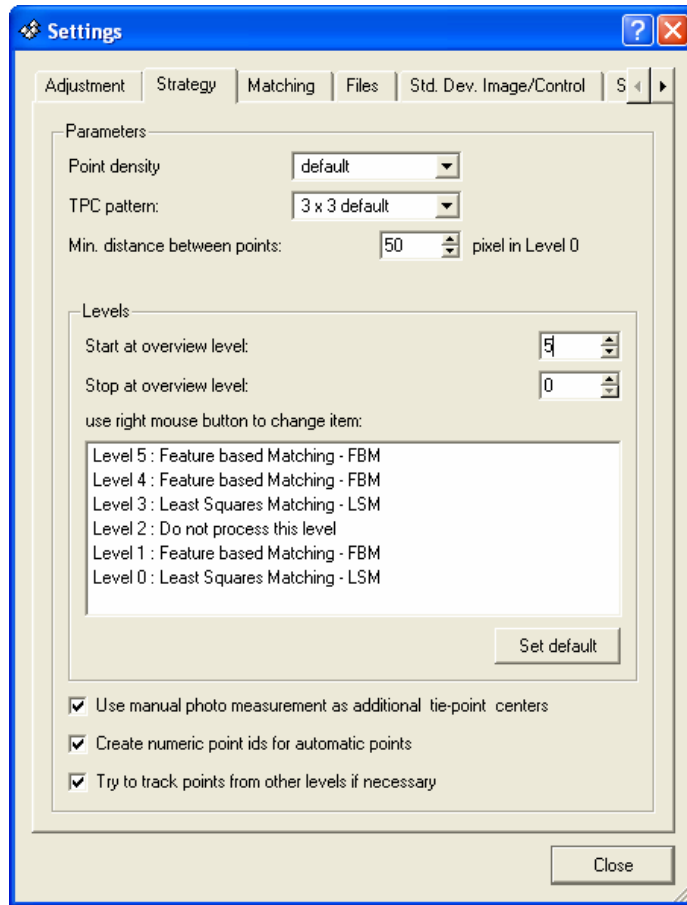
Figure 5.10 Strategy settings.
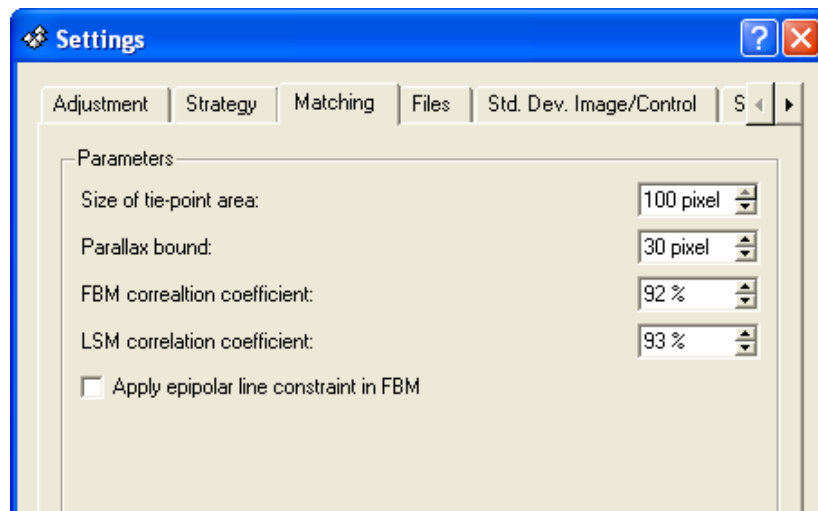
Figure 5.11 Matching settings.
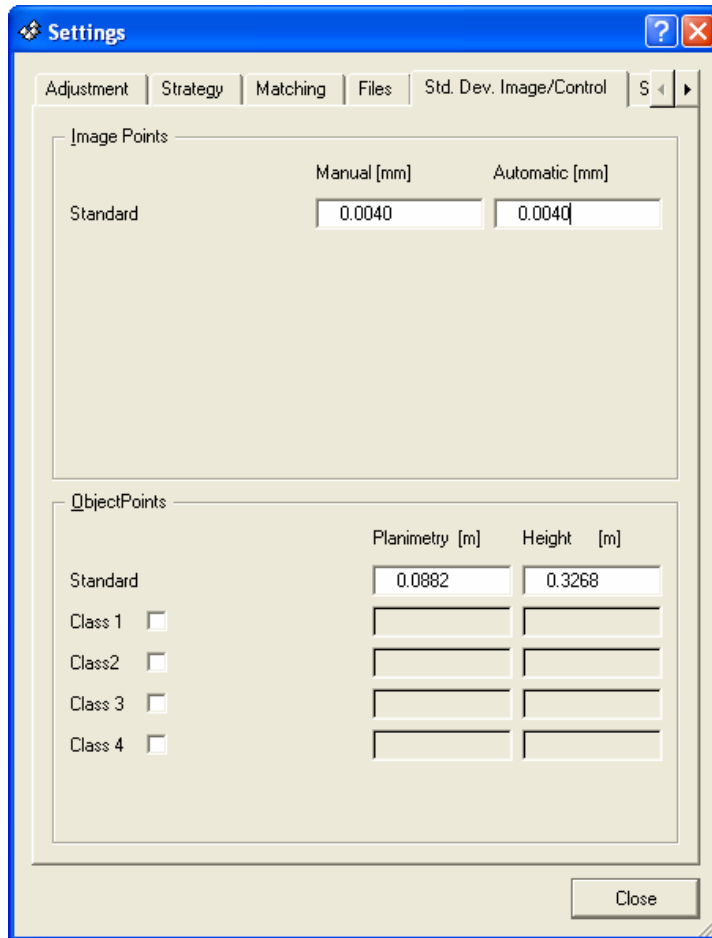
Figure 5.12 Standard deviations of image points.
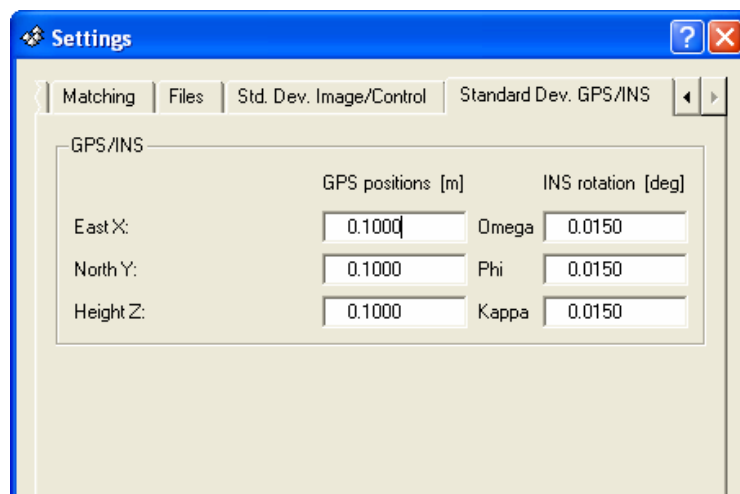
Figure 5.13 Standard deviations of GPS/INS.
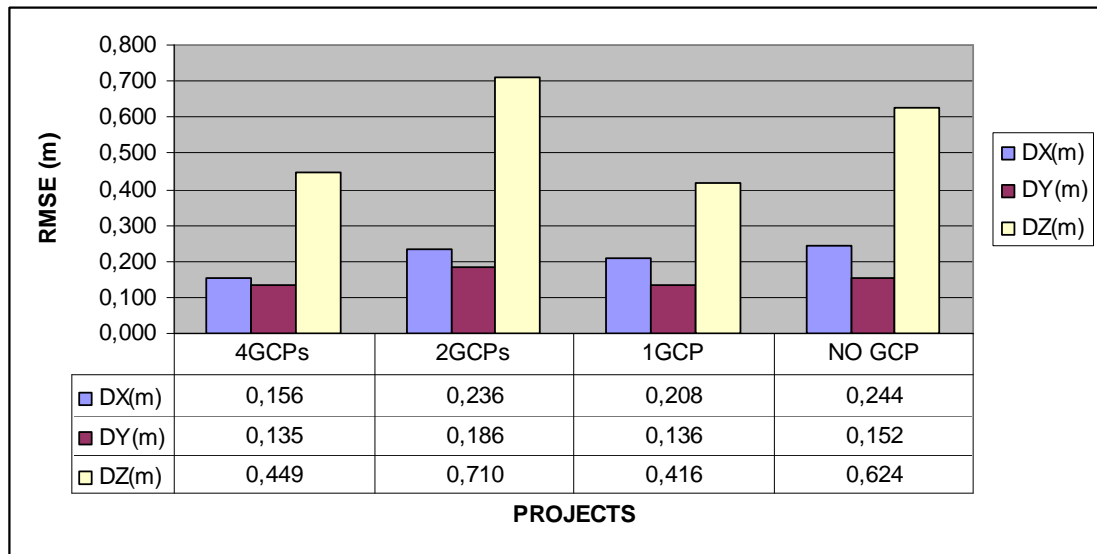
Figure 5.14 RMSE of Aero-triangulation results.

5.3 Boresight Calibration

The distance between IMU and camera sensor is measured physically when integrating IMU to the camera but the rotation angles between the camera and IMU axes cannot be measured. It is computed with the boresight calibration. Boresight calibration (dω, dφ, dκ, dx, dy, dz) is obtained by the differences between adjusted and GPS/INS results.

In order to implement boresight calibration a small area enclosing 5 GCPs is determined (Figure 5.15). Bundle block adjustment is applied using GPS/INS data as initial parameters. Then boresight parameters are determined using AeroOffice software (Table 5.2)

Table 5.2 Boresight Calibration Results

BORESIGHT CALIBRATION RESULTS						
SCALE	ROLL (degree)	PITCH (degree)	YAW (degree)	EASTING (m)	NORTHING (m)	HEIGHT (m)
1:60.000	0.3874	-0.0352	-0.1155	-0.03	-0.014	-37.329
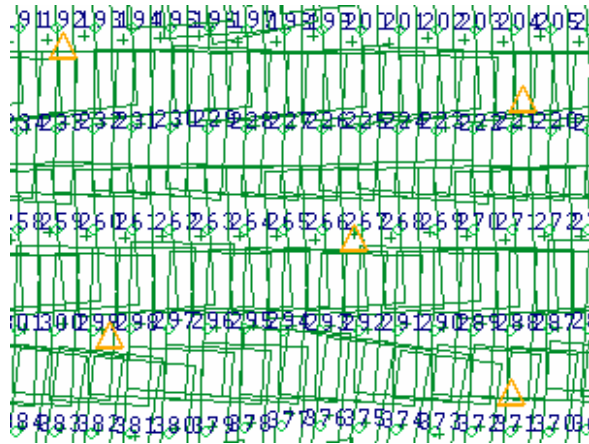
Figure 5.15 Boresight calibration area.

5.4 GPS Process with PPP

Perspective center coordinates (X_0, Y_0, Z_0) are determined with kinematic GPS method. Kinematic method is applied with the use of the air and ground GPS data and solved by kinematic differential method. In this method it is aimed to remove the satellite orbit and clock errors with double differencing. Alternatively there is another method to solve the GPS data named as Precise Point Positioning. The concept in this method is point positioning using air and precise ephemeris data. Corrected satellite coordinates and clock errors are included in precise ephemeris data. Thus precise results can be obtained. The advantage of PPP is no need of ground (base) GPS observations.

According to this concept PPP is performed by using air GPS and precise ephemeris data. GPS/INS integration is implemented with PPP results and corrected with boresight calibration parameters. Both block adjustment and direct georeferencing are performed. Stereo models are constructed in Datem Summit Evolution software and GCPs are measured in the models. Horizontal and vertical coordinate differences between the measured and adjusted coordinates are determined, mean error and root mean square error (RMSE) are computed (Figure 5.16). Detailed results are shown in Appendix-D.

	DG (DGPS)	DG (PPP)	ADJUSTED (DGPS)+GCP	ADJUSTED (PPP)+GCP
dX (m)	0,835	0,968	0,008	0,121
dY (m)	0,603	0,635	0,015	0,230
dZ (m)	0,550	0,747	0,035	0,491

PROJECTS
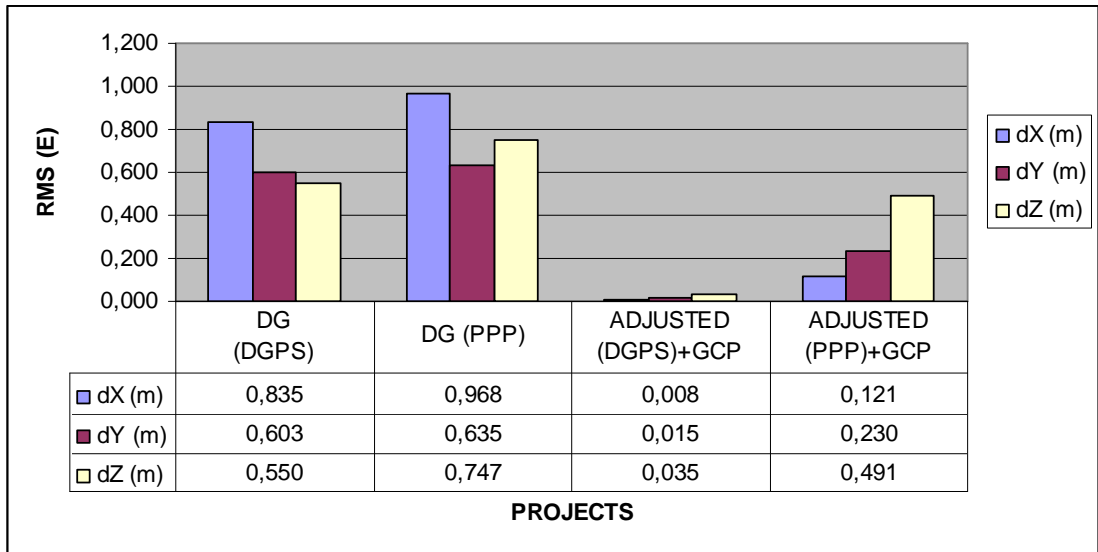
Figure 5.16 PPP and DGPS results in block adjustment and direct georeferencing.

CHAPTER 6

IMPLEMENTATION OF RECTIFICATION METHODS

In this chapter DRM of which the theory is explained in Chapter 3 will be implemented. Besides forward orthorectification (DRM) and polynomial rectification method will be implemented in order to compare the results.

6.1 Implementation of DRM

While implementing this algorithm direct georeferencing results as exterior orientation parameters are used.

In order to implement DRM an operational program is written in Matlab. For the rectification procedure the required data: raw image, the file includes exterior orientation parameters and DEM should be supplied to the folder that the program code runs.

After obtaining necessary data for rectification, the pixel by pixel transformation is performed. Firstly, the pixel coordinates are transformed into photo coordinates and the lens distortion corrections are applied. By using focal length of the camera corrected image coordinates are transformed into camera coordinates. The direction vector measured in camera coordinate system is transformed to the Local Geodetic Frame NED by the attitude angles obtained from file. The direction vector in local frame is transformed into the Earth Centered Earth Fixed Reference Frame.

Intersection point of the direction vector with WGS84 ellipsoid is computed by solving the quadratic equation. At this stage the cartesian coordinates are converted to the geodetic coordinates and the direction vector is transformed to

the local coordinate system and its zenith and azimuth angles are computed. By using the zenith angle and atmospheric parameters, atmospheric refraction coefficients are computed for 7 layers and the initial intersection position is corrected.

After the atmospheric refraction correction, relief displacement corrections are performed by iterative method. At this stage the elevation information is obtained from DEM. YUKPAF is used for the elevation data in this method. This file contains elevation data at every 10 m interval for both Northing and Easting. Elevation data are stored in ASCII format (X, Y, Z). Elevation data are constructed as grid data using mesh function (Figure 6.1).
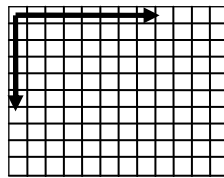
Figure 6.1 Illustration of elevation storage order in DEM [3].

After getting the corrected ground coordinates of each pixel, resampling with bilinear interpolation is applied in order to get a regular grid data. Thus orthorectified image is obtained (Figure 6.2).

Figure 6.2 Example of orthorectified image.

Finally, horizontal ground coordinates of GCPs of which the adjusted coordinates are known with GPS observations are measured on the orthorectified image. Coordinate differences between the adjusted and measured coordinates are determined, mean error and root mean square error (RMSE) (Table 6.1) are computed. Detailed results are shown in Appendix E.

Table 6.1 RMSE and mean error of horizontal coordinates for DRM.

ROOT MEAN SQUARE ERROR (RMSE)		MEAN ERROR	
DX (m)	DY (m)	DX (m)	DY (m)
1,303	2,557	1,128	2,148

6.2 Implementation of Polynomial Rectification

In order to compare the results with DRM, polynomial rectification is applied as 2nd order and 3rd order. The higher order polynomial functions do not correspond to any physical reality of the image acquisition system and it should be remembered that, in general, a higher degree 2nd polynomial may fit the GCPs but it will produce undesired distortions far away from them [4, p.25].

According to this concept polynomial rectification is applied as 2nd order and 3rd order with using Erdas Imagine 9.1 software (Figure 6.3). Horizontal ground coordinates of which the adjusted coordinates are known with GPS observations are measured on the rectified image. Coordinate differences between the adjusted and measured coordinates are determined, mean error and root mean square error (RMSE) (Table 6.2) are computed. Detailed results are shown in Appendix F.

Table 6.2 RMSE and mean error of horizontal coordinates for polynomial rectification.

Polynom Order	ROOT MEAN SQUARE ERROR (RMSE)		MEAN ERROR	
	DX (m)	DY (m)	DX (m)	DY (m)
2nd	4,763	19,671	3,129	9,800
3rd	4,622	13,960	3,631	8,427
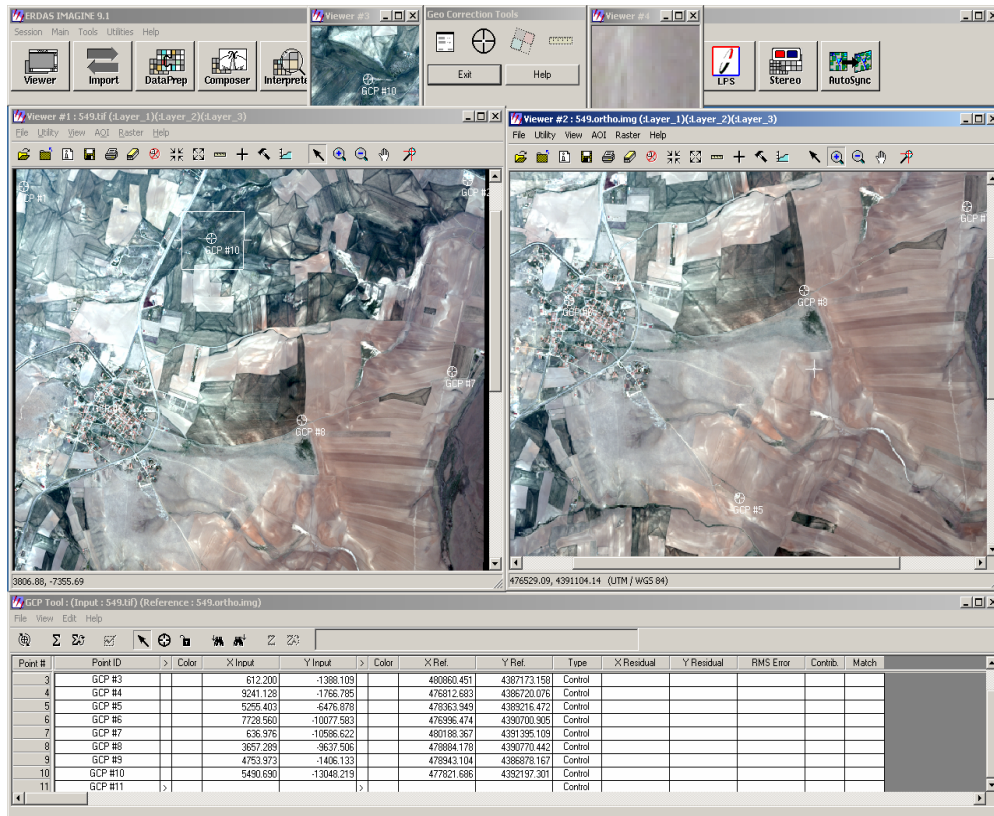
Figure 6.3 An example of polynomial rectification with Erdas Imagine 9.1.

6.3 Implementation of orthorectification with Inpho OrthoMaster 5.2

In this section images are orthorectified with different DEM data and GPS process methods in order to compare the results.

6.3.1 Orthorectification with direct georeferencing

Firstly, GPS data are post-processed as Carrier Phase Differential Positioning (CPDP) method and Precise Point positioning method. Then GPS/INS data are integrated with Kalman filtering in AeroOffice software. Both results, obtained from integration are used in orthorectification by Inpho OrthoMaster. The parameters used in orthorectification is shown in Figure 6.4 - 6.9. Horizontal ground coordinates are measured on the orthorectified image. Coordinate

differences between the adjusted coordinates are determined, mean error and root mean square error (RMSE) (Table 6.3, 6.4) are computed. Detailed results are shown in Appendix-G.
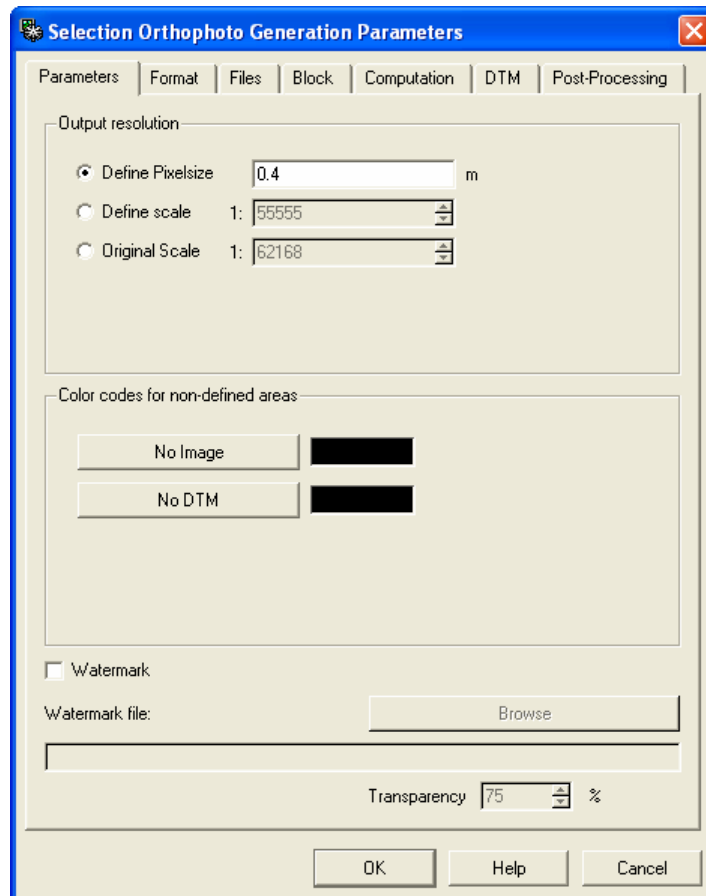
Figure 6.4 Pixel resolutions.
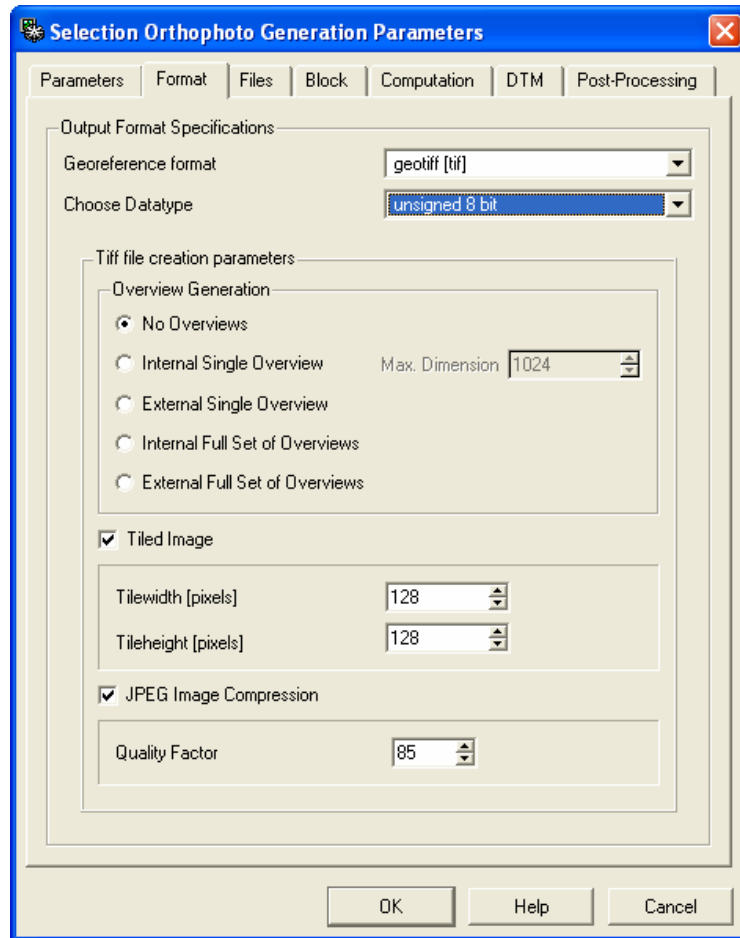
Figure 6.5 File format.
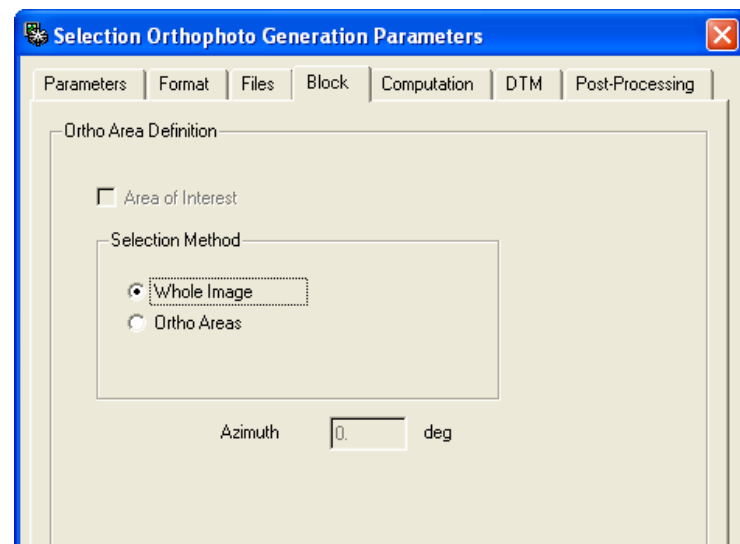
Figure 6.6 Selection method.
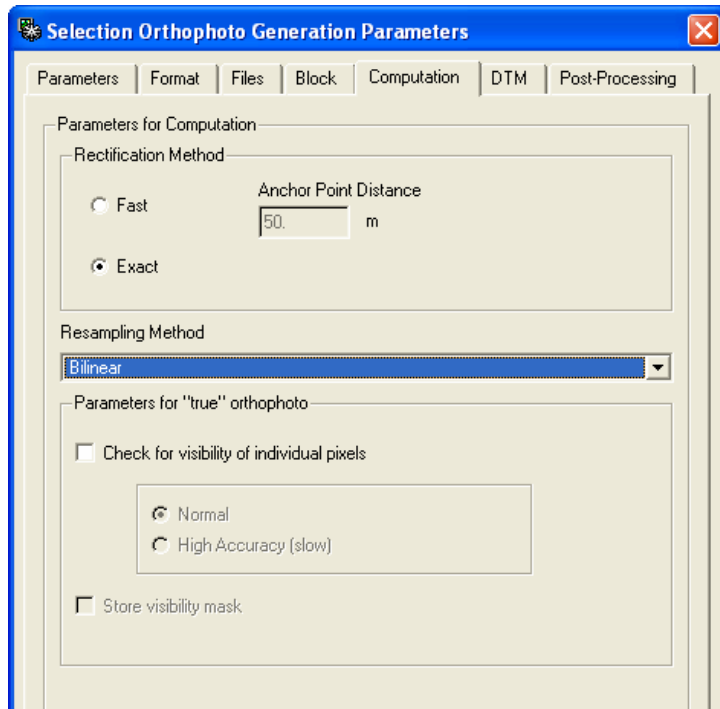
Figure 6.7 Resampling method
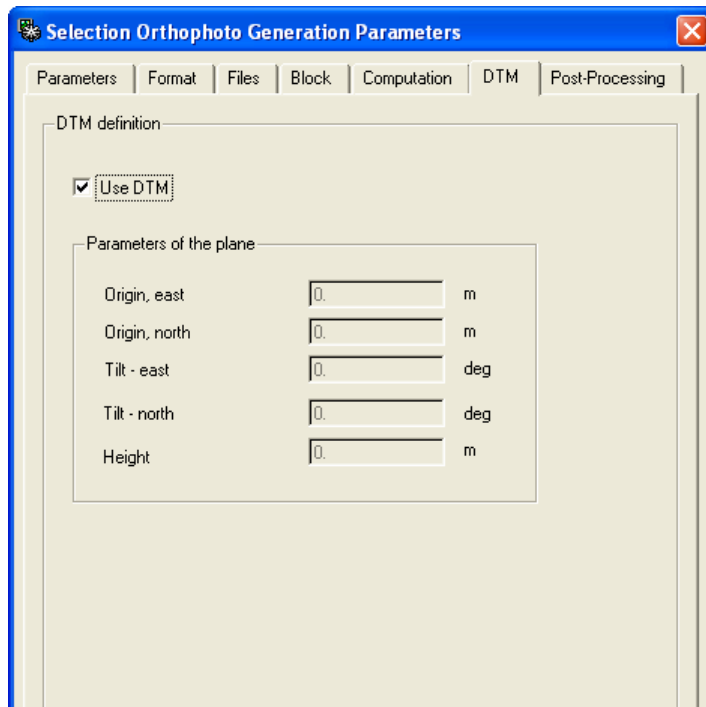
Figure 6.8 Used DEM.
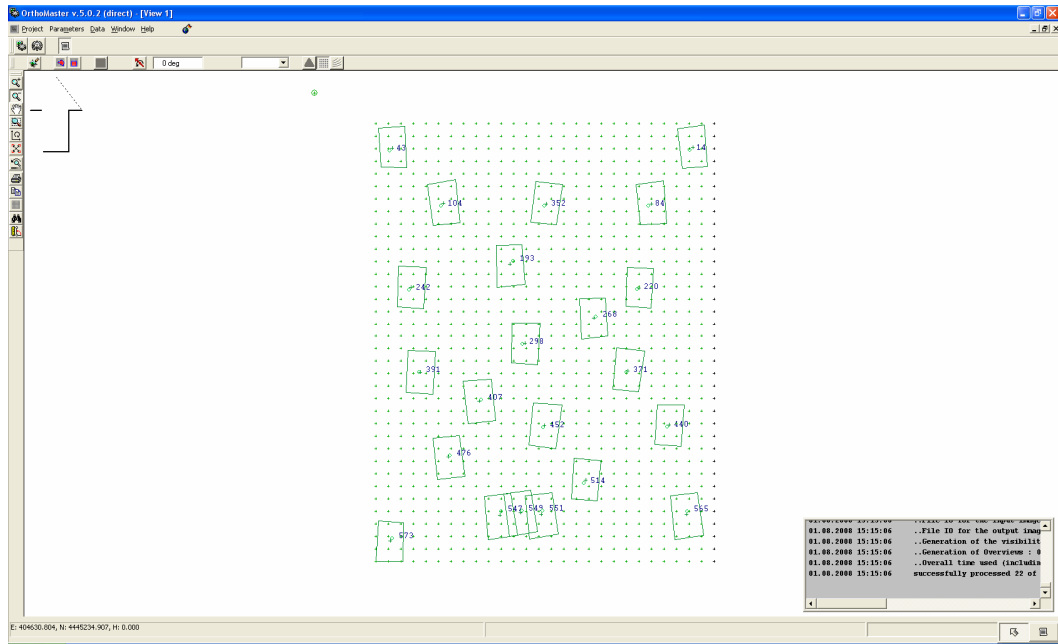
Figure 6.9 Footprint of images.

Table 6.3 RMSE and mean error of horizontal coordinates for orthorectification (CPDP).

ROOT MEAN SQUARE ERROR (RMSE)		MEAN ERROR	
DX (m)	DY (m)	DX (m)	DY (m)
0,981	0,980	0,812	0,734

Table 6.4 RMSE and mean error of horizontal coordinates for orthorectification (PPP).

ROOT MEAN SQUARE ERROR (RMSE)		MEAN ERROR	
DX (m)	DY (m)	DX (m)	DY (m)
1,079	0,961	0,900	0,714

6.3.2 Orthorectification with various DEM

In order to determine the effect of the DEM in orthorectification, SRTM and YUKPAF are used. In this implementation, adjusted exterior orientation parameters are used for orthorectification. After generating the orthorectified images horizontal ground coordinates of which the adjusted coordinates are known with GPS observations are measured. Coordinate differences between the adjusted and measured coordinates are determined, mean error and root mean square error (RMSE) (Table 6.5) are computed. Detailed results are shown in Appendix-H.

Table 6.5 RMSE and mean error of horizontal coordinates for orthorectification.

DEM	ROOT MEAN SQUARE ERROR (RMSE)		MEAN ERROR	
	DX (m)	DY (m)	DX (m)	DY (m)
YUKPAF	0,436	0,823	0,320	0,514
SRTM	1,401	1,913	1,052	1,173

CHAPTER 7

DISCUSSION OF RESULTS AND CONCLUSIONS

In this chapter, an overall evaluation of the analysis and the thesis will be performed and some recommendations will be made for the future studies. Evaluation and suggestions will be made for the thesis and an overall conclusion will be written for the thesis study.

Aero-triangulation and direct georeferencing are performed using GPS/INS data for the test area. RMSE of direct georeferencing results are 0.835 m, 0.603 m and 0.550 m for X, Y and Z respectively. These results seem to be sufficient enough for small scale applications. RMSEs of aero-triangulation results with 4 GCPs in the order of X, Y, Z is 0.156 m, 0.135 m and 0.449 m for X, Y and Z respectively. These are the expected results because of the bundle block adjusted parameters. If no GCP is used in aero-triangulation the results are also satisfactory with the RMSE of X, Y, Z as 0.244 m, 0.152 and 0.624 m respectively. It can be concluded as there is no need for GCP from now, on the other hand it should be known that there will not be the control of the results if there is no GCP. However, in order to be able to control the results 1 GCP can be used for the applications. RMSEs of aero-triangulation by using 1 GCP X, Y, Z are 0.208 m, 0.216 m and 0.416 m respectively. It can be concluded that the use of GPS/INS reduces the GCP amount used in the application block. Also automatic aero-triangulation reduces the cost of personnel and time. Besides, PPP solution of GPS data are also satisfactory with the RMSE X, Y, Z as 0.968 m, 0.635 m, and 0.747 m respectively for direct georeferencing and 0.121 m, 0.230 m and 0.491 m respectively for aero-triangulation.

DRM is implemented with respect to the algorithm explained in chapter 3 (Figure 3.4). Besides images are rectified with different parameters and DEM data in order to compare the results. Accuracy of DRM is compared with some of the existing methods (Figure 7.1). Results of comparison indicate that DRM has higher accuracy for aerial frame cameras and DRM method performance is very pleasing since polynomial transformation method shows significant decrease in accuracy especially in mountainous areas. The results of the polynomial method seem good in flat areas but the accuracy decreases if the height difference is big and it has no consistency. Besides, 3rd order polynomial seems better in accuracy especially in mountainous area with respect to 2nd order polynomial but there seems no correlation between them. On the other hand, DRM algorithm results have consistency in the whole test area. This shows that DRM can be implemented for the rectification of mountainous areas with confidence.
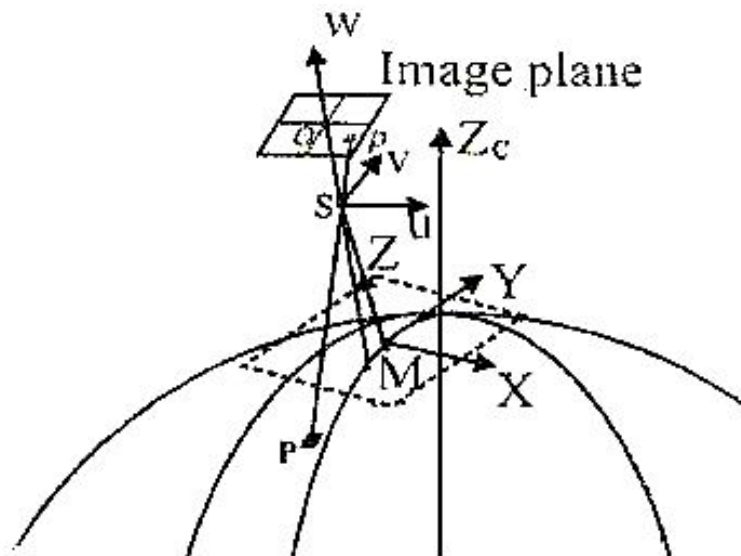
(a) Classical differential rectification procedure
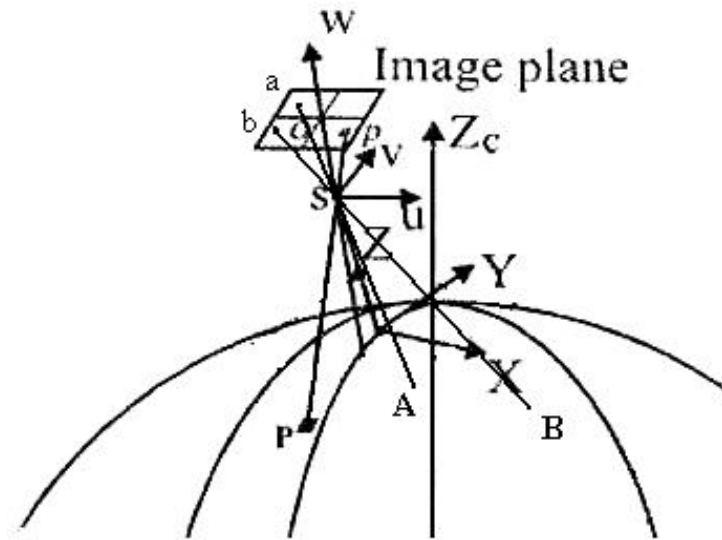
(b) DRM method

Figure 7.1 Comparison of the DRM with classical differential rectification method
[3, p.176].

As shown in Figure 7.1 DRM maps the image coordinates directly on to the reference ellipsoid while the classical rectification methods project the pixels on a plane. Although earth curvature corrections are applied after the projection, error caused by the assumption can not be completely removed. Furthermore, if the image is not taken in nadir direction, error caused by the classical rectification methods increases considerably. However, oblique images do not introduce significant errors in DRM, the only error is the effect of elevation anomaly on the horizontal coordinates. This can easily be overcome by using precise DEM [3].

Besides DRM, images are orthorectified with different DEM data and GPS process methods in order to compare the results. Orthorectification by SRTM data and YUKPAF data shows that DEM data are significant for the orthorectification procedure. Orthorectified images constructed by using YUKPAF with 10 m resolution are more accurate than the ones constructed by using SRTM with

approximately 30 m resolution as expected. Also direct georeferencing results are obtained with both Carrier Phase Differential Positioning (CPDP) method and Precise Point Positioning (PPP) method. CPDP method is more accurate because of the double differencing advantage. However, PPP solution is also satisfactory and advantageous because it does not need any ground GPS data. This reduces the cost but post process can be made approximately 2 weeks later to get the ephemeris data. All implementation results can be compared from Table 7.1.

Table 7.1 Comparison of rectification methods.

PROJECTS	ROOT MEAN SQUARE ERROR (RMSE)		MEAN ERROR	
	DX (m)	DY (m)	DX (m)	DY (m)
DRM	1,303	2,557	1,128	2,148
POLYNOMIAL (2nd)	4,763	19,671	3,129	9,800
POLYNOMIAL (3rd)	4,622	13,960	3,631	8,427
CPDP	0,981	0,980	0,812	0,734
PPP	1,079	0,961	0,900	0,714
YUKPAF	0,436	0,823	0,320	0,514
SRTM	1,401	1,913	1,052	1,173

In this thesis, DRM is programmed and applied. Besides it is compared with different rectification methods by using exterior orientation parameters obtained by different methods. It can be concluded that direct georeferencing with GPS/INS can't be used for 1:25.000 scaled topographic mapping. However, when

GPS/INS data are used in combined aerial triangulation it reduces cost of personnel and time with automatic applications. In addition, orthorectification with direct georeferencing results are satisfactory. Besides, different DEM data are used in order to determine the effect of DEM in orthorectification. The results show that orthorectification accuracy increases significantly when DEM accuracy increases. Finally, boresight calibration can be integrated in this DRM algorithm for the future studies.

REFERENCES

[1]   Aksu O. "Analitik ve Dijital Fotogrametrik Nirengi Yöntemlerinin Araştırılması", Master Thesis, ITU September 1998.

[2]   Amhar F., "The Generation of True Orthophotos 3D Building Model in Conjunction With a Conventional DTM", IAPRS, Vol.32, Part 4 "GIS-Between Visions and Applications", Stuttgart, 1998.

[3]   Bettemir Ö.H. "Sensitivity And Error Analysis of A Differential Rectification Method For CCD Frmae Cameras and Pushbroom Scanners", Master Thesis METU, September 2006.

[4]   Brown L.G. "A survey of Image Registration Techniques", ACM Computing Surveys, Vol. 24, No. 4, December 1992.

[5]   Cramer M. "Performance of GPS/Inertial Solutions in Photogrammetry" Photogremmetric Week, Heidelberg 2000.

[6]   Cramer M. and Stallmann D.   "System Calibration For Direct Georeferencing" Stuttgart/Germany, 2002.

[7]   Cramer M. and Stallmann M., "On the use of GPS/inertial exterior orientation parameters in airborne photogrammertry", Photogrammetric Week 2001, Fritsch/Spiller (eds.), Wichmann Verlag, Heidelberg, Germany.

[8]   Cramer M., Stallmann D. and Haala N., "Sensor Integration and Calibration of Digital Airborne Three-line Camera Systems", Commission II, Working Group-1.

[9]   Cramer M., Stallmann D., Haala N."Direct Georeferencing Using Gps/Inertial Exterior Orientations For Photogrammetric Applications", IAPRS, Vol. XXXIII, Amsterdam, 2000

[10] Dorota A. "Direct Exterior Orientation of Airborne Imagery with GPS/INS System: Performance Analysis", Navigation, Vol. 46, No. 4, pp. 261-270, 1999

[11] Dörstel C., Jacobsen K., Stallmann D., "DMC – Photogrammeteric Accuracy – Calibration Aspects and Generation of Synthetic DMC Images", Technical Session.

[12] Ellum C., El-Sheimy N., "The Common Adjustment of GPS and Photogrammetric Measurements", From Pharaohs to Geoinformatics FIG Working Week 2005 and GSDI-8, 2005.

[13] Erdoğan M. "Investigating The Effect Of Digital Elevation Model Accuracy On The Planimetric Accuracy Of Orthorectified Spot Imagery", Master Thesis METU, September 2000.

[14] ESRI, http://www.gisdevelopment.net/technology/ip/fio_1.htm, 12/06/2008.

[15] Ettarid M., M'Hand A.A. and Aloui R., "Digital True Orthophotos Generation", From Pharaohs to Geoinformatics FIG Working week 2005 and GSDI-8 Cairo, Egypt April 16-21, 2005.

[16] Forlani G."A Single Step Calibration Procedure For Imu/Gps In Aerial Photogrammetry" Commission III, WG III/1, 2002

[17] Fritsch D., Stallmann D., "Rigorous Photogtammetric Processing of High Resolution Satellite Imagery", ISPRS, Vol. XXXIII, Amsterdam, 2000.

[18] Grussenmeyer P., Khalil O.A., "Solutions for Exterior Orientation in Photogrammetry: A Review", Photogrammetry Record, 17(100):615 – 634 (October 2002).

[19] Haala N., Stallmann D. and Cramer M., "Calibration of Directly Measured Position and Attitude by Aerotriangulation of Three-line Airborne Imagery", Commission III, Working Group 1.Instidude of Photogrammetry (ifp) University of Stuttgart, Germany.

[20] Heipke C., Jacobsen K., Wegmann H. Andersen Q., Nilsen B. "Test Goals And Test Set Up For The Oeepe Test (Integrated Sensor Orıentatıon)" Hannover 2002.

[21] Honkavaara E. "In-Flıght Camera Calıbratıon For Dırect Georeferencıng", Finnish Geodetic Institute, Department of Remote Sensing and Photogrammetry, Finland 2004.

[22] Institute for photogrammetry, University of Stuttgart, http://www.ifp.uni-stuttgart.de/forschung/photo/georef-Dateien/georef.en.html, 25/07/2008.

[23] Jacobsen K. "Calibration Aspects In Direct Georeferencing Of Frame Imagery", Pecora 15/Land Satellite Information Iv/Isprs Commission I/Fıeos Conference Proceedings, 2002.

[24] Ji O., Costa M., Haralick R.M., Shapiro L.G., "A Robust Linear Least-Squares Estimation of Camera Exterior Orientation Using Multiple Geometric Features", ISPRS Journal of Photogrammetry & Remote Sensing 55 (2000) 75 – 93.

[25] Kamiya İ. "Development Of Orientation And Dem/Orthoimage Generation Program For Alos Prism", ACRS 2006.

[26] Karslioglu M.O., Jurgen F. "A New Differential Geometric Method to Rectify Digital Images of the Earth's Surface Using Isothermal Coordinates", IEEE Transactions on Geoscience and Remote Sensing, Vol. 43, No. 3, March 2005.

[27] Kowoma, http://www.kowoma.de/en/gps/errors.htm, 06/07/2008.

[28] Legat K., Skaloud J. "Reliability of Direct Georeferencing –A Case Study On Practical Problems And Solutions", Report to EuroSDR Commission 1, 2006

[29] Lithopoulos E., "The Applanix Approach to GPS/INS Integration", Photogrammetric Week, Heidelberg 1999.

[30] Manual of Photogrammetry Fifth Edition, (2004), American Society for Photogrammetry and Remote Sensing.

[31] Microsoft, http://download.microsoft.com/download/8/5/a/85a3648b-b4f5-46d6-80e6-c0698a2ee109/ULTRACAM-Specs.pdf . 11/08/2008.

[32] Ok A.Ö."Accuracy Assessment of the Dem and Orthoimage Generated From ASTER", Master Thesis METU, September 2005.

[33] Pateraki M., Baltsavias E., Recke U. "Experiences On Automatic Image Matching For Dsm Generation With ADS40 Pushbroom Sensor Data" Commission II, IC WG II/IV, 2004.

[34] Paul R. Wolf, Bon A. Dewitt, "Elements of Photogrammetry with Applications in GIS" Third Edition Mc Graw Hill.

[35] Reinartz P., Lehner M., Müller R., Rentsch M. and Schroeder M., "First Results on Accuracy Analysis for DEM and Orthoimages Derived from SPOT HRS Stereo Data over Bavaria".

[36] Remondino F., Fraser C. "Digital Camera Calibration Methods: Considerations And Comparisons", ISPRS Commission V Symposium 'Image Engineering and Vision Metrology', 2006

[37] Rummel R. and Peters T. "Reference systems in Satellite Geodesy" Technische Universitat München, Institut für Astronomiche und physikalische Geodasie, München 2001.

[38] Skaloud J., Lichti D., "Rigorous approach to bore-sight self-calibration in airborne laser scanning", ISPRS Journal of Photogrammetry & Remote Sensing 61 (2006) 47–59.

[39] Toth C., "Experiences With Frame CCD Arrays And Direct Georeferencing", Photogrammetric Week Heidelberg, 1999.

[40] Toth C., Dorota A. "Performance Analysis Of The Airborne Integrated Mapping System (Aims™)", USA 1998.

[41] Wikipedia, http://en.wikipedia.org/wiki/Inertial_navigation_system, 05/07/2008.

[42] Wolfgang T. "Geodesy" Third Edition. Walter de Gruyter Berlin 2001.

[43] Yastıklı N., Jacobsen K. "Investigation of Direct Sensor Orientation For DEM Generation", 2002.

[44] Zoej M.J., Yavari S. and Sadeghian S., "Mathematical Modeling of IKONOS Geo Image", ISPRS Workshop in ANKARA.

APPENDIX A

GCP COORDINATES

Table A.1 GCP coordinates computed by least square adjustment from GPS observations.

GCP ID	X (m)	Y (m)	Z (m)
1001	478936,505	4390731,643	1008,086
1002	481826,293	4390727,917	996,994
1003	482180,482	4388574,039	1014,323
1004	478812,143	4388756,076	1010,384
2501	458445,342	4444259,050	1159,131
2502	505370,543	4444700,115	1022,158
2503	505306,640	4387929,315	973,117
2504	458479,272	4387801,224	1133,785
2505	466518,511	4436370,420	830,258
2506	477618,816	4428274,204	977,772
2507	498147,217	4436267,692	958,880
2508	497329,923	4425998,611	1069,042
2509	464193,389	4413327,702	1224,120
2510	479619,906	4415660,590	893,751
2511	496841,350	4413195,980	1116,342
2512	483337,136	4403382,802	1015,748
2513	488891,152	4396829,274	1401,780
2514	476039,113	4390932,736	1132,284
2515	482099,726	4437300,907	1362,451
2516	502583,110	4404687,821	1385,683
2517	462116,284	4424747,120	789,877
2518	466320,285	4398570,588	1287,171
2519	490068,554	4419954,012	952,063
2520	473487,407	4406252,022	1173,893

APPENDIX B

DIRECT GEOREFERENCING RESULTS

Table B.1 Measured coordinates in stereo model constructed using exterior orientation parameters obtained by direct georeferencing.

GCP ID	MEASURED COORDINATES (m)		
	X	Y	Z
1001	478935,623	4390731,525	1008,162
1002	481825,386	4390728,168	997,867
1003	482179,627	4388574,251	1014,437
1004	478811,310	4388755,966	1010,260
2501	458445,330	4444258,042	1159,320
2502	505370,641	4444701,929	1022,299
2503	505305,621	4387929,588	972,510
2504	458478,032	4387801,505	1133,633
2505	466518,199	4436370,489	829,315
2506	477618,781	4428274,362	977,772
2507	498146,763	4436268,145	958,880
2508	497329,943	4425998,505	1068,288
2509	464194,752	4413326,875	1223,665
2510	479620,412	4415660,271	893,798
2511	496842,197	4413195,383	1116,038
2512	483338,552	4403383,212	1016,203
2513	488891,584	4396829,350	1401,135
2514	476038,142	4390932,553	1132,626
2515	482099,066	4437302,096	1363,668
2516	502583,858	4404688,223	1384,924
2517	462117,147	4424746,950	790,490
2518	466319,239	4398570,221	1288,044
2519	490068,436	4419954,243	952,157
2520	473486,261	4406252,630	1174,007

Table B.2 Differences between measured and adjusted coordinates.

GCP ID	COORDINATE DIFFERENCES (m)		
	DX	DY	DZ
1001	-0,882	-0,118	0,076
1002	-0,907	0,251	0,873
1003	-0,855	0,212	0,114
1004	-0,833	-0,110	-0,124
2501	-0,012	-1,008	0,189
2502	0,098	1,814	0,141
2503	-1,019	0,273	-0,607
2504	-1,240	0,281	-0,152
2505	-0,312	0,069	-0,943
2506	-0,035	0,158	0,000
2507	-0,454	0,453	0,000
2508	0,020	-0,106	-0,754
2509	1,363	-0,827	-0,455
2510	0,506	-0,319	0,047
2511	0,847	-0,597	-0,304
2512	1,416	0,410	0,455
2513	0,432	0,076	-0,645
2514	-0,971	-0,183	0,342
2515	-0,660	1,189	1,217
2516	0,748	0,402	-0,759
2517	0,863	-0,170	0,613
2518	-1,046	-0,367	0,873
2519	-0,118	0,231	0,094
2520	-1,146	0,608	0,114

Table B.3 RMSE and mean error of coordinate differences.

ROOT MEAN SQUARE ERROR (RMSE)			MEAN ERROR		
DX (m)	DY (m)	DZ (m)	DX (m)	DY (m)	DZ (m)
0,835	0,603	0,550	0,699	0,426	0,412

APPENDIX C

AERIAL TRIANGULATION RESULTS

Aerotriangulation results with bundle block adjustment using 4 GCP.

Table C.1 Computed as check points (CP) in bundle block adjustment (4 GCP).

GCP ID	CP COORDINATES (m)		
	X	Y	Z
1001	478936,401	4390731,654	1008,254
1002	481826,463	4390727,946	997,236
1003	482180,470	4388574,039	1014,584
1004	478812,202	4388756,079	1010,630
2501	458445,302	4444259,052	1159,130
2502	505370,545	4444700,115	1022,106
2503	505306,636	4387929,315	973,152
2504	458479,313	4387801,226	1133,804
2505	466518,431	4436370,426	830,426
2506	477619,048	4428274,258	977,992
2507	498147,345	4436267,708	959,143
2508	497329,896	4425998,612	1069,065
2509	464193,281	4413327,714	1224,318
2510	479620,002	4415660,599	893,826
2511	496841,443	4413195,989	1116,330
2512	483336,911	4403382,853	1015,702
2513	488891,250	4396829,284	1401,926
2514	476039,177	4390932,740	1132,548
2515	482099,537	4437300,943	1362,155
2516	502583,277	4404687,849	1385,594
2517	462116,041	4424747,179	789,860
2518	466320,240	4398570,590	1287,356
2519	490068,602	4419954,014	952,236
2520	473487,385	4406252,022	1174,016

Table C.2 Differences between check points and adjusted GCP coordinates.

GCP ID	COORDINATE DIFFERENCES (m)		
	DX	DY	DZ
1001	-0,104	0,168	0,190
1002	0,170	0,242	-0,059
1003	-0,012	0,261	-0,060
1004	0,059	0,246	0,086
2501	-0,040	-0,001	-0,038
2502	0,002	-0,052	0,049
2503	-0,004	0,035	0,207
2504	0,041	0,019	-0,218
2505	-0,080	0,168	0,120
2506	0,232	0,220	0,366
2507	0,128	0,263	0,131
2508	-0,027	0,023	0,354
2509	-0,108	0,198	-0,244
2510	0,096	0,075	0,285
2511	0,093	-0,012	0,039
2512	-0,225	-0,046	-0,149
2513	0,098	0,146	-0,411
2514	0,064	0,264	-0,009
2515	-0,189	-0,296	-0,380
2516	0,167	-0,089	-0,345
2517	-0,243	-0,017	0,136
2518	-0,045	0,185	-0,660
2519	0,048	0,173	0,319
2520	-0,022	0,123	-0,080

Table C.3 RMSE and mean error of coordinate differences.

ROOT MEAN SQUARE ERROR (RMSE)			MEAN ERROR		
DX (m)	DY (m)	DZ (m)	DX (m)	DY (m)	DZ (m)
0,123	0,172	0,263	0,096	0,138	0,206

Aerotriangulation results with bundle block adjustment using 2 GCP.

Table C.4 Computed as check points (CP) in bundle block adjustment (2 GCP).

GCP ID	CP COORDINATES (m)		
	X	Y	Z
1001	478936,305	4390731,683	1008,183
1002	481826,368	4390727,923	997,164
1003	482180,374	4388574,051	1014,511
1004	478812,105	4388756,077	1010,559
2501	458445,105	4444259,106	1159,054
2502	505370,431	4444700,128	1021,775
2503	505306,498	4387929,335	973,210
2504	458479,319	4387801,226	1133,806
2505	466518,330	4436370,453	830,346
2506	477618,951	4428274,222	977,913
2507	498147,245	4436267,693	959,051
2508	497329,798	4425998,627	1068,986
2509	464193,184	4413327,744	1224,243
2510	479619,906	4415660,590	893,751
2511	496841,347	4413195,980	1116,253
2512	483336,816	4403382,904	1015,628
2513	488891,156	4396829,274	1401,853
2514	476039,081	4390932,737	1132,479
2515	482099,441	4437300,988	1362,077
2516	502583,181	4404687,826	1385,516
2517	462115,945	4424747,235	789,784
2518	466320,150	4398570,606	1287,282
2519	490068,505	4419954,014	952,157
2520	473487,290	4406252,036	1173,941

Table C.5 Differences between check points and adjusted coordinates.

GCP ID	COORDINATE DIFFERENCES (m)		
	DX	DY	DZ
1001	-0,026	0,105	0,044
1002	0,248	0,178	-0,205
1003	0,066	0,196	-0,206
1004	0,136	0,183	-0,060
2501	-0,014	-0,021	-0,156
2502	0,060	-0,374	0,046
2503	0,014	0,021	0,156
2504	0,221	0,029	-0,530
2505	-0,009	0,106	-0,033
2506	0,309	0,153	0,222
2507	0,201	0,180	-0,001
2508	0,047	-0,047	0,213
2509	-0,031	0,132	-0,390
2510	0,172	0,009	0,141
2511	0,170	-0,080	-0,106
2512	-0,148	-0,112	-0,292
2513	0,176	0,081	-0,554
2514	0,142	0,203	-0,153
2515	-0,112	-0,363	-0,525
2516	0,243	-0,159	-0,490
2517	-0,168	-0,083	-0,008
2518	0,038	0,120	-0,799
2519	0,124	0,105	0,175
2520	0,056	0,057	-0,222

Table C.6 RMSE and mean error of coordinate differences.

ROOT MEAN SQUARE ERROR (RMSE)			MEAN ERROR		
DX (m)	DY (m)	DZ (m)	DX (m)	DY (m)	DZ (m)
0,152	0,162	0,320	0,122	0,129	0,239

Aerotriangulation results with bundle block adjustment using 1 GCP.

Table C.7 Computed as check points (CP) in bundle block adjustment (1 GCP).

GCP ID	CP COORDINATES (m)		
	X	Y	Z
1001	478936,305	4390731,683	1008,183
1002	481826,368	4390727,923	997,164
1003	482180,374	4388574,051	1014,511
1004	478812,105	4388756,077	1010,559
2501	458445,105	4444259,106	1159,054
2502	505370,431	4444700,128	1021,775
2503	505306,498	4387929,335	973,210
2504	458479,319	4387801,226	1133,806
2505	466518,330	4436370,453	830,346
2506	477618,951	4428274,222	977,913
2507	498147,245	4436267,693	959,051
2508	497329,798	4425998,627	1068,986
2509	464193,184	4413327,744	1224,243
2510	479619,906	4415660,590	893,751
2511	496841,347	4413195,980	1116,253
2512	483336,816	4403382,904	1015,628
2513	488891,156	4396829,274	1401,853
2514	476039,081	4390932,737	1132,479
2515	482099,441	4437300,988	1362,077
2516	502583,181	4404687,826	1385,516
2517	462115,945	4424747,235	789,784
2518	466320,150	4398570,606	1287,282
2519	490068,505	4419954,014	952,157
2520	473487,290	4406252,036	1173,941

Table C.8 Differences between check points and adjusted coordinates.

GCP ID	COORDINATE DIFFERENCES (m)		
	DX	DY	DZ
1001	-0,200	0,097	-0,096
1002	0,075	0,170	-0,346
1003	-0,108	0,188	-0,347
1004	-0,038	0,175	-0,200
2501	-0,237	-0,077	-0,409
2502	-0,112	-0,383	-0,097
2503	-0,142	0,093	0,177
2504	0,047	0,021	-0,672
2505	-0,181	0,088	-0,170
2506	0,135	0,141	0,083
2507	0,028	0,171	-0,142
2508	-0,125	-0,056	0,073
2509	-0,205	0,123	-0,532
2510	0,000	0,000	0,000
2511	-0,003	-0,089	-0,247
2512	-0,320	-0,120	-0,431
2513	0,004	0,073	-0,694
2514	-0,032	0,195	-0,294
2515	-0,285	-0,374	-0,665
2516	0,071	-0,167	-0,629
2517	-0,339	-0,093	-0,145
2518	-0,135	0,111	-0,939
2519	-0,049	0,094	0,036
2520	-0,117	0,048	-0,361

Table C.9 RMSE and mean error of coordinate differences.

ROOT MEAN SQUARE ERROR (RMSE)			MEAN ERROR		
DX (m)	DY (m)	DZ (m)	DX (m)	DY (m)	DZ (m)
0,161	0,162	0,416	0,125	0,025	0,129

Aerotriangulation results with bundle block adjustment using no GCP.

Table C.10 Computed as check points (CP) in bundle block adjustment (No GCP).

GCP ID	CP COORDINATES (m)		
	X	Y	Z
1001	478936,403	4390731,587	1007,886
1002	481826,446	4390727,905	996,698
1003	482180,521	4388573,882	1014,130
1004	478812,256	4388755,908	1010,215
2501	458445,191	4444259,074	1159,329
2502	505370,281	4444699,909	1022,258
2503	505306,178	4387929,461	973,849
2504	458479,816	4387801,230	1133,655
2505	466518,486	4436370,639	830,713
2506	477619,000	4428274,374	978,079
2507	498147,045	4436267,893	959,220
2508	497329,601	4425998,622	1069,705
2509	464193,578	4413327,887	1224,262
2510	479619,967	4415660,642	893,799
2511	496841,093	4413195,961	1116,778
2512	483336,807	4403382,739	1015,274
2513	488891,134	4396829,278	1401,563
2514	476039,201	4390932,793	1132,195
2515	482099,353	4437300,755	1361,822
2516	502582,662	4404687,706	1385,788
2517	462116,339	4424747,127	789,853
2518	466320,443	4398570,711	1286,176
2519	490068,416	4419954,092	952,111
2520	473487,517	4406252,105	1174,159

Table C.11 Differences between check points and adjusted coordinates.

GCP ID	COORDINATE DIFFERENCES (m)		
	DX	DY	DZ
1001	-0,102	-0,056	-0,200
1002	0,153	-0,012	-0,296
1003	0,039	-0,157	-0,193
1004	0,113	-0,168	-0,169
2501	-0,151	0,024	0,198
2502	-0,262	-0,206	0,100
2503	-0,462	0,146	0,732
2504	0,544	0,006	-0,130
2505	-0,025	0,219	0,455
2506	0,184	0,170	0,307
2507	-0,172	0,201	0,340
2508	-0,322	0,011	0,662
2509	0,189	0,185	0,142
2510	0,061	0,052	0,048
2511	-0,257	-0,019	0,436
2512	-0,329	-0,063	-0,474
2513	-0,018	0,004	-0,217
2514	0,088	0,056	-0,089
2515	-0,373	-0,152	-0,629
2516	-0,448	-0,115	0,105
2517	0,055	0,007	-0,024
2518	0,158	0,123	-0,995
2519	-0,138	0,080	0,048
2520	0,110	0,083	0,266

Table C.12 RMSE and mean error of coordinate differences.

ROOT MEAN SQUARE ERROR (RMSE)			MEAN ERROR		
DX (m)	DY (m)	DZ (m)	DX (m)	DY (m)	DZ (m)
0,244	0,152	0,624	0,208	0,103	0,328

APPENDIX D

GPS PROCESSING WITH PPP

D.1 Bundle Block Adjustment

GPS post-processed with PPP and then the results integrated with INS. Integration results are used as initial parameters of bundle block adjustment.

Table D.1 GCP coordinates measured from stereo model constructed using PPP results.

MEASURED COORDINATES			
GCP ID	X (m)	Y (m)	Z (m)
1001	478936,554	4390731,686	1008,684
1002	481826,266	4390727,802	997,822
1003	482180,552	4388574,104	1014,415
1004	478812,089	4388756,196	1010,832
2501	458445,4	4444258,772	1158,395
2502	505370,595	4444700,256	1021,79
2503	505306,675	4387929,397	973,025
2504	458479,278	4387801,36	1133,417
2505	466518,509	4436369,947	829,982
2506	477618,624	4428273,901	977,956
2507	498146,946	4436267,232	958,88
2508	497329,849	4425998,379	1069,502
2509	464193,513	4413327,254	1223,695
2510	479619,606	4415660,538	894,119
2511	496841,365	4413195,812	1116,48
2512	483337,378	4403382,536	1016,645
2513	488891,175	4396829,343	1402,228
2514	476039,233	4390932,789	1132,732
2515	502583,062	4404687,898	1385,832
2516	462116,23	4424746,834	790,613
2517	466320,312	4398570,52	1287,711
2518	490068,536	4419953,97	952,615
2519	473487,386	4406251,856	1174,341
2520	478936,554	4390731,686	1008,684

Table D.2 Differences between adjusted and measured GCP coordinates.

CORDINATE DIFFRENCES (m)		
DX	DY	DZ
0,049	0,043	0,598
-0,027	-0,115	0,828
0,070	0,065	0,092
-0,054	0,120	0,448
0,058	-0,278	-0,736
0,052	0,141	-0,368
0,035	0,082	-0,092
0,006	0,136	-0,368
-0,002	-0,473	-0,276
-0,192	-0,303	0,184
-0,271	-0,460	0,000
-0,074	-0,232	0,460
0,124	-0,448	-0,425
-0,300	-0,052	0,368
0,015	-0,168	0,138
0,242	-0,266	0,897
0,023	0,069	0,448
0,120	0,053	0,448
-0,048	0,077	0,149
-0,054	-0,286	0,736
0,027	-0,068	0,540
-0,018	-0,042	0,552
-0,021	-0,166	0,448

Table D.3 RMSE and mean error of coordinate differences.

RMSE			MEAN ERROR		
X (m)	Y (m)	Z (m)	X (m)	Y (m)	Z (m)
0,121	0,230	0,491	0,078	0,173	0,400

D.2 Direct Georeferencing

GPS post-processed with PPP and then the results integrated with INS. Integration results used as directly in stereo model construction (direct georeferencing).

Table D.4 GCP coordinates measured from stereo model constructed by PPP results.

	MEASURED COORDINATES		
GCP ID	X (m)	Y (m)	Z (m)
1001	478935,45	4390731,732	1009,604
1002	481825,013	4390728,089	998,259
1003	482179,678	4388574,687	1014,576
1004	478811,314	4388756,77	1010,763
2501	458446,242	4444260,661	1159,786
2502	505371,324	4444701,602	1021,503
2503	505305,831	4387929,957	972,358
2504	458477,349	4387801,617	1133,279
2505	466518,164	4436370,508	829,396
2506	477618,711	4428274,329	977,197
2507	498146,585	4436268,322	958,88
2508	497329,908	4425998,355	1068,755
2509	464194,821	4413326,83	1223,833
2510	479620,325	4415660,241	894,038
2511	496841,984	4413195,46	1116,629
2512	483338,481	4403382,887	1016,61
2513	488891,626	4396828,453	1401,78
2514	476037,956	4390932,836	1133,169
2515	482098,921	4437301,558	1363,693
2516	502583,739	4404687,806	1385,108
2517	462116,918	4424746,899	790,739
2518	466319,056	4398570,736	1288,321
2519	490068,061	4419954,212	952,35
2520	473486,009	4406252,344	1174,18

Table D.5 Coordinate differences between adjusted and measured GCP coordinates.

COORDINATE DIFFERENCES (m)			
GCP ID	DX	DY	DZ
1001	-1,055	0,089	1,518
1002	-1,280	0,172	1,265
1003	-0,804	0,648	0,253
1004	-0,829	0,694	0,379
2501	0,900	1,611	0,655
2502	0,781	1,487	-0,655
2503	-0,809	0,642	-0,759
2504	-1,923	0,393	-0,506
2505	-0,347	0,088	-0,862
2506	-0,105	0,125	-0,575
2507	-0,632	0,630	0,000
2508	-0,015	-0,256	-0,287
2509	1,432	-0,872	-0,287
2510	0,419	-0,349	0,287
2511	0,634	-0,520	0,287
2512	1,345	0,085	0,862
2513	0,474	-0,821	0,000
2514	-1,157	0,100	0,885
2515	-0,805	0,651	1,242
2516	0,629	-0,015	-0,575
2517	0,634	-0,221	0,862
2518	-1,229	0,148	1,150
2519	-0,493	0,200	0,287
2520	-1,398	0,322	0,287

Table D.6 RMSE and mean error of coordinate differences.

RMSE			MEAN ERROR		
X (m)	Y (m)	Z (m)	X (m)	Y (m)	Z (m)
0,968	0,635	0,747	0,839	0,464	0,614

APPENDIX E

DRM RESULTS

Table E.1 GCP coordinates measured from orthorectified imagery constructed using DRM.

MEASURED COORDINATES		
GCP ID	X (m)	Y (m)
1001	478935,586	4390732,811
1002	481824,492	4390729,495
1003	482179,573	4388571,752
1004	478811,245	4388754,058
2501	458446,494	4444255,983
2502	505371,47	4444697,939
2503	505305,903	4387926,422
2504	458477,778	4387806,139
2505	466518,477	4436368,717
2506	477619,019	4428272,395
2507	498146,832	4436265,971
2508	497330,581	4426001,018
2509	464195,626	4413330,424
2510	479620,935	4415659,895
2511	496843,106	4413198,816
2512	483339,366	4403383,934
2513	488892,109	4396834,645
2514	476038,155	4390934,548
2515	482101,201	4437299,545
2516	502584,593	4404692,363
2517	462117,64	4424747,291
2518	466318,127	4398569,911
2519	490068,017	4419953,067
2520	473486,626	4406250,473

Table E.2 Differences between adjusted and measured GCP coordinates.

GCP ID	COORDINATE DIFFRENCES (m)	
	DX	DY
1001	-0,919	1,168
1002	-1,801	1,578
1003	-0,909	-2,287
1004	-0,898	-2,018
2501	1,152	-3,067
2502	0,927	-2,176
2503	-0,737	-2,893
2504	-1,494	4,915
2505	-0,034	-1,703
2506	0,203	-1,809
2507	-0,385	-1,721
2508	0,658	2,407
2509	2,237	2,722
2510	1,029	-0,695
2511	1,756	2,836
2512	2,230	1,132
2513	0,957	5,371
2514	-0,958	1,812
2515	1,475	-1,362
2516	1,483	4,542
2517	1,356	0,171
2518	-2,158	-0,677
2519	-0,537	-0,945
2520	-0,781	-1,549

Table E.3 RMSE and mean error of coordinate differences.

RMSE			MEAN ERROR		
X (m)	**Y (m)**	**Z (m)**	**X (m)**	**Y (m)**	**Z (m)**
1,303	2,557	1,128	2,148	1,303	2,557

APPENDIX F

POLYNOMIAL RECTIFICATION RESULTS

F.1 2nd Order Polynomial Rectification

Table F.1 GCP coordinates measured from rectified imagery constructed by using 2nd order polynomial rectification.

MEASURED COORDINATES		
GCP ID	X (m)	Y (m)
1001	478937,229	4390730,324
1002	481825,047	4390728,889
1003	482180,122	4388574,275
1004	478812,198	4388757,065
2501	458447,150	4444261,442
2502	505367,253	4444704,154
2503	505311,167	4387940,155
2504	458478,641	4387825,040
2505	466517,592	4436374,555
2506	477617,141	4428272,182
2507	498146,642	4436270,585
2508	497328,257	4425992,173
2509	464197,463	4413336,475
2510	479616,876	4415654,694
2511	496840,957	4413204,211
2512	483339,564	4403392,553
2513	488881,522	4396913,672
2514	476037,753	4390935,448
2515	482095,657	4437289,226
2516	502599,093	4404708,645
2517	462114,063	4424743,050
2518	466325,525	4398576,475
2519	490062,431	4419945,428
2520	473484,331	4406256,311

Table F.2 Differences between adjusted and measured GCP coordinates.

GCP ID	COORDINATE DIFFRENCES (m)	
	DX	DY
1001	0,724	-1,319
1002	-1,246	0,972
1003	-0,360	0,236
1004	0,055	0,989
2501	1,808	2,392
2502	-3,290	4,039
2503	4,527	10,840
2504	-0,631	23,816
2505	-0,919	4,135
2506	-1,675	-2,022
2507	-0,575	2,893
2508	-1,666	-6,438
2509	4,074	8,773
2510	-3,030	-5,896
2511	-0,393	8,231
2512	2,428	9,751
2513	-9,630	84,398
2514	-1,360	2,712
2515	-4,069	-11,681
2516	15,983	20,824
2517	-2,221	-4,070
2518	5,240	5,887
2519	-6,123	-8,584
2520	-3,076	4,289

Table F.3 RMSE and mean error of coordinate differences.

RMSE		MEAN ERROR	
X (m)	Y (m)	X (m)	Y (m)
4,763	19,671	3,129	9,800

121

F.2 3rd Order Polynomial Rectification

Table F.4 GCP coordinates measured from rectified imagery constructed by using 3rd order polynomial rectification.

MEASURED COORDINATES		
GCP ID	X (m)	Y (m)
1001	478937,043	4390729,245
1002	481824,054	4390728,877
1003	482180,243	4388575,243
1004	478812,230	4388755,936
2501	458446,972	4444261,967
2502	505366,567	4444704,762
2503	505310,332	4387941,086
2504	458477,679	4387820,565
2505	466516,328	4436376,589
2506	477616,177	4428270,876
2507	498157,282	4436256,666
2508	497334,471	4426014,571
2509	464199,451	4413336,475
2510	479616,876	4415652,601
2511	496834,863	4413196,577
2512	483338,008	4403391,505
2513	488893,776	4396883,446
2514	476035,244	4390932,114
2515	482095,669	4437288,803
2516	502593,161	4404696,912
2517	462114,958	4424745,866
2518	466323,512	4398577,978
2519	490061,097	4419948,364
2520	473482,743	4406258,068

Table F.5 Differences between adjusted and measured GCP coordinates.

GCP ID	COORDINATE DIFFRENCES (m)	
	DX	DY
1001	0,538	-2,398
1002	-2,239	0,960
1003	-0,239	1,204
1004	0,087	-0,140
2501	1,629	2,917
2502	-3,976	4,647
2503	3,692	11,770
2504	-1,593	19,341
2505	-2,183	6,169
2506	-2,639	-3,328
2507	10,065	-11,026
2508	4,548	15,960
2509	6,062	8,773
2510	-3,030	-7,989
2511	-6,487	0,597
2512	0,872	8,703
2513	2,624	54,172
2514	-3,869	-0,622
2515	-4,057	-12,104
2516	10,051	9,091
2517	-1,326	-1,254
2518	3,227	7,390
2519	-7,457	-5,648
2520	-4,664	6,046

Table F.6 RMSE and mean error of coordinate differences.

RMSE		MEAN ERROR	
X (m)	Y (m)	X (m)	Y (m)
4,622	13,960	3,631	8,427

APPENDIX G

CPDP AND PPP IN ORTHORECTIFICATION

G.1 Direct Georeferencing with CPDP results

GPS post-processed with CPDP and then the results integrated with INS. Integration results used directly as exterior orientation parameters in orthorectification.

Table G.1 GCP coordinates measured from orthorectified imagery constructed using by CPDP results.

MEASURED COORDINATES		
GCP ID	X (m)	Y (m)
1001	478935,2732	4390729,617
1002	481824,7221	4390727,523
1003	482179,5875	4388575,217
1004	478811,2773	4388757,516
2501	458446,3805	4444259,866
2502	505371,436	4444701,129
2503	505306,4145	4387927,638
2504	458478,1273	4387803,344
2505	466518,1041	4436370,658
2506	477619,0883	4428273,568
2507	498146,8404	4436268,477
2508	497330,0898	4425998,584
2509	464194,4488	4413326,112
2510	479620,0503	4415660,46
2511	496841,5896	4413195,166
2512	483339,0565	4403383,275
2513	488891,5935	4396829,673
2514	476038,1853	4390932,883
2515	482100,9972	4437300,502
2516	502583,8999	4404688,21
2517	462116,7863	4424747,19
2518	466318,3667	4398570,096
2519	490068,2016	4419954,014
2520	473486,5667	4406252,383

Table G.2 Differences between adjusted and measured GCP coordinates.

GCP ID	COORDINATE DIFFERENCES (m)	
	DX	DY
1001	-1,232	-2,026
1002	-1,571	-0,394
1003	-0,894	1,178
1004	-0,866	1,440
2501	1,038	0,816
2502	0,893	1,014
2503	-0,226	-1,677
2504	-1,145	2,120
2505	-0,407	0,238
2506	0,272	-0,636
2507	-0,377	0,785
2508	0,167	-0,027
2509	1,060	-1,590
2510	0,144	-0,130
2511	0,240	-0,814
2512	1,921	0,473
2513	0,441	0,399
2514	-0,928	0,147
2515	1,271	-0,405
2516	0,790	0,389
2517	0,502	0,070
2518	-1,918	-0,492
2519	-0,352	0,002
2520	-0,840	0,361

Table G.3 RMSE and mean error of coordinate differences.

RMSE		MEAN ERROR	
X (m)	Y (m)	X (m)	Y (m)
0,981	0,980	0,812	0,734

G.2 Direct georeferencing with PPP results

GPS post-processed with PPP and then the results integrated with INS. Integration results used directly as exterior orientation parameters in orthorectification.

Table G.4 GCP coordinates measured from orthorectified imagery constructed using by PPP results.

MEASURED COORDINATES		
GCP ID	X (m)	Y (m)
1001	478935,179	4390730,057
1002	481824,771	4390728,616
1003	482179,559	4388575,701
1004	478811,317	4388757,832
2501	458446,253	4444259,968
2502	505371,295	4444701,323
2503	505306,442	4387928,179
2504	458477,459	4387803,273
2505	466518,035	4436370,727
2506	477619,085	4428273,64
2507	498146,766	4436268,581
2508	497330,057	4425998,544
2509	464194,627	4413326,374
2510	479619,958	4415660,491
2511	496841,706	4413195,338
2512	483338,936	4403382,877
2513	488889,363	4396828,392
2514	476038,221	4390933,268
2515	482101,164	4437300,921
2516	502583,936	4404687,558
2517	462116,742	4424746,954
2518	466318,585	4398570,672
2519	490068,081	4419953,902
2520	473486,425	4406252,114

Table G.5 Differences between adjusted and measured GCP coordinates.

GCP ID	COORDINATE DIFFRENCES (m)	
	DX	DY
1001	-1,326	-1,586
1002	-1,522	0,699
1003	-0,923	1,662
1004	-0,826	1,756
2501	0,911	0,918
2502	0,751	1,208
2503	-0,198	-1,136
2504	-1,813	2,049
2505	-0,477	0,307
2506	0,269	-0,564
2507	-0,451	0,889
2508	0,134	-0,067
2509	1,238	-1,328
2510	0,052	-0,099
2511	0,356	-0,642
2512	1,800	0,075
2513	-1,789	-0,882
2514	-0,892	0,532
2515	1,438	0,014
2516	0,826	-0,263
2517	0,458	-0,166
2518	-1,700	0,084
2519	-0,473	-0,111
2520	-0,982	0,092

Table G.6 RMSE and mean error of coordinate differences.

RMSE		MEAN ERROR	
X (m)	Y (m)	X (m)	Y (m)
1,079	0,961	0,900	0,714

ORTHORECTIFICATION WITH YUKPAF AND SRTM

H.1 Orthorectification with YUKPAF

Exterior orientation parameters are obtained by bundle block adjustment and YUKPAF DEM is used in orthorectification.

Table H.1 GCP coordinates measured from orthorectified imagery constructed using YUKPAF DEM.

MEASURED COORDINATES		
GCP ID	X (m)	Y (m)
1001	478936,715	4390729,488
1002	481826,275	4390728,109
1003	482180,664	4388575,132
1004	478812,331	4388757,108
2501	458445,173	4444259,159
2502	505370,539	4444700,233
2503	505307,523	4387927,126
2504	458479,658	4387802,586
2505	466518,152	4436370,427
2506	477619,311	4428273,226
2507	498147,308	4436267,853
2508	497329,949	4425998,758
2509	464192,942	4413327,827
2510	479618,939	4415661,05
2511	496840,841	4413195,825
2512	483337,455	4403383,166
2513	488891,045	4396829,712
2514	476039,443	4390932,786
2515	482099,718	4437300,968
2516	502583,135	4404688,289
2517	462115,878	4424747,218
2518	466319,959	4398570,413
2519	490068,803	4419953,694
2520	473486,425	4406252,114

Table H.2 Differences between adjusted and measured GCP coordinates.

GCP ID	COORDINATE DIFFRENCES (m)	
	DX	DY
1001	0,210	-2,155
1002	-0,018	0,192
1003	0,182	1,093
1004	0,188	1,032
2501	-0,169	0,109
2502	-0,004	0,118
2503	0,883	-2,189
2504	0,386	1,362
2505	-0,359	0,007
2506	0,495	-0,978
2507	0,091	0,161
2508	0,026	0,147
2509	-0,447	0,125
2510	-0,967	0,460
2511	-0,509	-0,155
2512	0,319	0,364
2513	-0,107	0,438
2514	0,330	0,050
2515	-0,008	0,061
2516	0,025	0,468
2517	-0,406	0,098
2518	-0,326	-0,175
2519	0,249	-0,318
2520	-0,982	0,092

Table H.3 RMSE and mean error of coordinate differences.

RMSE		MEAN ERROR	
X (m)	Y (m)	X (m)	Y (m)
0,436	0,823	0,320	0,514

H.2 Orthorectification with SRTM

Exterior orientation parameters are obtained by bundle block adjustment and SRTM DEM is used in orthorectification.

Table H.4 GCP coordinates measured from orthorectified imagery constructed using SRTM DEM.

MEASURED COORDINATES		
GCP ID	X (m)	Y (m)
1001	478935,594	4390731,027
1002	481824,567	4390727,895
1003	482179,746	4388573,358
1004	478811,353	4388756,147
2501	458446,272	4444258,291
2502	505371,052	4444702,328
2503	505305,400	4387931,034
2504	458478,000	4387801,573
2505	466518,098	4436370,645
2506	477619,773	4428270,455
2507	498147,042	4436269,102
2508	497330,838	4426000,78
2509	464197,719	4413330,144
2510	479619,931	4415660,493
2511	496841,491	4413195,169
2512	483339,395	4403383,487
2513	488892,364	4396835,882
2514	476038,060	4390932,593
2515	482100,553	4437299,437
2516	502584,103	4404688,462
2517	462116,703	4424747,003
2518	466318,247	4398570,237
2519	490068,379	4419954,144
2520	473486,205	4406252,691

Table H.5 Differences between adjusted and measured GCP coordinates.

GCP ID	COORDINATE DIFFRENCES (m)	
	DX	DY
1001	-0,911	-0,616
1002	-1,726	-0,022
1003	-0,737	-0,681
1004	-0,790	0,071
2501	0,929	-0,759
2502	0,509	2,213
2503	-1,240	1,719
2504	-1,272	0,349
2505	-0,413	0,225
2506	0,957	-3,749
2507	-0,174	1,410
2508	0,915	2,169
2509	4,330	2,442
2510	0,025	-0,097
2511	0,141	-0,811
2512	2,259	0,685
2513	1,212	6,608
2514	-1,053	-0,143
2515	0,827	-1,470
2516	0,993	0,641
2517	0,419	-0,117
2518	-2,038	-0,351
2519	-0,175	0,132
2520	-1,202	0,669

Table H.6 RMSE and mean error of coordinate differences.

RMSE		MEAN ERROR	
X (m)	Y (m)	X (m)	Y (m)
1,401	1,913	1,052	1,173